DOCTORAL THESIS

Analytical and Approximate Methods in Rogue Wave Theory

Author:
Mahyar Bokaeeyan

Supervisors:
Nail Akhmediev
Adrian Ankiewicz
Wonkeun Chang

Research School of Physics
The Australian National University (ANU)

A thesis submitted to the Australian National University as a requirement of the degree for *Doctor of Philosophy*.

AUGUST 2020

ACKNOWLEDGMENTS

The production of a dissertation is a formidable, arduous and demoralizing task. For me, the effort has been considerably reduced by the support of many people. This list, obviously, is so long that it is hard to decide where to begin.

First of all, I would like to express my deepest gratitude to my supervisors, Prof. Nail Akhmediev, Dr. Adrian Ankiewicz, and Dr. Wonkeun Chang, for providing both the essential background information and an appropriate atmosphere to investigate the enthralling field of rogue waves. They have always been friendly and readily approachable. This Ph.D. thesis would not have come into existence without their support and assistance. Professor Akhmediev should be especially acknowledged on his perceptive view of the concept, always advising me to tackle new challenging physical problems, while the professional and technical support of Dr. Ankiewicz has proved invaluable, guiding me towards my research targets. I particularly thank him for his affection and kindness for spending his invaluable time proofreading and providing fruitful comments on my thesis and publications. He is, indeed, my best teacher, mentor, and friend. I am grateful to Dr. Wonkeun Chang for his help with advice on programming and numerical techniques, his technical support, and his useful discussions.

I cannot forget to thank all members of the Optical Sciences Group, especially Peter Vouzas, Matthew Crabb and Dr. Chong Liu, an industrious visitor from North-west University, Xían, China. You are a brilliant group of scientists, I really enjoyed listening to everyone's ideas, comments and discussions. This made my stay at the RSP very fruitful because, apart from my own research topic, I got the chance to learn about what other people are doing, thus broadening my knowledge in nonlinear physics. This period has really been a time of tremendous learning and growth for me, both scientifically and personally.

I would like to express my appreciation to the contributor of the 'Ben Williams student support grant' for providing me with essential funding when I was facing a financial hardship. Herewith, I thank Karen Nulty, Luda Mangos and Professor Lan Fu for helping me on various administrative tasks.

I would like to thank my wife, Mahsa Nazemi Moghaddam for her support and help, and for creating a peaceful atmosphere for me to do my best in this work. This thesis would not have been possible without her help and suport.

Lastly, I extend my thanks to TOTAL who provided me with the ANU scholarships. I am most grateful to them.

Mahyar Bokaeeyan
The Australian National University
April 2020

Dedication

To my wife, my love, my life.

I am indebted to you for your love, support and encouragement through everything. I could not have done it without you.
Thank you.

Author's declaration

I *Mahyar Bokaeeyan*, declare that this thesis titled, 'Analytical and Approximate Methods in Rogue Wave Theory' and the work presented here, except where indicated by particular reference in the text, is entirely the candidate's own work. The works of other authors in any forms (like ideas, equations, figures, programming codes, tables) are mentioned at any spots of their use. A list of the references is properly included.

SIGNED: .... DATE: ....

List Of Publications

1. "Rogue waves under influence of Raman delay"
   Journal of Optical Society of America B **35**, p. 899-908 (2018).
   Adrian Ankiewicz, Mahyar Bokaeeyan, and Nail Akhmediev.
   *Recieved a "**Spotlight**" remark from the Optical Society of America.*

2. "Rogue waves in higher-order systems: Lagrangian approach"
   Physica Scripta **94**, p. 035203 (2019).
   Mahyar Bokaeeyan, Adrian Ankiewicz, and Nail Akhmediev.

3. "Shallow-water rogue waves: An approach based on complex solutions of the Korteweg-de-Vries equation"
   Physical Review E (*Rapid Communication*) **99**, no. 5, p. 050201 (2019).
   Adrian Ankiewicz, Mahyar Bokaeeyan, and Nail Akhmediev.

4. "Bright and dark rogue internal waves: The Gardner equation approach"
   Physical Review E **99**, no. 6, p. 062224 (2019).
   Mahyar Bokaeeyan, Adrian Ankiewicz, and Nail Akhmediev.

5. "Infinitely extended complex KdV equation and its solutions: solitons and rogue waves"
   Physica Scripta **95**, p. 035201 (2020).
   Adrian Ankiewicz, Mahyar Bokaeeyan, and Nail Akhmediev.

6. "Integral relations for rogue wave formations of Gardner equation"
   Nonlinear Dynamics, **99**, p. 2939 (2020).
   Adrian Ankiewicz, Mahyar Bokaeeyan

7. "Real-valued rogue waves in dusty plamsa" (Submitted)
   Mahyar Bokaeeyan, Adrian Ankiewicz, Nail Akhmediev, Wonkeun Chang

8. "Understanding general rogue wave solutions of the Gardner Equation" (Submitted)
   Adrian Ankiewicz, Mahyar Bokaeeyan, Wonkeun Chang

Abstract

Rogue waves are defined as localized structures in both space and time. They can be described as isolated large-amplitude waves that unexpectedly appear on a relatively calm background. They usually bring destruction and damage. Rogue waves are ubiquitous, found in oceans and in the atmosphere. They exist in various areas of physics such as plasmas and optics. The mechanism of formation of these unusual waves can vary depending on the subject. Mathematically, such waves can be modeled by specific (rational) solutions of the nonlinear Schrödinger equation. This equation is a generic model for wave propagation in dispersive media with weak nonlinearity.

This thesis is devoted to investigation of rogue waves in various nonlinear systems, including water waves, plasma, and optical fibers. In particular, modeling rogue waves using other equations has been considered. Rational solutions have been found for the Gardner equation which is known to be an accurate model for the propagation of internal waves in multi-layer fluids. The first four 'bright' and 'dark' exact rational solutions to the Gardner equation are given as a mathematical description for internal rogue waves that occur in three-layer fluids. These are the lowest-order solutions of the corresponding hierarchies of rogue-wave solutions of this equation.

Another subject covered in the thesis is the formation of rogue waves in shallow water. Namely, the three lowest-order exact rational solutions to the complex-valued Korteweg-de Vries (KdV) equation are found. These solutions can serve as a likely model for shallow water rogue waves. It is found that the amplitude amplification factor of such waves is much larger than the amplitude amplification factor of rogue waves occurring in deep water. The practical aspect of finding these solutions is in demonstration that shallow water rogue waves can be a potential hazard for coastal areas. Further progress is reached in extending the complex-valued KdV equation to a more general equation that contains an infinite number of high-order terms with arbitrary real coefficients. This equation is shown to be integrable allowing us to find a general form of soliton and rogue wave solutions for this equation. The latter are described by the rational solutions of this generalised equation.

Rogue waves in dusty plasma is another application of the theory developed in the thesis. Namely, a long wave-length model in a plasma with cold and heavy dust particles at thermal equilibrium has been considered. The detailed derivation leads to the Gardner equation which is an accurate model for weakly nonlinear and dispersive wave propagation in the regime of small amplitude waves. A discrete hierarchy of rational solutions describing rogue waves in dusty plasma shows that a considerable amount of energy (or electric charge) could become concentrated in a relatively small area of plasma at certain instance of time. This feature is similar to those of rogue waves in the ocean or in fiber optics. This study shows that the dust electric potential amplitude of rogue waves strongly depends on the ratio between the ion and electron temperatures and densities in the plasma.

When exact solutions cannot be found, approximate methods are used for modeling rogue waves. In this thesis, we use a Lagrangian approach for finding rogue wave solutions of the

extended nonlinear Schrödinger equation (NLSE). The higher-order terms in the equation distort the rogue wave solutions leaving the main features such as localisation in space and time intact. When the equation with higher-order terms is integrable, the approximate wave forms naturally coincide with the exact rogue wave solutions. This is demonstrated in several well-known cases such as the Hirota equation, The Lakshmanan-Porsezian-Daniel (LPD) equation, and the Kundu-Echkaus equation. However, the main advantage of using the Lagrangian approach is achieved in cases of non-integrable equations when finding exact solutions is impossible.

In particular, we used this technique to evaluate the effects of fourth and sixth order dispersion on rogue waves. We also considered the influence of Raman delay as an example of treating the nonlinear terms. In order to confirm the applicability of the technique, the results are compared with solutions found by numerical simulations of the original equation. Good agreements have been found confirming the usefulness of the approach. In order to further simplify the approach for users, a table of Lagrangian components for variety of possible terms in the extended equation is provided. This way, the analysis of rogue waves solutions for any extended equations becomes a simple and straightforward exercise. The direct summation of the components is a major point in achieving this simplicity.

Table of Contents

Page

List of Tables

List of Figures

Figure **Page**

Chapter 1

Introduction

The rogue wave phenomena has received much attention over the past few decades nearly in all branches of physical science. We can mention oceanography, nonlinear optics and plasmas [7–9], and even economics [10]. There is still no general strict definition of a rogue wave that is universally applicable to all of these subjects. We can describe it as a very large wave that unexpectedly appears on a relatively calm background. Generation of rogue waves in a variety of conditions is a subject under intense investigation [11–14]. Several mechanisms have been suggested for the emergence of rogue waves. The terms "rogue wave" or "freak wave" were first applied in the study of giant waves that suddenly emerge in the ocean. A few other technical terms commonly used in different contexts are "killer waves", "monster waves" and "giant waves" [15]. Another imaginative description for rogue waves is "waves that appear from nowhere and disappear without a trace" [16].

The stories of enormous waves are used to be spread by fishermen who have encountered large walls of water in the ocean. There are many anecdotes narrating such an event in seas [17]. Historically, the ill-famed rogue waves possibly capsized the third voyage of Columbus' fleet in 1498. They might have sunk the Mary Rose battleship, erected on the King Henry VIII's order, in 1545. They also, perhaps, destructed Daniel Steinmann, a hefty iron steamer ship in 1884 and has led to disappearance of an Australian ship, the SS Waratah in 1909 [18].

In the late 20th century, these stories became more credible as giant waves have been captured in photos. One testimony of the existence of such waves is a picture of a 30-meter-high rogue wave taken by a professional photographer, Karsten Peterson, on the foredeck of Stolt Surf [18]. Another proof of their existence is the significant destruction of mechanical and electrical equipment on vessels and marine structures during the rogue wave events. These events include structural damage to the hull of Wilstar, the Norwegian tanker, hit by a steep wave in South

Africa in 1974 [19], or the drowned drilling oil platform Ocean Ranger [20].

However, the first direct proof of the existence of rogue waves has happened on the first day of 1995 when the laser wave height sensor installed at the Draupner platform in the North Sea reported a wave with an astonishingly high peak of 25.6 meters [21]. This event created a wave of interest to this topic that resulted in significant advancement in the knowledge bank. Despite the fact that today we know much more about these waves than in the past, rogue waves still are a major cause of material damage or loss of lives in oceans. Among recent events, we can mention the catastrophe of Rabaul Queen in 2012 and an incident with a rogue wave that hit Divina, a Cruise ship, in November 2015. The two other ships that were hit by a rogue in 2017 are a German supply tender vessel Drifa, and a passenger ship Trollfjord [22].

Rogue waves do not necessarily bring a destruction. One of the businesses that profited from rogue waves is the film industry. The rogue waves is the central subject in recent blockbusters such as “The perfect storm” (2000), “The day after tomorrow” (2004), “Poseidon” (2006), “Haeundae” (2009), “2012” (2009), “San Andreas” (2015), “The fifth wave” (2016), “Geostorm” (2017), “Open water III” (2017) and the Oscar winner “Interstellar” (2014). The combined profit due to release of these movies is over 3.5 billion dollars. By a cursory glance at the giant water wave in the aforementioned movies, we can realize they are rogue waves rather than tsunami, a tidal wave or a flood wave. Namely, they occur in a perfectly calm sea condition and have a sharp crest.

The generation mechanism of oceanic rogue waves in different physical models is a matter of debate which has taken much effort from the oceanographic society [23]. Although there are a few feasible suggestions for this mechanism, each of them can be valid in distinctive physical and natural conditions. The linear [24] and nonlinear mechanisms [25] are two most important theories to explain that kind of wave. In linear theory, a wave superposition of numerous small amplitude linear waves with different wave characteristics, i.e. amplitude and phase, moving in various ways in an arbitrary area of an ocean is suggested. This superpositions can be easily written as:

$$\psi(x,t) = \sum A(\vec{K}) cos(\vec{K}.\vec{x} - \omega t + \eta(\vec{K})),$$

where ψ is the elevation and $A(\vec{K})$ is the amplitude of the wave. η is the phase, $\vec{x}$ is a directional position, and t is the time. The wave-number vector $\vec{K}$ is dependent on the angular frequency ω by the dispersion relation as:

$$\omega^2 = gK \tanh(hK),$$

where $K = |\vec{K}|$ and g is the gravity. It can be proved that in the limit of deep water ($Kh \to \infty$) the phase velocity is twice as big as the group velocity. It means that the larger wave-length yields the faster propagation speed.

The local amplification process, thus, can be led by the geometrical focusing of waves which happens usually as a result of inhomogeneous wind flow in deep water.

In the case of very sharp and steep waves, the linear theory, which is based on the harmonic waves, may not be valid and thus nonlinear mechanism can be suggested instead. Nonlinear wave interaction eases the energy exchange between different wave elements and, therefore, the background can affect the propagation of uniform waves. This can result in the instability of the amplitude modulation of the waves. This has proved that the nonlinearity can, indeed, escalate the probability of the rogue wave more than what is predicted by the linear theory [23].

Importantly, rogue waves have not only been observed in oceans but also have been studied in laboratories. They have been investigated in water tanks, in plasma, and in fibre optics [13].

1.0.1 Rogue waves in water tanks

Direct observations of rogue waves in the ocean are difficult and dangerous. Hunting for these rare events would requires expensive equipment and involvement in risk as the rogue wave appearance is tightly related to stormy weather and large average wave amplitude. Moreover, observations in nature cannot provide sufficient information regarding the formation, excitation and other major features of rogue waves. Therefore, water tank experiment is a better alternative for rogue wave studies. A brief summary of such observations of water rogue waves is presented below.

A very first experimental observation was carried out in a wave-current flume at University of Wisconsin in the Environmental Fluid Mechanics Laboratory in 2004 [26]. A man-made channel of 46 m long, 0.91 m wide and 0.6 m depth filled with tap water has been used in this experiment. An even bed for this flume was constructed. An appropriate wave generator was assembled at the bottom of one end of the channel. At the other end of the flume, there was a slope acting as a provisional beach that absorbed almost all incoming monochromatic waves. The results of this measurement were quite staggering. First, wave group formation and its spectral content were proved to be important in the emergence and the appearance of rogue waves. Spectral bandwidth played a crucial role in the formation of rogue waves. Large-amplitude confronting currents increased the steepness of the waves beyond the ordinary waves sharpness. It was found that the energy of waves has been transferred to higher frequencies at the location of the freak wave. The main sources of the generation of these huge waves have been found to be the wave-current interaction and dispersive spatial-temporal focusing of random waves. However, these studies were not supported by an accurate theory of rogue waves.

An experiment based on the theory of rogue waves based on Peregrine solution of the wave equation has been done in [27]. These studies have been done at the Hamburg University of Technology in 2011. The water tank used in this experiment had the size 15 m length, 1.6 m wide and 1 m depth. Waves in the tank have been excited using computer controlled paddle located at one end of the tank. Waves have been dissipated by a beach installed at the other end. These experiments have confirmed that the Peregrine solution can serve as the prototype for the first order rogue waves. The wave profile had accurately followed the theoretical curve that included two deep troughs at each side of the wave crest. The wave evolution after reaching the maximum of the wave decayed symmetrically, in reverse order to the growth observed before the maximum.

This reversibility is exactly what is expected in the theory. In addition, the rogue waves measured in this experiment were 3 times larger than the average height of waves around it. This fact showed once again that the observed rogue wave satisfied the definition given in [28].

The experimental research followed a year later [29] confirmed the theoretical prediction of the existence of higher-order rogue waves. The second order rogue wave solution had the amplitude that is 5 times higher than the background while the amplitude of the third order rogue wave was 7 times higher than the background.

The works mentioned above clearly demonstrated that rogue waves in a laboratory are much easier to study than in an open sea. These studies can be done in a controlled conditions with prescribed parameters of excited waves. Exciting rogue waves at any desired instant allows one to shorten time required for investigations. Besides, it is not necessarily surface water waves that can be used for rogue wave research. This can be done in various areas of physics. One of them is optics. The next section provides a brief review of extreme wave propagation in optical systems. We will start with the derivation of nonlinear wave equation in the absence as well as in presence of higher order nonlinear effects. We will also consider the formation of coherent structures in optical fibres.

1.1 Optical fibers and nonlinear Schrödinger equation

Optical communication is the next stage of the information revolution. Digital processing and transmission of information more than ever, demands light as a crucial means to be used in the communication lines as extensively as possible. Due to ever growing demand of the internet, the web traffic will shortly surpass an unprecedented figures of thousands of terabytes per second per connection. This sharp upsurge requires more transmission capacity and reliability of optical links. This is possible with the use of optical fiber as an efficient terrestrial information transmission medium. The fibre offers ultra-broadband communication for connecting millions of desktop computers at home and governmental organisations.

The birth of optical fibers dates back to 1966, soon after the invention of the laser in 1960 [30]. During this period, researchers attempted to find an advanced medium for communications. In 1966, the optical fiber seemed to be the best option for signal transmission due to potentially larger bandwidth than copper wires. The principle of the total internal reflection, which was first demonstrated by John Tyndall in 1870, is the theoretical concept behind the optical fibers [31]. This principle allows light to propagate within the fiber very much the same way as electrons move within a metal wire. The first optical fibers were made from transparent glass and then silica [30].

Potentials of the optical fibres are not limited to linear light transmission. With the invention of the laser, which can produce high intensity monochromatic optical fields, the boundaries of the linear optics were broken. In high intensity optical fields, the relation between the electric field and dielectric polarisation becomes nonlinear. This has many consequences. In particular, the nonlinear optics led to the observation of new optical phenomena such as propagation of stable forms of pulses (solitons) in optical fibers [32]. As mentioned, in nonlinear optics, the linear response of the dielectric to the applied electric field is no longer valid. Polarisation can be presented as a power series expansion of the electric field:

$$\vec{P} = \epsilon_0 \left[\chi^{(1)} \vec{E} + \chi^{(2)} \vec{E}^2 + \chi^{(3)} \vec{E}^3 + \dots \right]$$

where ϵ_0 is the vacuum permittivity and $\chi^{(j)}$ ($j = 1, 2, \dots$) is j^{th} order susceptibility which is generally a tensor of the rank $(j+1)$. The first term here is responsible for the linear effect. The second term is responsible for parametric processes involving three frequencies and the second-harmonic generation. The third term is responsible for the third harmonic generation, the four-wave mixing and nonlinear refraction. The latter phenomenon, i.e. nonlinear refraction, represents the fact that the refractive index is not only the function of the frequency but also depends on the intensity of light. Namely, $n = n(\omega, |E|^2) = n_0 + n_2|E|^2$, where n_0 is the linear refraction index approximated by the Sellmeier equation [33] and $n_2 = (3/8n)\Re(\chi^{(3)}_{xxxx})$, where $\Re$ stands for the real part.

The wave equation describing the light propagation in an optical fiber can be derived from the Maxwell's equations taking into account the nonlinear dielectric polarisation given above. Eliminating the magnetic field B and the electric flux density D for a nonmagnetic medium $M = 0$, we obtain:

$$\nabla \times \nabla \times \vec{E} = -\frac{1}{c^2} \frac{\partial^2 \vec{E}}{\partial t^2} - \mu_0 \frac{\partial^2 \vec{P}}{\partial t^2},$$

where $c = 1/\sqrt{\mu_0 \epsilon_0}$ is the speed of light in vacuum. The next stage of derivation is the separation of fast and slow variables. In the approximation of slowly varying amplitude, for the wave envelope, we find the Nonlinear Schrödinger equation [32, 34–36]:

$$\frac{\partial E}{\partial z} + \beta_1 \frac{\partial E}{\partial t} + i\beta_2 \frac{\partial^2 E}{\partial t^2} + \frac{\alpha}{2} E = i\gamma |E|^2 E, \tag{1.1}$$

where, E is the slowly varying electric field envelope, z is the coordinate along the propagation direction, t is the retarded time. For an isotropic medium, such as glass, $\gamma = \frac{n_2 \omega_0}{c A_{eff}}$ is a scalar, where A_{eff} is the effective core area, $\beta_m = \left(\frac{d^m \beta}{d\omega^m} \right)_{\omega = \omega_0}$ is the dispersion coefficient, which is the m^{th} term of the Taylor expansion of the wave number $\beta(\omega)$ near the central frequency ω_0. Namely, β_1 describes the group velocity of the pulse envelope, i.e. $\beta_1 = 1/v_g$, while β_2 describes the group-velocity dispersion. The latter is positive if the wavelength is below the zero-dispersion wavelength λ_D and β_2 is negative if the wavelength is bigger than λ_D. This parameter can change sign along the fibre of special design [32, 35]. Finally, α is the total fiber loss. When loss is zero, this wave equation can be transformed to the non-dimensional form which is known as the NLSE.

1.1.1 Higher-order dispersion and Raman delay

The wave equation (1.1) explains, roughly, nonlinear effects in a fiber. However, it may need refinements for shorter pulses. When pulse duration is less than 1 ps, some assumptions used in deriving Eq.(1.1) have to be reconsidered. Pulses with a wide spectrum ($> 0.1THz$) require additional terms in the equation related to time delayed nonlinear material response [32]. One of the consequences is the energy transfer from the high-frequency components of the pulse spectrum to lower-frequency components. This process is known as the intrapulse Raman scattering. It causes the so-called self-frequency shift in the case of soliton propagation along the fiber.

In order to describe these effects, the third-order susceptibility must be presented in time domain. In this case, it serves as a kernel of an integral transform:

$$\chi^{(3)}(t-t_1, t-t_2, t-t_3) = \chi^{(3)} R(t-t_1)\delta(t-t_2)\delta(t-t_3),$$

where t_1, t_2 and t_3 are time delay variables in the transform. Delta functions here assume instantaneous response while R is the normalised nonlinear response function describing the time delay. It is normalised such that $\int_{-\infty}^{\infty} R(t)dt = 1$. Substituting this kernel into the integral transform and assuming the fiber is lossless, we obtain more general evolution equation than Eq.(1.1) [32, 35, 37]:

$$i\frac{\partial E}{\partial z} + \sum_{m=1}^{\infty} \frac{i^m \beta_m}{m!}\frac{\partial^m E}{\partial t^m} + \gamma\left(1 + is\frac{\partial}{\partial t}\right)\left(E\int_0^{\infty} R(t')|E(t-t')|^2 dt'\right) = 0. \tag{1.2}$$

Here, the infinite sum describes all orders of dispersion while the next term describes the nonlinear response with time delay and self-steepening with the corresponding coefficient s. In practice, only a few lowest order terms are used to describe the dispersion with sufficiently high accuracy. The integral term in this equation can be approximated by [38]:

$$R(t) = (1 - f_R)\delta(t) + f_R h_R(t),$$

where f_R represents the Raman delay response of the nonlinear polarization and $h_R(t) = \frac{\tau_1^2+\tau_2^2}{\tau_1\tau_2^2}\sin(\frac{t}{\tau_1})e^{(\frac{-t}{\tau_2})}$ is the simplest mathematical form of the Raman response function with two adjustable parameters (τ_1 and τ_2). In these approximations, Eq.(1.2) becomes [32, 35]:

$$i\frac{\partial E}{\partial z} + \sum_{m=1}^{n} \frac{i^m \beta_m}{m!}\frac{\partial^m E}{\partial t^m} + \gamma\left(|E|^2 E + is\frac{\partial}{\partial t}(|E|^2 E) - \tau_R E\frac{\partial |E|^2}{\partial t}\right) = 0, \tag{1.3}$$

where $\tau_R = f_R \int_{-\infty}^{\infty} h_R(t)dt$ is a constant. The two last terms describe the self-steepening and the intrapulse Raman delay phenomena, respectively. In optical fibers, the effect of the latter term on the propagation of very short pulses can dominate the effect of the former one. This equation is used in Chapter 7 for the analysis of solitons and rogue waves in media where such effects are important.

1.1.2 Coherent structures

Solitons

Research on solitons covers areas such as water waves, nonlinear optics, plasma physics and other fields in physics. The soliton research in optics started with the seminal work of Hasegawa and Tappert [39]. They predicted, theoretically, the possibility of the soliton propagation in optical fibers with the profile in time described by the sech-function. In 1980, Mollenauer, Stolen and Gordon provided first experimental confirmation of this novel idea [40]. They have shown how the nonlinearity in the index of refraction can counterbalance the pulse broadening.

Presently, all basic features of solitons have been confirmed experimentally. In particular, it has been shown that solitons can interact without changing their shapes [41]. Spatial solitons have been studied in nonlinear crystals [42], glasses [43] and liquids [44]. Theoretically, it was found that many other integrable equations admit soliton solutions with the same properties as in the case of the NLSE [45]. These studies established new branch of physics: solitons.

As solitons do not change their shape during propagation along the fibre, they have been naturally considered as bits of information in optical communication systems. However, if used in long distance telecommunications, a variety of unwanted effects such as two-photon absorption, harmonic generation, Raman and Brillouin scattering may distort the pulses [46] and lead to soliton interaction between various channels [47]. Another difficulty is the interaction between solitons and the background noise. Solving these problems took several years of intensive research. The use of efficient multiplexers and demultiplexers allowed researchers to overcome some of these difficulties [48]. As a result, a practical soliton-based system has been built for Amcom `IP1` by *Marconi* company for long distance telecommunication between Adelaide and Perth [49]. This is the longest optical long-haul soliton-based optical link built so far.

The use of the word "soliton" caused a debate between mathematicians and nonlinear optics community [50, 51]. According to the mathematical definition, solitons are localized, stable modes of an integrable system described by the NLSE or another completely integrable evolution equation. In optics, stable localised pulses can propagate long distances in a fibre due to the balance between nonlinearity and dispersion. This may happen no matter whether the physical system is integrable or not. Hence, scientific terms like "solitary waves", "self-trapped beam", "localized stationary state" and "localized stable structure" have been used in physics literature along with the name "soliton".

Modulation instability and Akhmediev Breathers

Modulation Instability (MI) is a ubiquitous phenomenon that leads to the growth of weak periodic modulation on top of a plane wave in space or a continuous wave in time. As a result, the periodic modulation becomes stronger and may brake the constant amplitude wave into a periodic sequence of pulses or into a periodic self-focused beams. This happens due to four-wave interaction between the central carrier frequency and side-bands separated from it by the modulation frequency [52]. In case of water waves, this phenomenon is known as Benjamin-Feir instability [53]. In the optics of spatial beams, it is called Bespalov-Talanov instability or small-scale filament formation [54]. The MI phenomenon in fiber-optics has been predicted by Hasegawa and Brinkman [55, 56]. Modulation in the latter case develops in time.

The theory of MI has been developed using small-amplitude linear perturbation analysis [52]. However, this theory is approximate and leads to the unphysical exponential growth of the perturbation. In order to avoid this, a family of exact solutions have been found with the initial stage corresponding to the MI [57]. This family of solutions is known as Akhmediev Breathers (AB) [52, 58]. These solutions have far reaching consequences in physics. The AB theory can cast light on the initial stage of supercontinuum generation which is seeded by the noise-driven MI [59]. This theory provides an accurate description of periodic pulse train generation in optical fibres [57]. It can also explain the process of excitation of rogue waves [60, 61].

The family of AB solutions is a new class of solutions of the NLSE physically different from solitons. It describes different physical phenomena thus adding new aspects of research to nonlinear physics. Similar to multi-solitons, ABs can be combined when constructing multi-breather solutions [62]. The ABs expand significantly the range of problems in physics that can be solved analytically. The concept of AB has been applied to other integrable equations [63] demonstrating the universality of this notion. The number of publications on AB is continuously growing thus demonstrating their practical usefulness [64]. Generally speaking, both the ABs and solitons are particular cases of even more general 'first order solutions' of the NLSE. This, ones again, expands the range of phenomena that can be explained with the solutions of the NLSE [65]. The research on this general class of solutions presently gains momentum [64–67].

Optical rogue waves

Rogue waves do exist not only in the oceanic settings but also in optics. Solli *et al* [60] were the first to experimentally observe rogue waves in optics [68]. Namely, they studied the process of supercontinuum generation in the form of a chaotic sequence of pulses as the output radiation from an optical fibre. Calculation of probability density function of the amplitudes of these pulses have shown that some of these pulses have the features of rogue waves. These pulses create long (L-shaped) tails in the probability distribution function.

Akhmediev, Ankiewicz and Taki in 2009 suggested that rogue waves can be described mathematically by doubly localised rational solutions of the NLSE [16]. There is an infinite hierarchy of these solutions with the amplitude increasing linearly with the order of the solution. The first order rational solution in this hierarchy is named after Peregrine who derived it as a limiting case of a soliton on a background [69]. The higher order solutions have been found by Akhmediev *et al* [1]. In some works, they are called Akhmediev-Peregrine solutions [70]. In optics, the first-order Peregrine waves have been observed by Kibler *et al* [71]. Higher-order rogue waves have also been observed experimentally [72]. The latter can split into its fundamental components [73]. In this case, they appear in the form of self-organised patterns [74, 75]. Analytical expressions for higher-order solutions are progressively more complicated [75]. Rogue wave solutions can be found for Sasa-Satsuma equation (SSE) [76], Ablowitz-Ladik equation [77] and various sets of coupled NLSE equations [78]. Equation like SSE include terms describing a higher-order dispersion and self-steepening effects. The corresponding solutions provide better accuracy in describing wave propagation in optical fibres. When the wave evolution equation is not integrable, the rogue wave solutions can be found numerically. Approximate techniques is another way for finding analytic solutions.

There are several optical settings where L-shaped probability distribution functions can be observed. They include spatially extended optical systems with linear mechanism of rogue wave formation [13, 79, 80] and nonlinear optical cavities [81]. In each case, the elongated, non-Gaussian statistics of high amplitude formations can be observed. Optical lasers in chaotic regime of pulse generation can also produce high amplitude pulses creating the long tail statistics. These are presently known as 'dissipative rogue waves' [82]. They have been predicted theoretically [82] and observed in fibre lasers [83, 84] and in erbium-doped fiber systems [85]. Dissipative rogue waves have also been observed in passively mode-locked solid state laser [86]. Recent works on rogue waves include supercontinuum generation in a fiber [68, 87, 88], their emergence in guided wave optics [89] in photonic crystal fibers [90] and Raman fibre amplifiers [91].

1.1.3 Numerical analysis

The absence of analytic solutions in non-integrable systems in the form of rogue waves and solitons requires other methods to be developed. The most powerful among them are the numerical techniques. For example, a comprehensive study of nonlinear structures with highly complex behaviours, such as dissipative solitons, is only possible with the aid of numerical analysis. Several alternative methods have been used for finding numerical solutions of a nonlinear differential equation. Each of those methods has its own weaknesses and strengths.

One of the oldest and straightforward techniques to solve differential equations is the finite differences method (FDM). The advent of this technique in numerical applications originated in the early 1950s. Since the emergence of computers that provided a running platform for this technique, it has been used in dealing with many complex problems in science and engineering. Important issues in applications of the FDM for solving partial differential equations are the convergence, stability and accuracy [92–94]. Derivatives in the differential equation in this technique are approximated by finite differences. This leads to the discretisation or truncation error [93]. The smaller steps in calculations lead to a smaller error as long as the scheme remains stable. This scheme has been employed in the case of soliton solutions of the NLSE in earlier studies. The strength of the FDM is relatively high accuracy achieved at the expense of large computational time [94].

The split-step Fourier method (SSFM) is another efficient scheme that is widely used for solving nonlinear partial differential equations and particularly the NLSE. In this scheme, the nonlinear and linear (dispersion) parts in each step are solved separately [95]. Fast Fourier transform (FFT) plays a central role for solving the linear parts of the equation. Iterative methods such as Runge-Kutta method can be used to solve the nonlinear parts. Using a smaller step sizes in this scheme, like in all numerical methods, leads to a higher accuracy, however, requires longer processing time. Therefore, a compromise between precision and computational time has to be found. One of the advantages of using this scheme is simplicity and availability of standard FFT routines. There are various types of iterative schemes used in the SSFM with different degrees of accuracy, stability and required computational time [95, 96].

Some specific types of evolution with sharp peaks may need adaptive step size techniques. Otherwise, essential features of the solution can be lost. An illustrative case in this regard is finding the spiny solitons [97]. These are regular or chaotic dissipative solitons with narrow spikes described by the complex cubic-quintic Ginzburg-Landau equation [97]. The adaptive step-size SSFM, which sometimes is called the local error method , adjusts the mesh size by estimating the local error when reducing the step size [98]. Although the conventional (uniform step-size) SSFM scheme can be used to achieve the same results, it needs to have a step size as small as 10^{-6}.

In this thesis, particularly in chapter 7, where the numeric results are used to verify the approximate solutions, the pulse propagation is simulated by using the highly efficient SSFM technique with fourth-order Runge-Kutta algorithm for solving the nonlinear parts of the equation. The fast Fourier transform algorithm (*FFT*) of the Matlab software is used for solving the dispersion parts.

The basic idea of the SSFM is splitting the linear and nonlinear operators [34]. In the case of the normalised NLSE, for example, this may lead to:

$$\frac{\partial \psi}{\partial z} = (\hat{D} + \hat{N})\psi$$

where $\psi = \psi(z,t)$ is a slow-varying envelope of a pulse, z is the propagation variable, t is the transverse variable, while $\hat{D} = \frac{i}{2}\frac{\partial^2}{\partial t^2}$ and $\hat{N} = i|\psi|^2$ are the dispersion and nonlinear operators, respectively. The approximate solution can be obtained after sequential use of these operators in each step [99]:

$$\psi(z + \delta z, t) \approx \exp(\delta z \hat{D}) \exp(\delta z \hat{N}) \psi(z,t).$$

The exponential operators are, in turn, can be represented in the form:

$$\exp(\delta z \hat{D})\psi(z,t) = F^{-1}\{\exp(\hat{D}(i\omega)\delta z) F[\psi(z,t)]\},$$

and

$$\exp(\delta z \hat{N})\psi(z,t) \approx \exp(i\delta z|\psi(z,t)|^2)\psi(z,t),$$

where F^{-1} and F are the inverse Fourier and direct Fourier-transform operators, respectively. ω is the frequency in the Fourier domain. To achieve better accuracy, the latter exponential can be approximated by using an iterative procedure such as the fourth-order Runge-Kutta algorithm. It should be noted that, in this scheme, a sufficiently wide transverse interval should be used, typically more than 10 times of the pulse width, to guarantee that the energy of the pulse remains restricted within the boundaries. The total spectral interval also should be much larger than the width of the pulse spectrum.

The SSFM has been employed to a wide variety of physical problems. These include propagation of nonlinear waves in the earth ionosphere, short pulses in graded-index fibers [100], the study of pulse generation in passively mode-locked lasers [101], and switching processes in waveguide couplers [102]. This approach has been used extensively in the study of solitons, spiny solitons and rogue waves in optical fibers.

1.2 Recent developments

Solitons in dissipative systems are known as dissipative solitons [103–105]. They have been studied intensively in physics, biology and chemistry [106]. These solitons, in addition to the balance between dispersion and nonlinearity, require balance between gain and loss. Such complex balance can keep their shape intact for extended periods of time. Dissipative solitons can exist in lasers and fiber lasers [104]. They can be modeled by the complex cubic-quintic Ginzburg-Landau equation [107]. This equation is non-integrable and it is an extension of the nonlinear Schrödinger equation complemented with several dissipative terms. The extension may include Raman term like in the case of an optical laser generating pulses in femto-second range [103]. These pulses may reach energy values up to 25 nanojoules for low repetition rates. This upper limit is caused by the stimulated Raman scattering [103]. Dissipative solitons in two- and three dimensions may find potential applications in optical memory and laser microscopy [108]. Their shapes may vary in wide range. For example, the emergence of stable asymmetric rotating dissipative solitons in three dimensions has been studied in [109]. Short-living dissipative solitons can be turned into dissipative rogue waves [82].

Optical rogue waves can be found in telecommunications due to cross-interaction of pulses in multiplicity of channels [110]. They can be also observed in fibre lasers in the form of single, twin and triple peaks [111]. Duration of optical rogue waves can be in the range of picoseconds or smaller. Thus, they need special equipment for experimental observations such as time-lens technique.

Rogue waves can appear in a group. A group of moving dark rogue waves due to the interaction of two orthogonal pulses in a random weakly birefringent fibre has been observed in an optical fibre [112]. A theoretical background for these observations has been provided earlier in [113].

Rogue waves can be found in systems described by Manakov or Fokas-Lenells equations. Their features may differ from those modelled by the NLSE [114]. For example, the wave amplitude of these rogue waves can reach a peak up to 5 times the background level. The tails of this rogue wave decay slower than those described by the NLSE.

In the last few years, there has been much attention to higher-order (super) rogue waves in optical fibers [29, 115]. A phenomenon of super-chirped rogue wave has been found in the case of the cubic-quintic NLSE with non-negligible self-steepening coefficient [116]. Here, the optical rogue waves experience a frequency shift and have a sharp peak at the centre with symmetrically rotating tails.

An interesting phenomenon is super-regular breather which is a nonlinear superposition of quasi-Akhmediev breathers [117]. It was found experimantally in the case of the NLSE [118]. Chong Liu *et al* [119] found a family of super-regular breathers in a system modeled by the Chen-Lee-Liu equation where the self-phase modulation term is replaced by the self-steepening one. These breathers are similar to the NLSE ones except that they are asymmetric regardless of the initial conditions.

Rogue waves can be found also in specially designed electrical systems made of inductors and capacitors that are governed by the NLSE equation [115].

Turbulence is a natural wave field for existence of rogue waves. It can be created in passive resonant optical cavities pumped by a continuous wave providing conditions for rogue wave observation [120, 121]. The light circulation in this system can be modelled either by the generalised NLSE [121] or by the Lugiato-Lefever (LL) equation [120]. Theoretical background for the integrable turbulence described by the NLSE has been provided in the work [122, 123].

As mentioned earlier, rogue waves do exist in other physical systems just like they do in the oceans. Since optical experiments can be carried out in a laboratory, studies of optical rogue waves may be useful in providing insight into the properties of oceanic rogue waves. Vice versa, some ideas from oceanic observations can be translated to optics. For example, the phenomenon of the so-called three-sister rogue waves observed in the Great Lakes of northern America can be repeated in optics [113] and hydrodynamics [124].

1.3 Thesis overview

The content of this thesis is the study of rogue waves in several areas of physics such as water waves, dusty plasma and nonlinear optics. Both exact solutions and approximations are used for modelling the rogue waves. In particular, a theory based on the complex valued KdV equation that may explain shallow water rogue waves is suggested. A detailed mathematical theory of internal rogue waves based on Gardner equation is developed. Exact solutions for dust acoustic rogue waves in plasma are found. More detailed description of the thesis content is given below.

Chapter 2 provides the theory of internal waves in the ocean caused by stratification of water. These waves are invisible on the surface of the ocean. However, their amplitudes may exceed the amplitude of the surface ocean waves several times. The three-layer model of such stratification leads to the Gardner equation describing the internal waves. New rational solutions of Gardner equation are found that correspond to rogue waves. These solutions have a high and sharp peak at the centre and long tails. A scaling transformation is presented that can convert bright rogue waves to dark ones and vice versa. This Chapter is based on the work [125].

The well known Korteweg de Vries (KdV) equation that describes shallow water nonlinear waves does not have rogue wave solutions. On the contrary, observations show that rogue waves in coastal areas are common [126]. Finding rogue wave solutions for complex-valued KdV equation solves this controversy. These solutions are presented in Chapter 3. Namely, a set of complex-valued rational solutions has been found for the KdV equation. These solutions and the corresponding expressions for water surface elevation may explain the emergence of rogue waves in shallow waters. This Chapter is based on the work [127].

Although the extension to complex variables solves the problem of rogue wave existence in shallow waters, the KdV equation has to be supplemented with higher-order terms in order to improve the accuracy of wave modelling. In Chapter 4, the infinitely extended Korteweg de Vries equation is considered that retains the integrability. It is shown that this equation also has rogue waves solutions. Explicit expressions for them that include variable coefficients of the equation are presented. The suitable choice of these coefficients may improve the accuracy of description of shallow water rogue waves. This Chapter is based on the work [128]

Chapter 5 presents a study of rogue waves in dusty plasma. The set of equations for the motion of charged and neutral particles in plasma can be reduced to Gardner equation. The latter has been found to have bright and dark rogue wave solutions with continuous transformation between them. Thus, there is a one parameter family of solutions that can describe variety of rogue wave phenomena in dusty plasma. Moreover, there is a discrete hierarchy of such solutions with increasing order and the linearly growing amplitude.

Chapter 6 provides the basics of Lagrangian approach in the theory of localised solutions. The theory is based on trial functions that potentially may approximate such solutions. The technique has been previously used for modelling solitons that are localised either in time or in space. Rogue waves as solutions localised both in space and in time require more involved calculations. To start with, the Lagrangian approach is applied to rogue wave solutions of integrable equations. This allows us to justify the possibility of using it for finding such solutions in other systems. Several integrable models are chosen to prove the applicability of this method. This Chapter is based on the work [129].

Chapter 7 is devoted to the investigation of optical rogue waves in non-integrable systems. The latter are described by the extended NLS equations that do not have exact solutions in the form of rogue waves. Solutions can be approximated by trial functions with parameters that can be found using Lagrangian approach. In order to show that these solutions are reasonably close to real solutions, comparisons with numerical simulations are done. The latter are based on the split-step Fourier method. A close agreement is found between the analytical results and numerical simulations. This Chapter is based on two works [129] and [130].

The final Chapter 8 draws a conclusion from this study and provides the perspectives for future work.

CHAPTER 2

INTERNAL ROGUE WAVES

2.1 Introduction

Internal waves are waves in layered media [131]. In the ocean, they propagate in the interior of water rather than on the surface. Internal waves strongly depend on stratification of the fluid [132]. Two examples of stratified media are the lower atmosphere and oceans. Stratification of water density in the ocean is defined by the salinity, temperature or underwater flows. In presence of vertical density gradients, called *pycnoclines*, the internal waves propagate horizontally. They are slower and have larger amplitudes than surface waves.

Generally, internal waves may have both horizontal and vertical velocity components as long as the density variation is continuous. There are various types of internal waves depending on their amplitudes, the presence of external forces or the way they are generated [131]. When the earth's rotation affects the dynamics of these waves, they are called inertia internal waves [133]. If a wind generates atmospheric internal waves over a hill or mountain, they are known as lee waves or mountain waves [134]. There are also internal solitary waves [135].

Investigating internal waves is important from various points of view. In oceanography, internal waves are responsible for mixing the nutrients in the oceans and the transportation of sediments near the shore [136]. In biology, these waves are important since they carry large amount of potential food for many species. Researches have documented the impact of these waves on living organisms on the bottom of the seas (benthic zone) and plankton [137]. These studies show how nutrients reach an uninhabitable environment and feed a wide variety of living organisms on the bottom of the ocean [131]. Internal waves can efficiently transport phytoplankton and zooplankton to shore lands [136]. They also can facilitate the process of reproduction of zooplankton by increasing its concentration. Thus, internal waves are vital for many living creatures in oceans [131, 136].

The knowledge of properties of internal waves is important in engineering. They can move oil production platforms [138]. In some cases, slow-moving ships are impeded because their engine energy is being transferred into an interfacial internal wave, although the water surface visibly stays calm. This phenomenon, first noted in 1893, is known as the 'dead water effect' [139]. Namely, the ship's propeller generates internal waves on the boundary between the two layers of fluid. The energy produced by the propellers is transferred to the internal waves instead of moving the vessel. Then boats cannot move faster than about three knots which is the average velocity of internal waves. Fridtjof Nansen, a Norwegian sailor (1861-1930), discovered the mechanism of this event. When he encountered stratified water, he realized that the surface of the sea was nearly drinkable and fresh, whilst beneath the ship keel, it was wholly salty [140]. This happens when a layer of freshwater from a thawed iceberg or from a river rests over denser and saltier sea water.

Large-amplitude internal waves are ubiquitous features in the marginal oceans and coastal seas [135]. Internal solitary waves have been observed in the 1960s when advanced instruments for recording vertical arrays internally became available. Perry *et al* [141] observed a family of internal waves with amplitudes up to 80 meters and wavelengths of more than a kilometer.

In the 1980s, Osborne *et al* [142] proved these large-amplitude waves can be generated by the tidal flow. They observed the generation of the internal waves propagating hundreds of kilometers off the Sumatra coastline by the tidal flows in channels in Andaman and Nicobar island. Generally, the internal waves can be caused by tidal forces, when mixing of river freshwater with seawater [143] and by the propellers or bow waves of ships.

Zeigenbein [144] was the first who showed that internal waves are not linear and in fact, they are non-linear. The reason is that their height is too large compared to the depth of the stratification. Due to the nonlinearity, they can remain coherent and last for a long time and long-distance. Therefore, they are called internal solitary waves (ISW) [135]. These waves can also be found in lakes, estuaries, and rivers. However, they are relatively smaller than those found in the oceans [145].

These large-amplitude bell-shaped internal waves displace waters vertically, upward (elevation) or downward (depression). Internal solitary waves often occur in packets and sometimes at particular phases of the internal tide [146]. A bunch of these waves can be observed in 95% of all coastlines, shown by satellite images [147] with a wavelength of 0.1 to 1 kilometer, the velocity of roughly 1 m/s, periods around 5-8 minutes and 10 to 100 meters height.

The importance of the ISWs in the layered structures of the atmosphere and the ocean should not be underestimated. These are the areas of human activity such as the movement of submarines and airplanes. ISWs can affect the acoustic signals emitted underwater and distort the transmission signals from submarines [148]. Strong currents might interfere with the movement of the underwater vessels and impose hazards for man-made structures in the

Figure 2.1: *The formation of the morning glory clouds, (left) Tasman sea (credit:Randall Lee, `scripps.ucsd.edu/projects`) and (right) Burketown, Australia (`en.wikipedia.org`).*

ocean. Large-amplitude ISWs can be especially dangerous in this regard. For example, they may unexpectedly shift submarines down to depths below the pressure capacity of the hull. They may have caused the Thresher submarine disaster in 1963 [138]. Possibly, the sinking was caused by a large ISW with high amplitude [149]. Thus, gaining understanding of internal waves and their properties is crucial for the safe flying of airplanes in the atmosphere and the safe operation of submarines and other underwater devices in the ocean. In the atmosphere, in particular, internal waves can be responsible for the formation of the clouds in uniform shapes with crests and troughs, referred to a “Morning Glory cloud”. Figure 2.1 shows two examples of this type of formation in the atmosphere [150].

Large-amplitude internal solitary waves can be observed in many parts of the world ocean. These include south China sea [151], Sulu Sea [152], Celebes Sea, Indonesia coasts, Australia east coast, northwest of Australia, Andaman sea, eastern and western parts of the Indian Ocean, southwest of Africa, the west-central African coast, west of Atlantic, northwest of South America, eastern pacific ocean, gulf of California [153]. Internal solitons have been often observed on the northwest of the Australian coast, while on the west-central African coast they have been seen only recently [153, 154]. Large-amplitude internal waves have been also detected in the Persian Gulf and near Oman sea [155]. Internal solitons can be mostly observed in the shore vicinity [154].

Satellite images (www.internalwaveatlas.com) show that ISWs are mostly concentrated around the coastal areas rather than in the deep ocean. For example, the East Shelf and North West Shelf (NWS) of Australia frequently experience huge internal waves [156].

ISWs may not reveal themselves on the ocean surface, but their vertical amplitudes under water can be several times higher than the amplitudes of the largest freak waves on the water surface. They can reach a height of 170 meters [151]. This amplitude exceeds 6 times the height of the ‘benchmark’ surface rogue wave known as the ‘Draupner wave’. The latter was ‘only’ 25.6 meters high [157].

The term 'rogue internal waves' has been coined by Grimshaw *et al* in [24]. Several approaches have been developed in order to model rogue internal waves. These include the long wave model described by the standard Korteweg-de Vries equation (KdV) [24], a model based on a variable-coefficient KdV equation [158], the one based on coupled nonlinear Schrödinger equations (cNLSE) [159], and and the model based on the Gardner equation (GE) [24]. Numerical simulations made in [24] provided a solid indication that this equation may have solutions describing the rogue waves. For the case of positive signs of all terms in this equation, its continuous wave solution is subject to modulation instability. This feature is common with the Nonlinear Schrödinger equation (NLSE).

In many works, the Gardner equation has been used to model internal solitary waves. Internal waves in the shallow fluid has been studied in [160]. Talipova *et al* [161] studied this type of waves in two-layer fluid. The ISWs of the Gardner equation with variable coefficients describing variable depth are studied in [162]. The corresponding adiabatic deformations of the soliton are found in [163]. For a step-like changes the solitons experience reflection and transmission [164]. Interaction of internal waves with solid ice on the water surface has been experimentally studied in [165].

A few approaches to study internal rogue waves have been done in more recent works. The possible formation of internal rogue wave due to the interaction between two or more solitions has been suggested by Shurgalina [166]. Generation of rogue waves in a turbulent wave field is discussed in [167].

Our approach is based on the analogy with rogue waves of the NLSE equation given by its rational solutions [16]. According to this analogy, rogue wave solutions of the GE are also expected to be given by rational expressions. The results presented in this Chapter confirm this conjecture. For deriving these solutions, we used the "billinear Hirota Method" (see Appendix). The first four rational solutions to the GE, showing localized wave amplification are presented below. These solutions have wider range of applications than internal waves. As the GE is known to be applicable to three-component plasmas [168] and surface waves [169], these solutions can also be useful in these areas of physics.

Chapter outline

In the following sections, we will present the Gardner equation, review some of its interesting properties and introduce a scaling transformation which generates a family of solutions adding a free parameter to a particular one. Two soliton solutions will be given that differ by the sign of the cubic coefficient in the equation. The main result presented in this Chapter is the hierarchy of rational solutions up to the fourth order that describe rogue waves of the Gardner equation.

2.2 Gardner equation and its special features

The GE describing the nonlinear internal waves in a stratified medium can be written as:

$$\phi_{x'} + \alpha_1 \phi \phi_{t'} + \alpha_2 \phi^2 \phi_{t'} + \gamma \phi_{t't't'} = 0. \tag{2.1}$$

Here, $\phi(x', t')$ is the normalised wave amplitude and the subscripts denote derivatives with respect to variables x' and t', respectively. Here x' is the propagation axis, whilst t' is a transverse axis. This equation can be derived based on the Euler equations for the stratified fluid [170]. The second and third terms are responsible for quadratic and cubic nonlinear effects, respectively. The last term describes the effect of the third-order dispersion. This equation is more general than the KdV or modified KdV (mKdV) equations. When $\alpha_1 = 0$, the Gardner equation (2.2) reduces to the mKdV equation, whilst if we set $\alpha_2 = 0$, it reduces to the well-known KdV equation. Therefore, Eq.(2.2) is also known as the mixed KdV-mKdV equation [171] or the extended KdV (eKdV) equation [172]. Throughout the thesis, I use the most common name for Eq.(2.2), *viz.* the Gardner equation.

The coefficients in Eq.(2.2) are defined by the density stratification and thickness of the layers. The coefficients α_1 can be either positive or negative and γ is always positive, while the sign of the coefficient α_2 depends on the stratification model [159, 173]. In the case of a two-layer fluid, it is always negative [148]. However, in a three-layer model and in the case of more complicated stratification with shear flows, this coefficient can be positive [159, 173, 174]. Without loss of generality, the dependent and independent variables can be renormalised, thus setting each of the three coefficients to unity. Then, Eq.(2.2) takes the form:

$$\psi_x + \psi \psi_t (1 + \psi) + \psi_{ttt} = 0, \tag{2.2}$$

when the cubic nonlinearity (α_2) is positive. Here:

$$\psi = \frac{\alpha_2}{\alpha_1}\phi, \quad t = \frac{\alpha_1}{\sqrt{\gamma \alpha_2}} t', \quad x = \frac{\alpha_1^3}{\sqrt{\alpha_2^3 \gamma}} x'.$$

An inverse rescaling transformation returns us to the original equation, Eq.(2.2), and its solutions, with all three coefficients included. Hereafter, the equation with positive cubic nonlinearity is called the Gardner equation (GE), while the equation with negative coefficient is called the negative Gardner equation ($GE-$). The main purpose of this chapter is to study and analyze the GE case and only in the next section, the $GE-$ will be briefly considered. The reason is that the solutions of the GE reveal richer dynamics than the solution of the $GE-$ [24]. The GE is used more frequently in other areas such as in studies of the atmosphere and in plasma research.

It is easy to show that if $\psi(x, t)$ is a solution of the Gardner equation (2.2), then the function

$$\hat{\psi}(x, t) = -\psi(x, t) - 1 \tag{2.3}$$

is also a solution of the same equation. The importance of the transformation (2.3) should not be underestimated, as it relates bright and dark solutions of the GE. Clearly, this transformation changes the background as well. The transformation 2.3 is a particular case of a more general one. It can be shown by direct substitution that if ψ is a solution of the GE, then Ψ is a solution to the GE:

$$\Psi(x,t) = \frac{k-1}{2} + k\psi(k^3x, kt + \frac{k(1-k^2)}{2}x), \tag{2.4}$$

here, k is an arbitrary real constant. The scaling transformation (2.4) expands a particular solution $\psi(x,t)$ into a one-parameter family of solutions $\Psi(x,t|k)$. Simultaneously, it changes the background by $(k-1)/2$ units. When $k=1$, the family of solutions is reduced to the original solution $\Psi = \psi$. On the other hand, if $k=-1$, then $\Psi = -1-\psi(-x,-t)$. Since the solutions of the GE can support an inversion-reflection symmetry (as shown in Appendix), we obtain $\hat{\psi} \equiv \Psi = -1-\psi(x,t)$ for the case $k=-1$. Thus, firstly, the background of the solution is adjustable. It depends on the parameter k. Secondly, the sign of the solution can be inverted. Namely, if $\psi(x,t)$ is a bright soliton, the transformed solution $\Psi = -\psi(x,t)-1$ is a dark soliton. Moreover, the amplitude of the soliton varies with k. In particular, it becomes zero when $k=0$. The velocities of the solitons also vary with k, as Eq.(2.4) clearly shows. The velocity correction in Eq.(2.4) becomes zero when $k=\pm 1$. As k is arbitrary, formally, the amplitude of the solution can be varied over an infinitely large interval from $-\infty$ to $+\infty$. Then, the background of the solutions, according to Eq.(2.4), can also be varied over an infinitely large interval.

As noted, the scaling (2.4) can be applied to any solution. These include solitons, breathers and rogue waves. Thus, the solutions governed by the Gardner equation, resemble linear waves in the sense that their amplitude can vary continuously. Clearly, the amplitude, velocity and the wave profile depend on initial conditions. Varying these values, the theoretical results can be adjusted to experimental data.

2.3 Soliton solutions

2.3.1 Gardner equation with negative cubic nonlinearity

In the deep areas of the ocean (with large *pycnocline*), a two-layer model leads to the Gardner equation with negative cubic nonlinearity ($GE-$):

$$\psi_x + \alpha_1\psi\psi_t - \alpha_2\psi^2\psi_t + \gamma\psi_{ttt} = 0,$$

Here, we let the quadratic nonlinearity coefficients α_1 be either positive or negative, while α_2 is only positive. The soliton solution of this equation has in the form:

$$\psi(x,t) = \frac{6\gamma}{\alpha_1 - \sqrt{\alpha_1^2 - 6\alpha_2\gamma}\cosh(t-\gamma x)}, \tag{2.5}$$

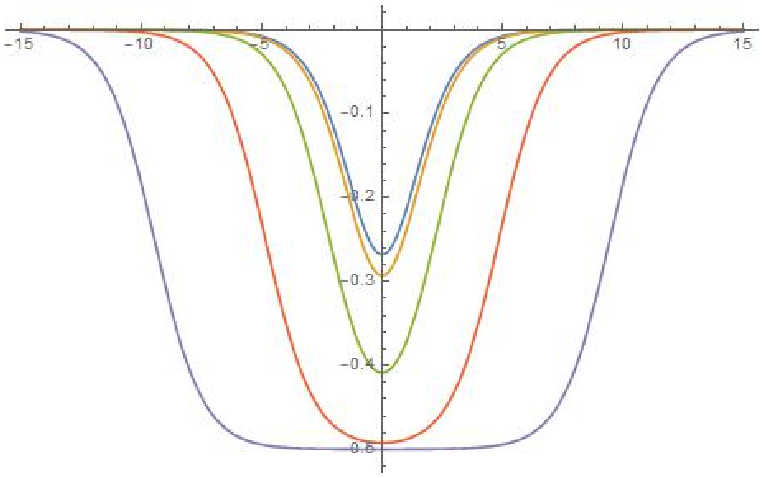

Figure 2.2: *Soliton solutions for the GE− Eq.(2.5) at* $x = 0$*. Here,* $\gamma = 1/6$ *and* $\alpha_1 = -2$ *in all cases, while* $\alpha_2 = 1$ *(blue),* 2 *(orange),* 3.8 *(green),* 3.999 *(red) and* 3.9999999*. The latter case corresponds to 'flat-top' soliton that nearly split into two kinks.*

We exclude the case $\alpha_1 < 6\alpha_2\gamma$, when this solution becomes a complex function. The physically meaningful real-valued profiles are shown in figure 2.2. The velocity of the soliton depends only on the dispersion γ. The amplitude of the soliton is $\frac{6\gamma}{\alpha_1 - \sqrt{\alpha_1^2 - 6\alpha_2\gamma}}$. There is an upper limit of the amplitude $\frac{6\gamma}{\alpha_1}$ which takes place at $\alpha_1 \approx 6\alpha_2\gamma$. This is the special case of a 'flat-top' soliton. The soliton consists of two fronts, or "kinks". The central part of this soliton can serve as a pedestal for other solitons or rogue waves.

Due to the geographical conditions of the bottom of the ocean or moderate changes in the stratification, the governing equation may have variable coefficients [170]. Then the shape of the solitary waves may change at the critical (turning) points. These points are reached when one or two parameters in the equation become zero. This is either the soliton of the KdV equation defined by $sech^2$ profile or the soliton of the mKdV equation, viz. $sech$.

2.3.2 Gardner equation with positive cubic nonlinearity

In the coastal areas of the ocean (small depth), the model involves three or more layers of stratification leading to Eq.(2.2). This equation has a wide range of solutions. One of the most widely-used solutions of this equation is the soliton solution [149, 168, 175]. The family of soliton solutions with a free real parameter α can be written in the form:

$$\psi(x,t) = \frac{1-\alpha^2}{\alpha\left\{\cosh\left[\frac{\sqrt{1-\alpha^2}\,(\alpha^2(6t+x)-x)}{6\sqrt{6}\,\alpha^3}\right]+\alpha\right\}}. \tag{2.6}$$

Here, the amplitude and velocity of the soliton are controlled by the arbitrary real parameter α. The range of this parameter is restricted by the conditions $|\alpha| \le 1$ and $\alpha \neq 0$. The amplitude of

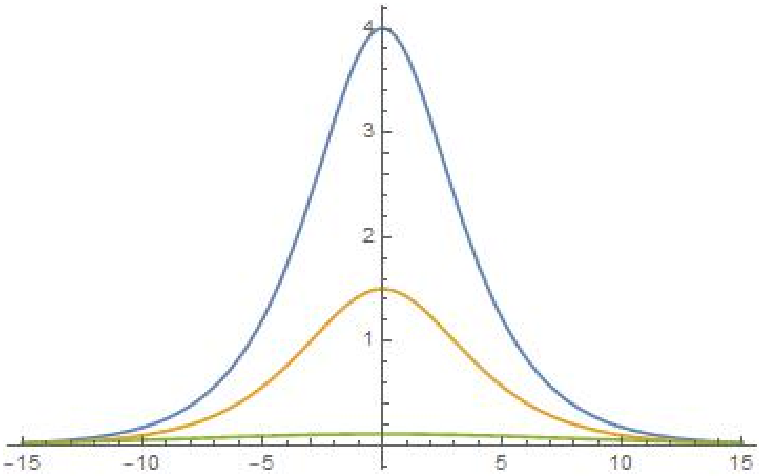

Figure 2.3: *Soliton solutions for the GE Eq.(2.2) at $x = 0$. Here, $\alpha = 0.2$ (blue), 0.4 (orange) and 0.9 (green) which has very low amplitude.*

the soliton is negative when $\alpha < 0$ and positive when $\alpha > 0$. The background is zero for any value of α. The velocity of the soliton, $v = (1-\alpha^2)/(6\alpha^2)$, is always positive. It does not depend on the sign of α. Lastly, the amplitude is $\frac{1-\alpha}{\alpha}$. Thus, Eq.(2.6) defines a one-parameter family of soliton solutions in the interval $-1 < \alpha < +1$. This family can be significantly extended using the scaling transformation (2.4), thus, adding one more parameter to the family.

The soliton profiles describing by Eq.(2.6) for several values of α are plotted in figure 2.3.

2.4 First-order rational solutions

The lowest order exact rational solution to the GE can be obtained by using the Lorentz transformation [169] applied to the first mKdV rational solution found in [2]. (See Eq.(3) of [2] for $\beta = 1$ and $\gamma_3 = -1$). Namely, let $u(x,t)$ be an exact solution to the mKdV equation,

$$u_x + u^2 u_t + u_{ttt} = 0. \tag{2.7}$$

Then, the function $\psi(x,t)$ defined as

$$\psi(x,t) = u\left(x, t + \frac{1}{4}x\right) - \frac{1}{2} \tag{2.8}$$

is an exact solution of the GE, Eq.(2.2).

Namely, using the exact lowest order rational solution of mKdV [2],

$$u_1(x,t) = \frac{12}{3 + 2(t-x)^2} - 1 \tag{2.9}$$

and the transformation (2.8), we obtain the exact lowest (first) order rational solution to the GE,

$$\psi_1(x,t) = \frac{12}{t^2 + 6} - 1. \tag{2.10}$$

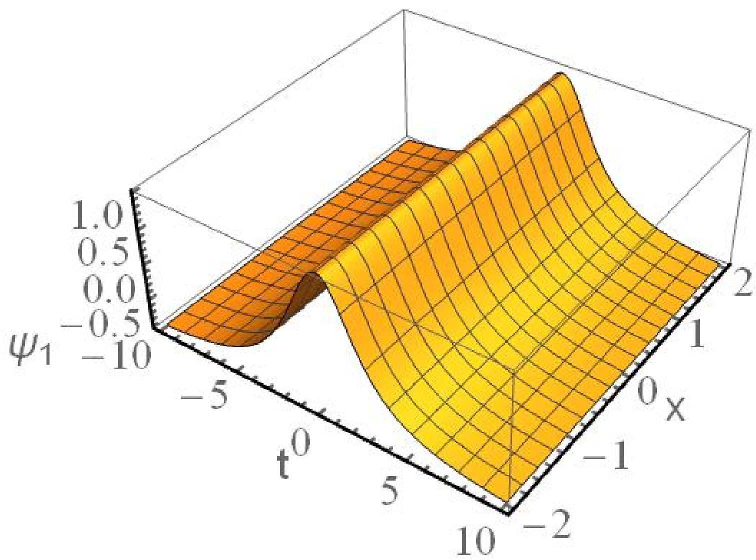

Figure 2.4: *The first order bright rational solution of the Gardner equation given by Eq.(2.10). Here, the background is* -1*. The maximum, at* $t = 0$*, is* 1*, thus giving an amplitude of* 2*.*

The form of this solution is shown in Fig. 2.4. The solution is stationary in x. The maximum amplitude relative to the background at $t = 0$ is 2, while the background level at $t \to \pm\infty$ is -1. It may look like a zero velocity soliton with positive amplitude but we have to keep in mind that this is rational solution rather than $sech$-function. The solution (2.10) has been derived earlier by Grimshaw *et al* in [158] as a limiting case of a $sech$-shaped soliton solution. This solution along with the higher order solutions will be directly obtained using the bilinear Hirota method in Appendix.

Now, using the transformation (2.3), we can easily find the inverted first-order solution:

$$\hat{\psi}_1(x,t) = -\psi_1(x,t) - 1 = -\frac{12}{t^2+6}, \tag{2.11}$$

This solution is plotted in Fig.2.5. This solution is also stationary in x. In contrast to the solution in Fig.2.4, this one resembles a dark soliton. For this solution, the background level is 0 and the minimum is -2.

Thus, we have two rational first-order solutions of the GE. One is given by Eq.(2.10) and the other by Eq.(2.11). This is not surprising because the transformation of Eq.(2.3) can be used with any solution of the GE, including rogue wave solutions of higher order. This transformation also means that there are two types of rogue waves: 'bright' ones, denoted $\psi_j(x,t)$ and 'dark' ones, denoted $\hat{\psi}_j(x,t)$. Although their background levels differ, their amplitudes relative to the background level are the same.

To connect this with soliton ideas, lets consider the soliton solution for the GE, i.e. Eq.(2.6).

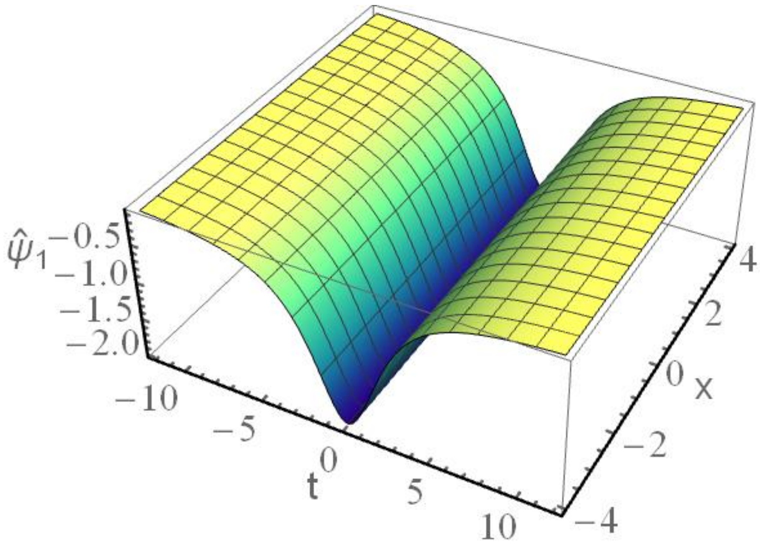

Figure 2.5: *The first order dark rational solution of the Gardner equation from Eq.(2.11). Here, the background level is* 0*. Minimum at $t = 0$ is* −2*. In order to see clearly the difference between the dark rogue wave solutions and the bright ones, a distinct colour scheme (yellow-green) is used here and in all figures below.*

In the limit $\alpha \to -1$, the solution (2.6) reduces to:

$$lim_{(\alpha\to-1)}\psi(x,t) = -\frac{12}{t^2+6},$$

i.e. the first order rational solution, Eq.(2.11).

2.5 Second order rational solutions as rogue waves

The general relation, Eq.(2.8), between the solutions of Gardner and mKdV equations allows us to construct higher-order rogue wave solutions. The second order rational solution of the mKdV equation has been obtained in [2] (see Eq.(5) therein). Taking the coefficients of the mKdV equation in [2] to be $\beta = 1$ and $\gamma_3 = -1$ and using one of the above-mentioned transformations, we find that the second order rational solution to the equation (2.2) is:

(2.12) $$\psi_2(x,t) = -36\,\frac{G_2}{D_2}$$

where

(2.13) $$G_2 = t^4 + 36t^2 - 24tx - 108$$

and

$$\begin{aligned} D_2 &= 18\left(t^4 - 24tx\right) + \left(t^3 + 12x\right)^2 + 972t^2 + 1944 \\ &= t^6 + 18t^4 + 24\left(t^2 - 18\right)tx + 972t^2 + 144x^2 + 1944, \end{aligned}$$

or, alternatively

$$\psi_2(x,t) = \frac{36\left(108 - t^4 - 36t^2 + 2tX\right)}{\left(t^3 - 18t + X\right)^2 + 54\left(t^2+6\right)^2}, \tag{2.14}$$

where $X = 12x$. This solution is shown in Fig.2.6. It has a high peak that we can view as a rogue wave. Indeed, the peak is localized, both in time and in space, thus representing an unexpected extreme event. This event is clearly seen in Fig.2.6. The background level of the solution, Eq.(2.14), is zero while the maximum amplitude of the rogue event is 2. The denominator of the solution in the form of Eq.(2.14) is a sum of squares. It is thus never zero, meaning that the solution is non-singular. Such a form has been given earlier in [176].

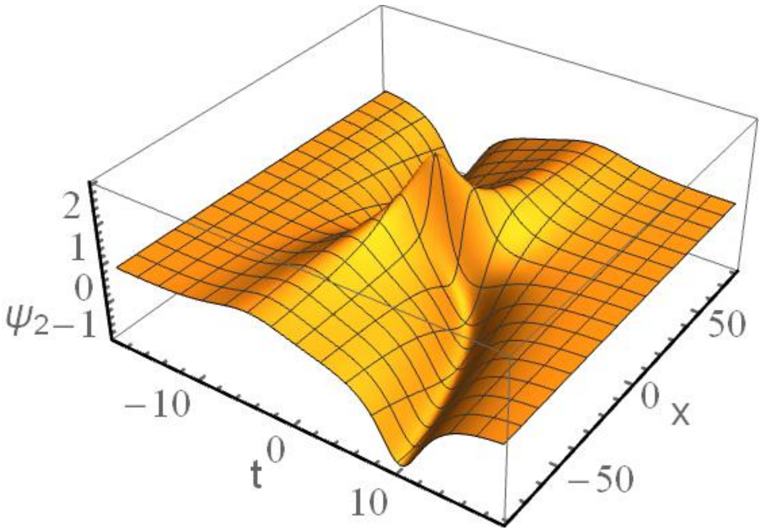

Figure 2.6: *The second order rational solution of the GE given by Eq.(4.3). The 'bright' rogue wave in the middle is clearly visible. Here, the background is* 0*. Maximum at the origin is* 2*.*

Using Eq.(2.3), we find the inverted second order solution:

$$\hat{\psi}_2(x,t) = 36\,\frac{G_2}{D_2} - 1. \tag{2.15}$$

In contrast to the solution given by Eq.(2.14), the background level here is -1 and the extremal amplitude of this rogue wave is -3. The profile of this solution is shown in Fig.2.7. We call this solution a 'dark rogue wave'.

2.6 Third order rational solutions

Starting with the third order solution of the mKdV given by Eq.(6) in [2] and using the Lorentz transformation, we are able to find the third rational solution of the GE:

$$\psi_3(x,t) = 72\,\frac{G_3}{D_3} - 1, \tag{2.16}$$

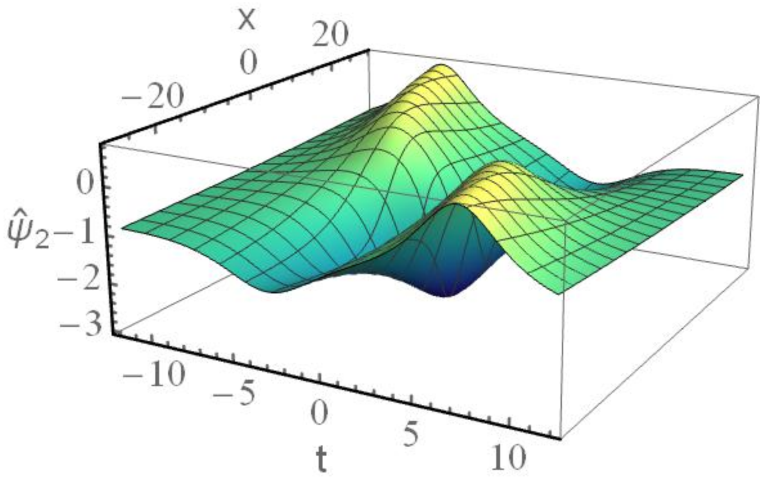

Figure 2.7: *The 'dark' second order rogue wave solution given by Eq.(2.15). Here, the background is* −1*. The central minimum is* −3*.*

where the numerator G_3 is

$$\begin{aligned} G_3 &= t^{10}+90t^8+7560t^6-4320t^5x+5400t^4\left(x^2-18\right)+259200t^3x \\ &\quad -32400t^2\left(2x^2+27\right)+43200tx\left(x^2+54\right)+194400\left(5x^2+27\right), \end{aligned}$$

while the denominator D_3 is

$$\begin{aligned} D_3 &= t^{12}+36t^{10}+120t^9x+4860t^8+2160t^6\left(x^2+234\right)-233280t^5x \\ &\quad +97200t^4\left(2x^2+45\right)-86400t^3x\left(x^2-108\right)-3499200t^2\left(x^2-27\right)+777600tx\left(2x^2-135\right) \\ &\quad +129600\left(4x^4+594x^2+729\right). \end{aligned}$$

This solution is plotted in Fig.2.8. It has the background level −1 and central amplitude 3 located at the origin due to the suitable choice of the co-ordinates.

Applying the transformation (2.3) to Eq.(2.16), we find the inverted third order solution:

$$\hat{\psi}_3(x,t) = -1-\psi_3(x,t) = -72\,\frac{G_3}{D_3}, \tag{2.17}$$

with the same values of G_3 and D_3 as above. This solution is plotted in Fig.2.9. The background level is now 0 and the minimum amplitude is −4. The two local maxima appear to have amplitudes around $\psi_{max} \approx 1.23$.

2.7 Fourth and higher order rational solutions

Applying the same technique as above to known higher order rogue wave solutions of mKdV equation, we can find higher order rogue wave solutions of the Gardner equation. Explicit

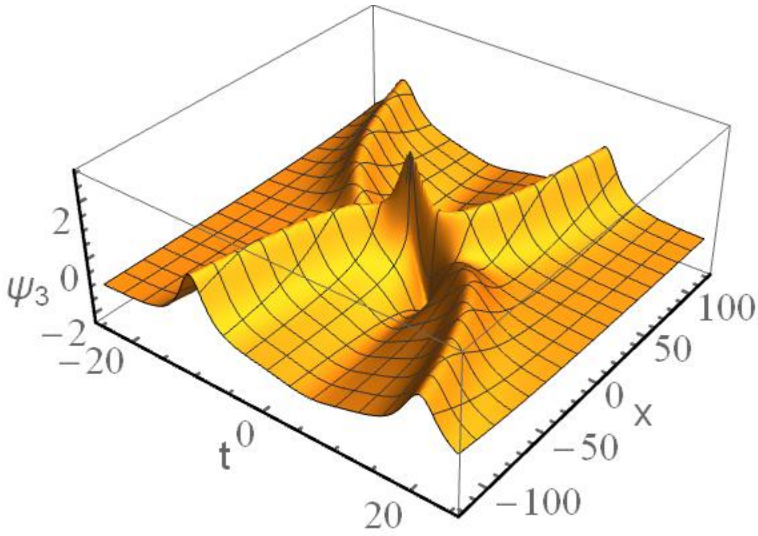

Figure 2.8: *Third order rogue wave solution of Gardner equation given by Eq.(2.16). Here, the background level is* -1 *while the maximal amplitude at the origin is* 3*.*

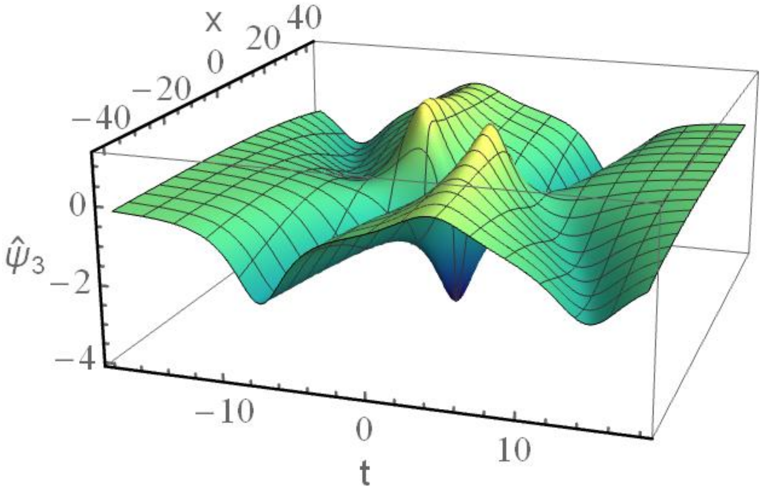

Figure 2.9: *'Dark' third order rational solution to the GE given by Eq.(2.17). This solution is inverted relative to Fig.2.8 and shifted down. Here, the background is* 0*. The central minimum is* -4*.*

mathematical expressions of these solutions are quite involved and the degree of complexity increases with the order of the solution. For example, for the case of the fourth order solution, we obtain:

$$\psi_4(x,t) = -120\,\frac{G_4}{D_4}, \tag{2.18}$$

where,

$$
\begin{aligned}
G_4 &= t^{18}+162t^{16}+144t^{15}x+32400t^{14}+22680t^{12}\left(x^2+180\right) \\
&- 544320t^{11}x+2449440t^{10}\left(x^2-57\right)-2116800t^9x\left(x^2-324\right) \\
&- 12247200t^8\left(35x^2+306\right)+97977600t^7x\left(2x^2+27\right) \\
&- 76204800t^6\left(2x^4-81x^2+729\right)-1371686400t^5x\left(7x^2-108\right) \\
&- 138883248000t^4\left(5x^2-36\right)-123451776000t^3x\left(2x^2+81\right) \\
&+ 10287648000t^2(8x^4+378x^2+3645)-1111065984000tx\left(5x^2+108\right) \\
&+ 2286144000\left(4x^6+1296x^4+2187x^2-19683\right)
\end{aligned}
$$

and

$$
\begin{aligned}
D_4 &= t^{20}+60t^{18}+360t^{17}x+14580t^{16}+8640t^{15}x+32400t^{14}\left(x^2+108\right) \\
&+ 1360800t^{12}\left(x^2+405\right)+604800t^{11}x\left(x^2-162\right)+220449600t^{10}\left(x^2+58\right) \\
&- 127008000t^9x\left(x^2-405\right)+27216000t^8\left(4x^4-1215x^2+29889\right) \\
&+ 17635968000t^7x\left(x^2-27\right)-1143072000t^6(8x^4-1215x^2-32076) \\
&- 740710656000t^5x\left(x^2+54\right)+4166497440000t^4\left(14x^2+45\right) \\
&- 11110659840000t^3x\left(5x^2-54\right)+22861440000t^2(4x^6+648x^4-24057x^2+98415) \\
&+ 33331979520000tx\left(14x^2-135\right)+68584320000\left(8x^6+3240x^4+83106x^2+19683\right),
\end{aligned}
$$

for the bright rogue wave. In order to show that there are certain rules that these solutions obey, we only illustrate them using the fourth order solution. It is shown in Fig.2.10. This solution also has a peak at the origin and its amplitude is 4. The background level is 0. Finally, the inverted version of the fourth order solution defined as

$$\hat{\psi}_4(x,t) = -1-\psi_4(x,t). \tag{2.19}$$

This is presented in Fig.2.11. It has the background level -1 and the minimum at the origin is -5.

2.8 Succinct Summary

In Table 2.1, we compare the rogue wave characteristics for hierarchies of rational solutions with increasing order, for the NLSE, taken from [1], the mKdV equation, taken from [2] and the bright rogue waves of the Gardner equation given in the present chapter. Further, in Table 2.2, we summarize the characteristics of dark rogue waves of the Gardner equation, also given in the present chapter. In the 'dark rogue wave case', the highest magnitude amplitudes are naturally negative, as they represent waves of depression, while 'bright rogue waves' show elevations.

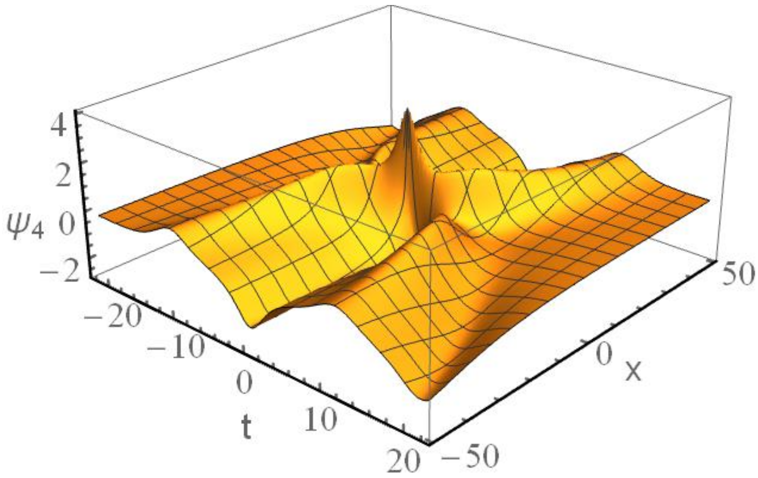

Figure 2.10: *Fourth order 'bright' rogue wave of the Gardner equation, given by Eq.(2.18). Here, the background level is* 0*. Maximal amplitude is* 4*.*

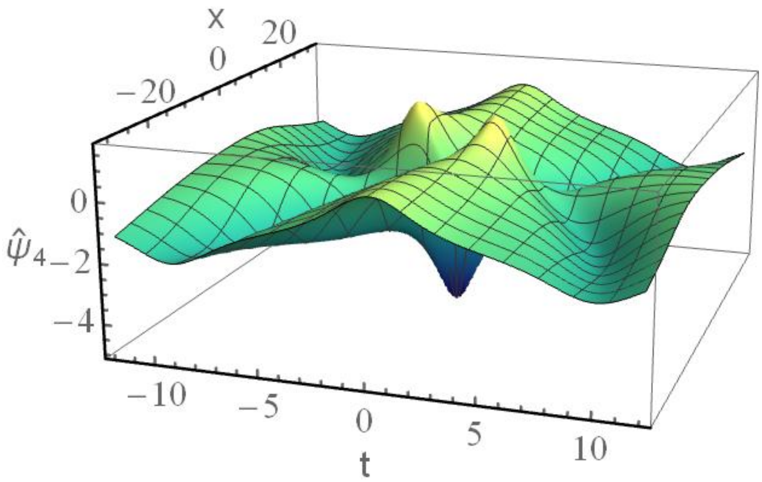

Figure 2.11: *'Dark' fourth order rational solution of the GE, given by Eq.(2.19) and Eq.(2.18). This solution is inverted relative to Fig.2.10 and shifted down. Here, the background is* −1*. The central minimum is* −5*.*

Clearly, the next question to answer is the robustness of these solutions. We leave this problem aside here, as it requires a complicated approach. We should also note that all solutions, including unstable ones, play significant roles in the complex chaotic dynamics that may occur in layered systems. Thus, knowledge of the form of the whole set of exact solutions of the Gardner equation, whether stable or not, is crucial for further progress in this field.

j	The background level of the NLS and mKdV rogue waves	Maximal amplitude of the NLS and mKdV rogue waves	The background level of the GE rogue waves	Maximal amplitude of the GE rogue waves
1	-1	3	-1	1
2	1	5	0	2
3	-1	7	-1	3
4	1	9	0	4
j	$(-1)^j$	$2j+1$	$\frac{1}{2}[(-1)^j-1]$	j

Table 2.1: *Main features (amplitude and the background level) of rogue waves of the NLSE [1], the mKdV [2] and the 'bright rogue waves' (ψ_j) of the Gardner equation. The j^{th} order rogue wave of the Gardner equation has amplitude j, so, in the dimensionless form, the amplitude is much lower than the corresponding rogue waves of the mKdV equation and the NLSE.*

j	Background level of 'dark rogue waves' of GE	Minimal amplitude of 'dark rogue waves' of GE
1	0	-2
2	-1	-3
3	0	-4
4	-1	-5
j	$\frac{1}{2}[-1-(-1)^j]$	$-(j+1)$

Table 2.2: *Main characteristics (background level and amplitude) of 'dark rogue waves' ($\hat{\psi}_j$) of the Gardner equation*

2.9 Conclusion

We have considered the characteristics of the internal waves and reviewed the works that show their utmost importance for living structures at the bottom and very deep places in the oceans. Then we investigated the special features of the GE, which is used as a reasonably-accurate model for the propagation of waves in the layered structures, and found a set of rational solutions describing rogue waves.

Having the first four rogue wave solutions in an explicit form, we are now in a position to predict the major characteristics of rogue waves of an arbitrary order, j. Moreover, we are able to compare them with the features of rogue waves of the NLS and mKdV equations found in previous works, [1] and [2], respectively. In all three cases, the rogue wave solutions are given in the form of rational solutions, and thus have much in common, even in this sense. Dimensionless forms of these equations allow us to make purely mathematical comparisons. The real world amplitudes are clearly another matter. The latter depend on particular parameters of the geometric structure of the layered media, and these may vary over a wide range.

One of the important predictions is related to the amplitude of rogue waves. Namely, the j^{th} member of the 'bright' set of rogue waves, denoted $\psi_j(x,t)$, has a positive central maximum of j, while the j^{th} member of the 'dark' set, denoted $\hat{\psi}_j(x,t)$, features a central minimum of amplitude $-j-1$.

The major difference between GE and mKdV rogue waves and those of the NLSE case is the presence of long tails, as can be seen from the plots above. They extend to infinity, thus modifying the background on which the rogue waves protrude with the higher amplitude. The presence of the tails may serve as a tool for predicting internal rogue waves much earlier than in the case of NLSE rogue waves, which lack such tails [16].

The presence of the central peak is the common feature in all three cases (mKdV, GE and NLSE), so a comparison of their amplitudes relative to the background levels (amplification factor) may provide further ideas for research on rogue waves. Rogue wave solutions are general features of many evolution equations, and are not just 'isolated' examples. They have been found for the NLSE [16], vector NLSE [177, 178], Sasa-Satsuma equation [76], three-wave resonant interaction problem [179], Davey-Sewartson equations [180] and for many other systems. These solutions are an essential part of the general waveform evolution in nonlinear systems, as the recent works [181, 182] have shown. This addition of a new hierarchy of rogue waves for the Gardner equation will further expand our knowledge in this exciting field of research.

Chapter 3

Shallow Water Rogue Waves

There is overwhelming evidence of the existence of rogue (or freak) waves in the oceans. Until the last two decades, they were mostly found in folk anecdotes or as a part of marine fictions which sometimes, due to highly unpredictable and unexplainable nature, were called "rabid-dog waves" by Asian fishermen [17]. However, thanks to the advances in engineering measurements, their existence has become indisputable and scientifically proven. The waves are identified as rogue waves when they have amplitudes at least twice the significant wave height [183]. The background significant wave height can be either measured by image processing of the satellite data or range finders assembled on active buoys and platforms. Rogue waves occur not only in the deepwater zones but also in shallow water or at the coast, where they were revealed as either abrupt inundations near the shore or huge splashes over sharp banks or sea barriers.

Indeed, they are confirmed to exist in shallow water and coastal areas [184, 185]. In Taiwan, for instance, in 50 years (1949 - 1999), more than 150 rogue events have been reported in the coastal zones [17]. In this report, the coastal rogue waves are one of the frequent and serious hazards among all Taiwan coastal disasters. This report describes the rogue wave as a sudden and large wave emerging from relatively calm (not treacherous) sea conditions with no advance notice or warning. The coastal and shallow water rogue waves act as traps which cause fatalities and serious injuries by abruptly engulfing people into the offshore. Furthermore, there were reports that vessels and ketches had been capsized and destroyed on the seashore regions as well [22, 184]. These reports have shown more than 496 fatalities and more than 35 capsized crafts in that period of 50 years in Taiwan owing to coastal freak waves [17]. This fact makes rogue waves the number one danger and the most perilous threat that jeopardizes and endangers the population. They kill more people than other coastal incidents such as shark attacks. We exclude from this list the tsunami wave in East Asia in 2004. The latter event caused a massive death toll of more than 220,000 people. This single event is clearly caused the highest number of fatalities.

In the years between 2006 and 2010, almost 70 extreme events reported in the world were confirmed to be rogue waves in the shallow water and coastal zones. These events caused more than 120 fatalities and almost 170 injuries in total. Out of these 70 events, 11 occurred on the Australian shoreline [126]. Counting only Australia coasts, 10 people have lost their lives and 40 people have received serious injuries. Fig.3.1 shows an example of a coastal rogue wave that happened in 2008. This picture is taken from the internet.

There are many tragedies related to rogue waves. One of these events happened in August 2010 when a ship with 60 people on board capsized and sank near Indonesian coast [126]. Only a third of those were rescued and the others have lost their lives. In 2006, three students with their teacher were washed off by an unexpected huge wave on a beach in Costa Rica.

The most recent rogue wave event occurred on Saturday, February 16, 2020, at Bondi Beach, Sydney, Australia. A large sudden wave has emerged in a perfectly calm sea conditions. It washed away a Russian couple walking along the sea rocks. This wave caused death for the man and severe injury for the woman [186].

Figure 3.1: *Coastal rogue wave in May 2008 on a beach. The wave amplitude can be estimated as 3 meters.*

There is no any regular pattern or a preferable season for rogue waves in shallow water and coastal zones. The increase of injuries and fatalities caused by rogue waves in March and May

[22, 184] may be explained by the beginning of holidays in the northern hemisphere. Nearly two-thirds of the rogue waves in the coastal areas have been reported next to sea walls and rocky beaches. The rest are near the slowly sloping sand beaches [184].

There are not many works explaining the origin of shallow water rogue waves. They can be divided into four categories [187]. The first category deals with probability distribution function of wave amplitudes. The second and third categories provide explanations based on the "linear" and "nonlinear" interaction of waves and currents. Superposition of waves at different frequencies is considered in the fourth category [187].

While significant efforts have been made to give explanations of rogue waves in the open ocean [13, 183, 188, 189], little has done about how to describe rogue waves that appear in coastal areas and shallow waters [190], although these constitute nearly 70% of the total number of extreme water wave events [126]. Thus, it is important to seek the best model of shallow water rogue waves which may mitigate this hazard and gain better understanding of the emergence of rogue waves.

Rogue waves in the ocean are described by the nonlinear Schrödinger equation (NLSE) [191] and it has solutions in the form of rogue waves as a set of rational solutions [16, 192]. These phenomena have been observed in water tanks [27], thus confirming the mathematical description of these devastating phenomena.

In shallow water, the mathematical description of water waves is usually based on solutions of the Korteweg-de Vries (KdV) or, in two dimensional case, the Kadomtsev-Petviashvili (KP) equations [190, 193]. The KdV equation [194] is known to have soliton solutions [195, 196] and these have been studied intensively, starting from the pioneering work of Zabusky and Kruskal [195]. It has, since then, found many applications in a wide variety of science branches such as crystal growth [197], plasma physics [198], nonlinear optics [199] and water waves [190].

The KdV equation is an approximate tool for modelling the shallow water waves. It can be derived from the set of the Navier-Stokes equations or their particular case - the Euler equations. The basic assumptions are zero viscosity, incompressibility and zero thermal conductivity. For an irrotational fluid, the set of equations consists of the Laplace equation, the momentum conservation and boundary conditions at the surface and the bottom of the fluid [200]:

$$\nabla^2\phi = 0, \tag{3.1}$$

$$\phi_t + \frac{1}{2}(\nabla\phi)^2 + g\psi = 0, \tag{3.2}$$

$$\phi_z - (\psi_x\phi_x + \psi_t) = 0, \tag{3.3}$$

$$\phi_z - (\eta_x\phi_x) = 0. \tag{3.4}$$

Here, ϕ is the velocity potential ($\nabla.\vec{v} = \phi$, $\vec{v}$ is the fluid velocity), g is the gravitational acceleration, $\psi \equiv \psi(t;x,z)$ is the surface elevation, η is the shape of the bottom, ∇ is the Del (nabla) operator and z, x and t are the spatial vertical and horizontal coordinates and time, respectively. Using the transformations [200]:

$$\hat{\phi} = \frac{H\phi}{LA\sqrt{gH}},$$

$$\hat{x} = \frac{x}{L}, \qquad \hat{z} = \frac{z}{H}, \qquad \hat{t} = \frac{t\sqrt{gH}}{L}$$

and

$$\hat{\psi} = \frac{H\psi}{A},$$

where H is the depth of the liquid, A is the wave amplitude, L is the average wavelength, for the case of a flat bottom, we can obtain the non-dimensional form of these equations:

$$\left(\frac{H}{L}\right)^2 \hat{\phi}_{2x} + \hat{\phi}_{2z} = 0, \tag{3.5}$$

$$\hat{\phi}_t + \frac{1}{2}\left(\frac{A}{H}\hat{\phi}_x^2 + \frac{AL^2}{H^3}\hat{\phi}_z^2\right)^2 + g\hat{\psi} = 0, \tag{3.6}$$

$$\left(\frac{L}{H}\right)^2 \hat{\phi}_z - \left(\frac{A}{H}\hat{\psi}_x\hat{\phi}_x + \hat{\psi}_t\right) = 0, \tag{3.7}$$

$$\hat{\phi}_z = 0. \tag{3.8}$$

Assuming a small depth, the velocity potential can be written as a series, $\hat{\phi}(t;x,z) = \sum_{m=0}^{\infty} \hat{z}^m \hat{\phi}^{(m)}(t;x)$. When inserting this approximation into Eq.(3.5), all odd powers of $\hat{z}$ vanish and only the even powers of $\hat{z}$ remain in the equation. For small depth, it is sufficient to keep the second powers of H/L. Eliminating $\hat{\phi}$ from the set of equations, we obtain one equation for evolution of the surface elevation:

$$\hat{\psi}_t + \hat{\psi}_x + \frac{3}{2}\left(\frac{A}{H}\right)\hat{\psi}\hat{\psi}_x + \frac{H^2}{6L^2}\hat{\psi}_{xxx} = 0.$$

This is essentially the KdV equation. It can be transformed into the standard form (3.11).

Taking into account more terms in the Euler equations (3.1) - (3.4), we can obtain the KdV equation with the higher-order terms [201]. This case will be considered in Chapter 4. The extended KdV equation can describe shallow water waves with higher accuracy. The corresponding works will be cited in Chapter 4. Needless to say, the KdV itself has a reasonable accuracy and a wide variety of applications in various branches of science [190, 197, 198].

In most of previous works, the authors studied the real-function KdV equation [202]. Namely, the wave function involved in this equation and spatial variables are taken to be real. For surface water waves, this approximation is valid as long as the vertical velocity components of the water particles are much smaller than the horizontal components [203].

Levi [203] was the first to derive the KdV equation where the wave function and the spatial variable are allowed to be complex. In particular, he took into account explicitly the vertical components of the velocity. Clearly, in this case, a whole new world of complex solutions of the KdV equation have to be discovered and their relevance to shallow water wave dynamics must be considered. Several complex-valued solutions have been found for the KdV equation in the works [204–207]. These are mostly related to soliton solutions. The rogue wave solutions, have been considered non-existent for the real-valued KdV equation. However, the complex KdV equation may have wider range of solutions that includes rogue waves.

This chapter offers the first step in solving this problem by presenting rogue wave solutions of the complex KdV equation. These are found in the form of complex rational solutions that may explain the emergence of rogue waves in shallow water. These solutions can be applied to the water surface elevation as shown at the end of the chapter.

Generally, there is a close connection between the KdV and NLS equations [208, 209]. Approximations of the NLSE by the KdV [210], or, inversely, the KdV by the NLSE [211, 212] are frequently presented. However, the difficulty of using such approximations lies in the fact that they relate a complex function of the NLSE to a real function of the KdV equation. Then, this transform loses a significant amount of information that is contained in the NLSE. Retaining the complexity of the function in the KdV equation provides a more detailed description of waves than that obtained from the purely real function KdV equation. As a result, it allows us to find rogue wave solutions that otherwise would be 'lost'.

Another equation connected to the KdV is the modified KdV (i.e. mKdV). Although it has a similar mathematical structure, the mKdV does not directly describe shallow water waves. The latter has been shown recently [2] to have rogue waves solutions. It was shown that many features of mKdV rogue waves are similar to those of rogue waves described by the NLSE solutions [2]. Namely, the hierarchy of rogue wave solutions in each case, mKdV and NLSE, have the same amplitudes that increase with the order of the solution. These observations lead us to the conclusion that the complex function KdV equation may also have rogue wave solutions.

Indeed, it is well known that all solutions of the KdV and mKdV equations are related through the Miura transformation [213, 214]. However, applying this transformation to the rogue wave solutions found in [2] leads to solutions that are singular and hence not physical. Thus, it is not the standard transformation that has to be used in this case. In fact, there is a so-called complex Mirua transformation that has been used in finding a complex solution of the KdV from the real solutions of the mKdV [215]. It has been shown, by using this transformation, that soliton solutions of the focusing mKdV can be mapped to complex soliton solutions of the KdV equation. However, this transformation cannot be used to convert real soliton solutions of the defocusing mKdV to solutions for the complex function KdV equation. Surprisingly, for rational solutions, it is a completely different matter. Here, we will show that rational solutions of the mKdV equation can be mapped to complex rational solutions of the KdV equation using the complex Mirua transformation.

The KdV equation has a variety of complex solutions, including solitons [204, 216]. Here, rogue wave solutions to the KdV are introduced for the first time. Similar to the cases of NLSE and mKdV, these are rational solutions that have maximum amplitude at the centre and decay to the background both in time and in space, thus satisfying the mathematical definition of rogue waves suggested in [16].

We start with the mKdV equation,

$$\phi_x + \beta\phi^2\phi_t + \gamma\phi_{ttt} = 0, \tag{3.9}$$

where x is the evolution variable (time), t is the spatial variable and $\phi(x,t)$ is a real function describing the wave profile. The value β and γ are the nonlinear and dispersion coefficients, respectively. Here and henceforth, subscripts t and x indicate derivatives with respect to the argument t and x. We set $\beta = 6$ and $\gamma = 1$ in order to deal with the focussing KdV. We take the known hierarchy of rogue wave solutions of the mKdV [2] and apply a complex Miura transformation [215]:

$$\psi_j(x,t) = -\phi_j(x,t)^2 + i(\phi_j)_t, \tag{3.10}$$

to them. Here $j = 1, 2, \cdots$ is the order of the solution. Then $\psi(x,t) = \psi_j(x,t)$ is a solution of the complex KdV:

$$\psi_x(x,t) - 6\psi(x,t)\psi_t(x,t) + \psi_{ttt}(x,t) = 0. \tag{3.11}$$

The transformation (3.10) differs from the ordinary Miura transformation. It provides the complex function as a result. This function is the solution of KdV in standard form but it is now complex. Direct substitution confirms that these functions are indeed complex solutions of the KdV equation.

3.1 First order rational solution

The first order rational solution of the mKdV can be written as [2]:

$$\phi_1 = \frac{12\gamma_3}{3\gamma_3 + 2\beta(t-\beta x)^2} - 1, \tag{3.12}$$

where velocity $v = \beta$. The solution resembles a soliton with a fixed velocity v. Thus, here, we have

$$\phi_1 = \frac{4}{4(t-6x)^2 + 1} - 1.$$

We use the above-mentioned complex Miura transformation for $j = 1$. Namely, using $\psi_1(x,t) = -\phi_1(x,t)^2 + i\phi_1^{(0,1)}(x,t)$ we obtain:

$$\psi_1(x,t) = \frac{8}{(2t-12x+i)^2} - 1. \tag{3.13}$$

The intensity is:

$$|\psi_1(x,t)|^2 = 16\frac{5-4(t-6x)^2}{\left[4(t-6x)^2+1\right]^2}+1, \tag{3.14}$$

Hence we have

$$\psi_1(x,t)+1 = \frac{8}{F_1^2} = -2\frac{\partial^2}{\partial t^2}\left(logF_1\right), \tag{3.15}$$

where $F_1 = 2t - 12x + i$. For convenience, $X = 12x$ and $T = 2t$ are set throughout this chapter. Hence, $F_1 = T - X + i$.

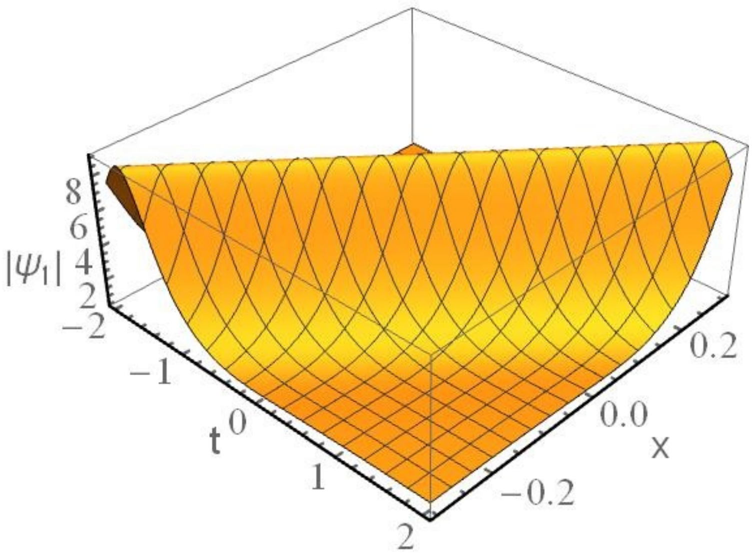

Figure 3.2: *First order rational solution, $|\psi_1|$ of complex KdV equation given by Eq.(3.13). The maximum is 9 and the background is -1.*

Fig.3.2 shows the absolute value profile of the solution (3.13). The maximal amplitude of the solution $|\psi_1| = 9$ occurs along a straight line. The maximum is remarkably high in comparison to the maximum of the first order NLSE and mKdV rogue waves that is 3 in each case. The background level here is -1. This solution was obtained in [217]. Clearly it cannot be defined as a rogue wave as the maximum is not a single peak. It resembles a soliton with a nonzero velocity, although it is not the usual KdV soliton either. Plainly, it is not a 'rogue wave', because the localization here is only in one dimension. However, it is the lowest order solution of the hierarchy with other items that do have rogue wave features.

3.2 Second order rational solution

The second order solution of the mKdV equation has been obtained in [2]. When $\beta = 6$ and $\gamma_3 = -1$, it is given by:

$$\phi_2 = \frac{12G_2}{D_2} + 1. \tag{3.16}$$

Here,

$$\begin{aligned} G_2 &= 3 - \left[(T-X)^3 + 2(3T-11X)\right](T-X) \\ &= 3 - 2\left[8(t-6x)^3 + 12(t-22x)\right](t-6x) \end{aligned}$$

and

$$\begin{aligned} D_2 &= 9 + T^6 - 6T^5X + 3T^4\left(5X^2+1\right) \\ &+4T^3X\left(1-5X^2\right) + 3T^2\left[5\left(X^2-2\right)X^2+9\right] \\ &-6TX\left(X^4-6X^2+17\right) + X^6 - 13X^4 + 139X^2. \end{aligned}$$

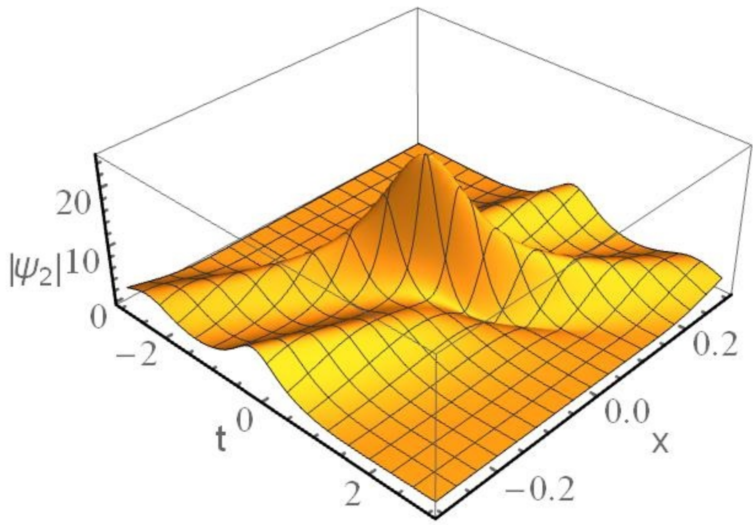

Figure 3.3: *The modulus of the second order rational solution, $|\psi_2|$ given by Eqs.(3.17) and (3.18). The maximum of $|\psi_2|$ is 25 and this occurs at the origin.*

We apply the complex Miura transformation to ϕ_2. Remarkably, we can write $\psi_2(x,t)$ in terms of one function only:

$$\psi_2(x,t) + 1 = -2\frac{\partial^2}{\partial t^2}(log F_2), \tag{3.17}$$

where

$$F_2 = (T-X)^3 + 11X - 3T - 3i[1+(T-X)^2], \tag{3.18}$$

with $X = 12x$ and $T = 2t$, as above. It can be noted that $\frac{\partial}{\partial t}(F_2) = 6(F_1^*)^2$, where * indicates complex conjugate. Thus,

$$\begin{aligned} F_2 &= 2\left[4t^3 - 72t^2x + t\left(432x^2 - 3\right) - 864x^3 \right. \\ & \left. +66x\right] - 3i\left[4(t-6x)^2 + 1\right]. \end{aligned} \tag{3.19}$$

Hence, $\psi_2(x,t) + 1 = 24\,\frac{N_2}{F_2^2}$, where

$$\begin{aligned} N_2 = & \quad T^4 - 4T^3(X+i) + 6T^2(X+i)^2 \\ & - \quad 4T\left(X^3 + 3iX^2 + X - 3i\right) \\ & + \quad (X^2+1)(9+4iX+X^2). \end{aligned} \tag{3.20}$$

The maximum of the solution Eq.(3.17) located at the point $(0,0)$ is 25. This is significantly higher than the maximum of the second order NLSE rogue wave solution. The wave profile resembles a peak on top of a moving soliton. As the peak is higher than the soliton, the central bump can be interpreted as a rogue wave. The profile of this solution, Eq.(3.17), is shown in Fig.3.3.

3.3 Third order rational solution

The third order rational solution can be obtained similarly:

$$\psi_3(x,t) + 1 = -2\,\frac{\partial^2}{\partial t^2}\,(log F_3), \tag{3.21}$$

where

$$\begin{aligned} F_3 &= T^6 - 6T^5(X-i) + 15T^4(X-i)^2 \\ &- 20T^3X\left(X^2 - 3iX - 5\right) + 15T^2(X-i)(X^3 \\ &- 3iX^2 - 11X - 3i) - 6T\left(X^5 - 5iX^4 - 30X^3\right. \\ &+ \left. 40iX^2 + 5X - 15i\right) + X^6 - 6iX^5 - 55X^4 \\ &+ 120iX^3 - 245X^2 - 450iX - 45, \end{aligned}$$

with $X = 12x$ and $T = 2t$.

Hence, we can write this solution in the form:

$$\psi_3(x,t) = 48\,\frac{N_3}{F_3^2} - 1, \tag{3.22}$$

where the explicit form of N_3 calculated from F_3 is given by:

$$
\begin{aligned}
N_3 \quad &= T^{10} - 10T^9(X-i) + 45T^8(X-i)^2 - 120T^7(X-i)^3 + 210T^6(X-i)^4 \\
&-36T^5\left(7X^5 - 35iX^4 - 70X^3 + 70iX^2 + 35X + 5i\right) + 30T^4(7X^6 - 42iX^5 \\
&-105X^4 + 140iX^3 + 185X^2 + 110iX + 45) - 120T^3\left(X^7 - 7iX^6\right. \\
&\left.-21X^5 + 35iX^4 + 115X^3 + 15iX^2 + 125X - 15i\right) + 45T^2(X-i)^2 \\
&\times\left(X^6 - 6iX^5 - 15X^4 + 20iX^3 + 335X^2 + 410iX + 15\right) - 10T\left(X^9 - 9iX^8 - 36X^7 + 84iX^6\right. \\
&\left.+1086X^5 - 1830iX^4 - 740X^3 - 4380iX^2 - 135X + 135i\right) + X^{10} - 10iX^9 - 45X^8 \\
&+120iX^7 + 2610X^6 - 7020iX^5 - 16250X^4 - 13000iX^3 - 17475X^2 - 5850iX - 2025.
\end{aligned}
$$

The profile of the solution magnitude, Eq.(3.22), is shown in Fig.4.1.

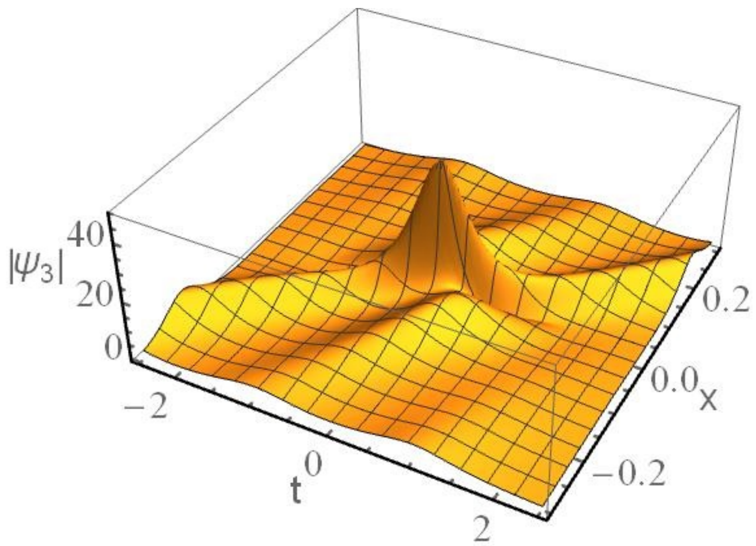

Figure 3.4: *The modulus of the third order rational solution, $|\psi_3|$ given by Eq.(3.22). The maximum is* 49 *and this occurs at the origin.*

A summary of these findings is presented in Table 3.1. The first column in the table shows the order of the solution while the second and third columns show the background and height involved in each ϕ (mKdV) solution. The fourth and fifth columns show the background and maximum amplitude involved in each ψ (complex KdV) solution. The last row shows the general expressions for the background and amplitude for any order j.

As we can see, the maximum amplitude increases rapidly with the order j. This is the main characteristic of these solutions that allows us to claim that they describe rogue waves. Taking into account the fact that the background level has unit magnitude, the ‘amplification factor’ can significantly exceed that for NLSE rogue waves. Our present results demonstrate, clearly, that shallow water rogue waves can, indeed, be considered as devastating.

j	background level of ϕ_j	height of ϕ_j	background level of $\lvert\psi_j\rvert$	maximum of $\lvert\psi_j\rvert$
1	-1	3	-1	$3^2 = 9$
2	+1	5	-1	$5^2 = 25$
3	-1	7	-1	$7^2 = 49$
j	$(-1)^j$	$2j+1$	(-1)	$(2j+1)^2$

Table 3.1: Background level and the amplitude of rational solutions of order j for mKdV (two left columns) and complex KdV (two right columns) equations.

In the next section, it will be shown how to calculate water surface elevation from these solutions.

3.4 Water surface elevation

The next question is how to apply these results to finding the water surface elevation in a channel with a constant depth. Rough estimates can be made on the basis of Levi's model [203]. Levi considered the flow of a homogeneous and irrotational fluid in a channel with parallel sides and uneven bottom. The flow is two dimensional with $\bar{x}$ and $\bar{y}$ parallel to the sides of the channel. The bottom corresponds to $\bar{y} = 0$ as shown in Fig.3.5. The $\bar{x} - axis$ is in the horizontal direction while the $\bar{y} - axis$ is in the vertical one. The velocity potential is defined by:

$$\omega(\tau;\bar{x},\bar{y}) = \mu(\tau;\bar{x},\bar{y}) - i\upsilon(\tau;\bar{x},\bar{y})$$

where $\mu(\tau;\bar{x},\bar{y})$ and $\upsilon(\tau;\bar{x},\bar{y})$ are the $\bar{x}$ and $\bar{y}$ components of the velocity field, respectively, while τ is time. The complex KdV equation can be written in terms of the complex velocity as [203]:

$$\rho_\tau + \alpha\rho\rho_\zeta - \beta\rho_{\zeta\zeta\zeta} = 0, \tag{3.23}$$

where $\rho \equiv \omega(\tau;\bar{x},\bar{y}) = \mu(\tau;\bar{x},\bar{y}) - i\upsilon(\tau;\bar{x},\bar{y})$, $\zeta = \bar{x} + i\bar{y}$ and α (the propagation velocity) and $\beta = \frac{1}{3}\frac{gq_0^3}{\alpha^4}$ are constant parameters. Here, g is the gravity acceleration and q_0 is the unperturbed flow.

Now, it seems that the real part of the function $\rho(\tau;\bar{x},\bar{y})$ corresponds to the horizontal component of the fluid velocity along the channel while the imaginary part corresponds to the vertical component of the velocity. With a rough estimation, if the complex velocity ρ is independent of $\bar{y}$ direction, a standard KdV equation with a complex-valued function is obtained and equation (3.23) can be converted to the equation (3.11) if $\tau \to -6\sqrt{\frac{6\beta}{\alpha^3}}x$ and $\zeta \to \sqrt{\frac{6\beta}{\alpha}}t$.

Let's look at the vertical velocity, which is now dependent only of time and $\bar{x}$ direction. This is the imaginary part of the complex solutions. The imaginary part of equation (3.11) is defined by the complex Miura transformation (3.10), i.e. the $t-$derivative of the mKdV solution (3.9). In this instance, the water elevation H is roughly defined by the indefinite integral of the imaginary

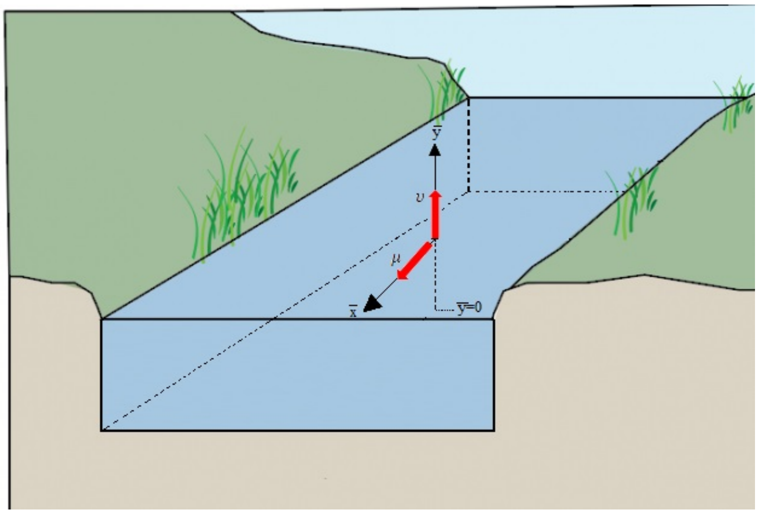

Figure 3.5: *Schematic figure of Levi's channel.*

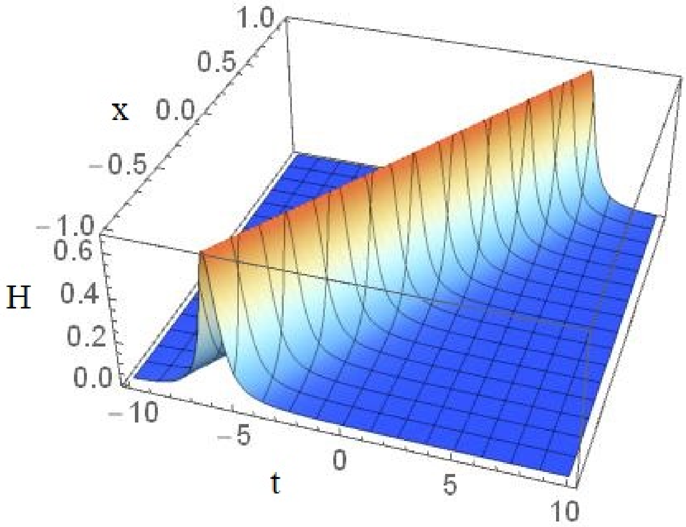

Figure 3.6: *Water level elevation for the first order rational solution equation (3.13).*

part of the complex field:

$$H \approx \int \frac{\partial}{\partial t}\left[\phi_j(x,t)\right] dx + C.$$

The integration constant, C, is normally chosen in such a way as to keep the water level at zero around the rogue wave event. For the first order rational solution (3.13), a soliton shape is obtained as we would expect. It is plotted in figure 3.6. Figure 3.7 shows two plots that have been constructed this way. The one in Fig.3.7(a) is for the second order solution and the one in Fig.3.7(b) is for the third order solution. The amplitudes here are not as dramatic as for the

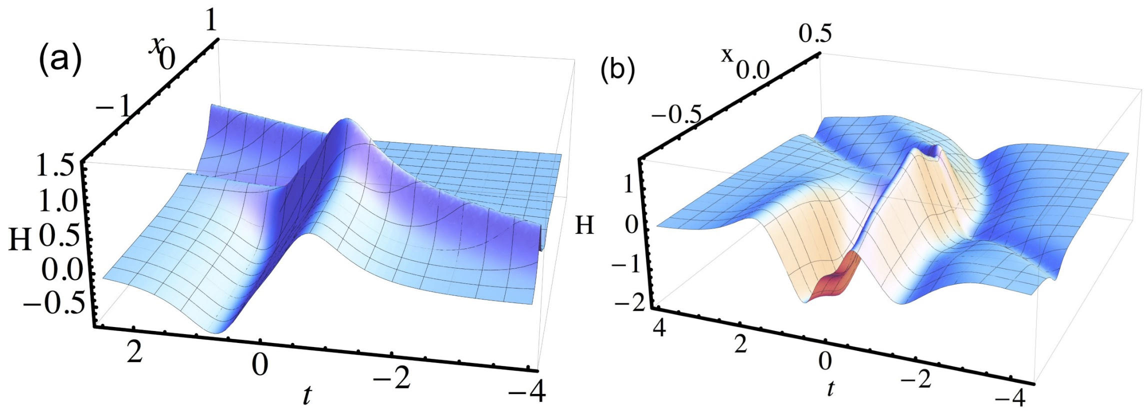

Figure 3.7: *Water level elevation for (a) second and (b) third order rational solutions of complex KdV equation.*

modulus of the function $|\psi|$, but the rogue wave peak is certainly there. Interestingly, it is not located at the origin. As it is said above, more accurate estimates should be made using the full scale theory provided by the work of Levi [203]. The latter requires not only the dependent but also the independent variables to be complex.

3.5 Conclusions

To summarize, we have presented the lowest order complex rational solutions of the KdV equation. These are the first three members of an infinite hierarchy of rogue wave solutions. We used the complex Miura transformation to derive them. However, other methods such as the Darboux transformation or equivalent can also be used to obtain the whole hierarchy, as is often done for other integrable equations [177]. These solutions imply the existence of shallow water rogue waves with amplitudes exceeding the soliton collision amplitudes of the real KdV equation. Namely, they are proportional to the square of the order of the solution [190]. Thus, a collision of solitons might not fully explain rogue waves. Indeed, the peak amplitudes at the point of soliton collision are too low to count them as rogue waves.

The significance of our findings is not restricted to water rogue waves. Our findings can be applied to optics, where the ideas of shallow water rogue waves are also applicable [218]. They can occur in diffusion-controlled unidirectional crystal growth [197]. One and two-soliton complex solutions of the KdV equation have been found. They are related to PT-symmetric systems [219], quantum mechanical scattering matrices in a semi-classical approximation [220] and to a number of other physical systems where the KdV is the governing equation.

Chapter 4

Extended Complex KdV Equation

The celebrated Korteweg-de Vries (KdV) equation became the first known integrable evolution equation for modelling nonlinear dispersive waves [213]. Originally, it was derived for modelling shallow water waves [194, 221]. The observation of a soliton by John Scott Russell demonstrated the existence of such waves in water canals [222]. Thereafter, it was found that the KdV equation is applicable to plasma waves [195, 223] and atto-second optical pulses that contain a few optical cycles, or even a fraction of one cycle [224]. In each case, soliton solutions are of primary interest as waves that keep undistorted profiles over large distances of propagation [225]. However, solitons are not the only structures that exist in the physical systems listed above. Rogue waves represent a different form of nonlinear structure that has received much attention in recent years. In particular, they do exist in shallow water [190]. In fact, they are understood much less than deep water rogue waves. One of the possible ways to model shallow water rogue waves is to use the KdV equation with complex functions [203, 226], rather than the real ones used in most previous publications. This has been done in the previous chapter 3.

Historically, the second nonlinear wave evolution equation found to be integrable was the Nonlinear Schrödinger Equation (NLSE) [227]. Solitons, breathers and rogue waves described by this equation are all known in analytical form. These solutions equally well model waves in optical fibres [228] and water waves in the deep ocean. It has been extended to include the Hirota equation [4], the Lakshmanan - Porsezian - Daniel (LPD) equation [229] and other higher-order equations, keeping integrability intact, and thus allowing one to find exact solutions for the relevant physical problems [230]. These equations provide the opportunity to increase the accuracy of modelling of nonlinear waves with the inclusion of higher-order dispersion or nonlinear terms. These higher-order equations are important for modelling oceanic waves [231],

[209] with high accuracy. They also cover a wider range of physical phenomena, such as the Heisenberg ferromagnetic spin chain [3], or effects like modulation instability [232] that do not exist in the case of the ordinary KdV equation.

In a similar fashion, expanding the KdV equation with the addition of higher-order terms may improve the accuracy of modeling of known phenomena as well as predicting new effects [200]. For example, this could describe water waves that are shorter but steeper (in the non-integrable case) [233]. It also can have better accuracy, compared to the KdV, in modeling shallow water waves facing an obstacle [234] or where the surface tension is not negligible [235]. However, it has been shown that the basic KdV equation describes half-cycle optical solitons in quadratic nonlinear media [225]. As another example, the 5-th order KdV equation has been found relevant to soliton collisions for weakly nonlinear long waves [233]. In these cases, only real solutions have been considered, despite the fact that allowing the solutions to encompass the complex space can significantly increase the variety of possible scenarios in wave evolution [217, 236].

Shallow water rogue waves can have considerable impact on the marine ecosystem and have caused significant coastal erosion [237]. A rogue wave hitting a crowded beach is of particular concern. For example, this occurred [238] in 1938 at Bondi beach in Sydney, Australia, where 'three tremendous waves rolled onto the beach', one after the other. This caused panic and swept many out into the sea. In the end, 5 people were killed and 250 rescued. It would be very useful to gain understanding of such phenomena, with an eye to possible early detection and warning. It is plausible that such waves can be modelled by the KdV equation and its expanded versions. In this work, we extend complex rogue wave ideas to the KdV expansion.

Higher-order KdV equations have been considered earlier in a number of publications [239–243]. They have been called 'hierarchies', as each separate one can be obtained from a lower order one using certain transformations [244]. The approach provided here is different in that we take them all together. Firstly, a single infinitely extended equation that includes, as a particular case, the basic KdV equation is considered. Secondly, a general solution that includes complex functions as potential solutions to this single equation is provided. The infinite extension contains higher-order operators with arbitrary real parameters, and this significantly increases the range of physical problems where this full equation can be applied. Below, we consider, separately, the cases of focusing and defocusing KdV extensions. These differ in signs of nonlinear terms, although a simple change of the sign of the function $u \to -u$ converts one case to the other.

4.1 Infinitely extended KdV equation

In Chapter 3, the plausibility of employing complex functions to describe rogue waves occurring in shallow water has been demonstrated. This involved only the 'standard' KdV equation. To extend this, we start with the well known 'defocussing' KdV equation,

$$u_x + \alpha_1 [u_{ttt} - 6u(t,x)u_t] = 0, \tag{4.1}$$

where t is the transverse variable and x is the variable along the wave propagation direction. In optics, x is the propagation distance, while t is a retarded time, as used in the optical few-cycle KdV example of [225, 245]. In water and other fluid systems, x is usually time while t is a transverse spatial variable. This is an evolution equation which means that waves evolve in the x-direction.

It is easy to show that if $u(x,t)$ is a solution of the 'defocusing' KdV, then $u(x,t) = -u(x,t)$ is a solution of 'focusing' KdV. Thus, the 'focusing' KdV solutions can be found from the 'defocusing' ones simply by changing the sign of the dependent variable.

We can write the infinitely extended equation (IEE) in the form similar to the one used in [230]:

$$u_x(t,x) + \sum_{m=1}^{\infty} \alpha_m K_m(u) = 0, \tag{4.2}$$

where $K_m(u)$ is the operator of order m. It include the function u and its derivatives up to order m. The lowest order operator here is:

$$K_1 = u_{ttt} - 6u(t,x)u_t.$$

When all coefficients except α_1 are zero, Eq.(4.2) reduces to the basic KdV equation (4.1). The next level operator, $K_2(u)$, is

$$K_2 = -\frac{15}{2} u_t u^2 + \frac{5}{2} u_{ttt} u + 5 u_t u_{tt} - \frac{1}{4} u_{5t}$$

while the operator $K_3(u)$ is given by

$$\begin{aligned} K_3 &= \frac{1}{16}\Big\{ 70 u_{ttt} u^2 - 140 u_t u^3 + +14[20 u_t u_{tt} - u_{5t}]u + 70(u_t)^3 \\ &- 70 u_{tt} u_{ttt} - 42 u_t u_{4t} + u_{7t} \Big\}. \end{aligned} \tag{4.3}$$

Here, each evolution equation, $u_x(t,x) + \alpha_n K_n(u) = 0$, obtained from Eq.(4.2) when all coefficients except one are zero can be written as

$$\frac{\partial u}{\partial x} + \alpha_n \frac{\partial F_n(u)}{\partial t} = 0,$$

where $F_n(u)$ is a polynomial in u. So

$$\frac{\partial F_n(u)}{\partial t} = K_n(u).$$

Hence, F_1 and F_2 are:

$$F_1 = u_{tt} - 3u^2, \tag{4.4}$$

$$F_2 = (-\frac{1}{4})(u_{4t} - 5u_t^2 - 10 u u_{tt} + 10u^3). \tag{4.5}$$

The coefficient α_1 in Eq.(4.1) is an arbitrary real parameter that commonly is taken to be 1. Eq.(4.1) can be called KdV-3 as it has the third-order derivative in the operator within the rectangular brackets. The set of operators can be continued indefinitely, thus making Eq.(4.2) infinitely extended.

The set of the operators for 'focusing' KdV, $u_x + \alpha_n W_n = 0$, can be found by setting $u(x,t) = -u(x,t)$, thus obtaining:

$$W_1 = u_{ttt} + 6u(t,x)u_t, \tag{4.6}$$
$$W_2 = -\frac{15}{2}u_t u^2 - \frac{5}{2}u_{ttt}u - 5u_t u_{tt} - \frac{1}{4}u_{5t}$$

and

$$\begin{aligned} W_3 &= \frac{1}{16}\Big\{70u_{ttt}u^2 + 140u_t u^3 + 14[20u_t u_{tt} + u_{5t}]u + 70(u_t)^3 \\ &+ 70u_{tt}u_{ttt} + 42u_t u_{4t} + u_{7t}\Big\}. \end{aligned} \tag{4.7}$$

As stated above, the parameters α_m are arbitrary real numbers that provide infinite variability for this equation. When all coefficients are zero except one, we obtain particular cases. For example, KdV-5 is an equation with 5-th order highest derivative in t:

$$u_x + \alpha_2 K_2 = 0. \tag{4.8}$$

Similarly,

$$u_x + \alpha_3 K_3 = 0, \tag{4.9}$$

can be called KdV-7, as its highest derivative is of seventh order in t. For each individual example, the equation with K_n can be called KdV-(2n+1), as its highest derivative is of order $2n+1$. It should be mentioned that the extensions of the KdV equation can possess different coefficients and parameters. The difference in the form of these equations stems from the different physical context, approximation and boundary conditions. The list of all possible coefficients is provided in [233]. For most of these cases, the extension of the KdV is proved to be non-integrable [201]. In this chapter, these constants are taken such that the equation becomes integrable and, thus, an analytical solution can be sought. The set of operators K_m provided above ensures the integrability of Eq.(4.2) and this means that solutions of Eq.(4.2) can be written in analytic forms. We demonstrate this by providing a few solutions to Eq.(4.2). We start with the most common – the soliton solution.

4.2 Soliton solutions

For KdV-3, the well-known soliton solution is:

$$u_1 = -2k^2 sech^2\left[k\left(t - 4\alpha_1 k^2 x\right)\right], \tag{4.10}$$

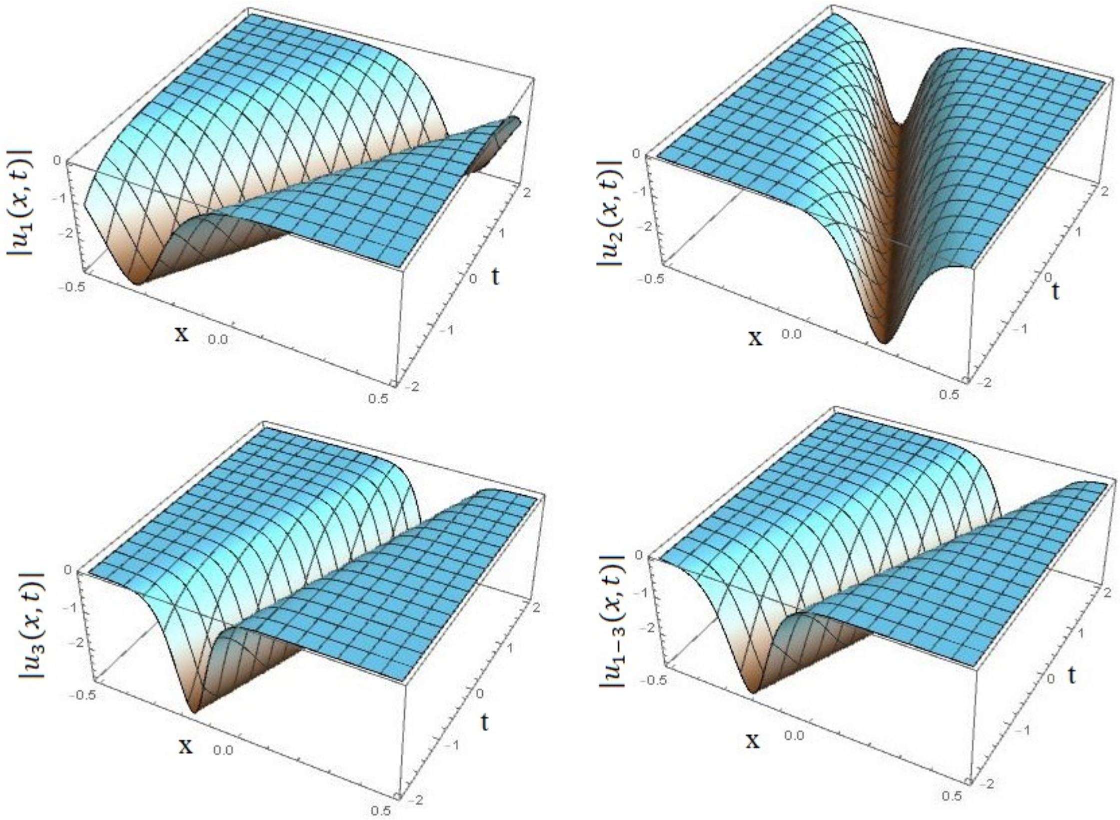

Figure 4.1: *3D plots for soliton solution Eq.(4.12), $|u_1|$, top left, when $\alpha_1 = 1$ and $\alpha_n = 0$ for $n \neq 1$, $|u_2|$, top right, when $\alpha_2 = 1$ and $\alpha_n = 0$ for $n \neq 2$, $|u_3|$, bottom left, when $\alpha_3 = 1$ and $\alpha_n = 0$ for $n \neq 3$, and $|u_{1-3}|$, bottom right, when $\alpha_1 = \alpha_2 = \alpha_3 = 1$ and $\alpha_n = 0$ for $n > 3$. In all cases, $k = 1.2$ is assumed. Clearly, all the solitons have the same amplitude but different velocities.*

where k is an arbitrary real constant that defines the amplitude and the velocity of the soliton.

We can write down the soliton solution in general form for the whole extended equation (4.2):

$$u(t,x) = -2k^2 sech^2 [k(t + J(x))], \tag{4.11}$$

where

$$J(x) = 4x \sum_{n=1}^{\infty} (-1)^n \alpha_n k^{2n}.$$

This can be written as

$$u(t,x) = -2[log(f(t,x))]_{tt}$$

where $f(t,x) = 1 + \exp[2k(t + J(x))]$. This solution is valid for any real values of the coefficients α_n which are present in the equation (4.2), even if there are infinitely many. Clearly, if some of these coefficients are zero, the solution is simplified, with a reduced number of the terms in the sum. For the case where only α_1 and α_2 are non-zero, this solution has been given in [246].

For example, if all of them are zero except for α_n, the solution becomes:

$$u_n = -2k^2 sech^2 \left\{k\left[t + 4(-1)^n \alpha_n k^{2n} x\right]\right\}, \tag{4.12}$$

where $n = 1, 2, 3, \cdots$. This is the soliton solution for KdV-(2n+1). By having a closer look at this form of the solution, we realize that for each KdV-(2n+1) (and setting $\alpha_n = 1$ and $k = 1$), we get the same solution, apart from the sign on the x term. This does not occur in the forms of the rational solutions, since we will obtain different shapes and solutions for each order of the KdV. In contrast to the non-integrable extensions of the KdV equation, which support the propagation of the steeper and narrower solitons [201, 247], the solution (4.12) demonstrates the same soliton shapes, in terms of width and amplitude at $x = 0$, but different velocities $(4(-1)^n \alpha_n k^{2n})$. This discrepancy in the velocity is plotted in figure 4.1. Furthermore, the soliton solutions given above in this section are real. However, in this thesis, complex solutions should be sought. Here we can add a parameter, ic, with c being an arbitrary real number, to the argument of the sech function in each of the above solutions. Hence

$$u_n = -2k^2 sech^2 \left\{k\left[t + 4(-1)^n \alpha_n k^{2n} x\right] + ic\right\} \tag{4.13}$$

is a valid solution of the equation of order n.

4.3 First order rational solutions.

The first order complex rational solution of KdV-3 has been given in chapter 3:

$$u_1 = \frac{8}{(2t - 12k\alpha_1 x + ic)^2} - k, \tag{4.14}$$

where k and c are arbitrary real constants, apart from the restriction that $c \neq 0$.

Now, this form of solution can be extended for other equations in the set. When only one α_n is non-zero, we obtain solutions of higher-order KdV equations. For example, for the KdV-5 case, the first order rational solution of Eq.(4.8), can be written as

$$u_2 = \frac{8}{(2t + 15k^2\alpha_2 x + ic)^2} - k. \tag{4.15}$$

Next, the first order rational solution of KdV-7, i.e. Eq.(4.9) can be written as:

$$u_3 = \frac{8}{\left(2t - k^3\alpha_3 \frac{35x}{2} + ic\right)^2} - k. \tag{4.16}$$

The first-order rational solution for KdV-9 is:

$$u_4 = \frac{8}{\left(2t + k^4\alpha_4 \frac{315x}{16} + ic\right)^2} - k. \tag{4.17}$$

We continue in this way, finding the coefficients needed.

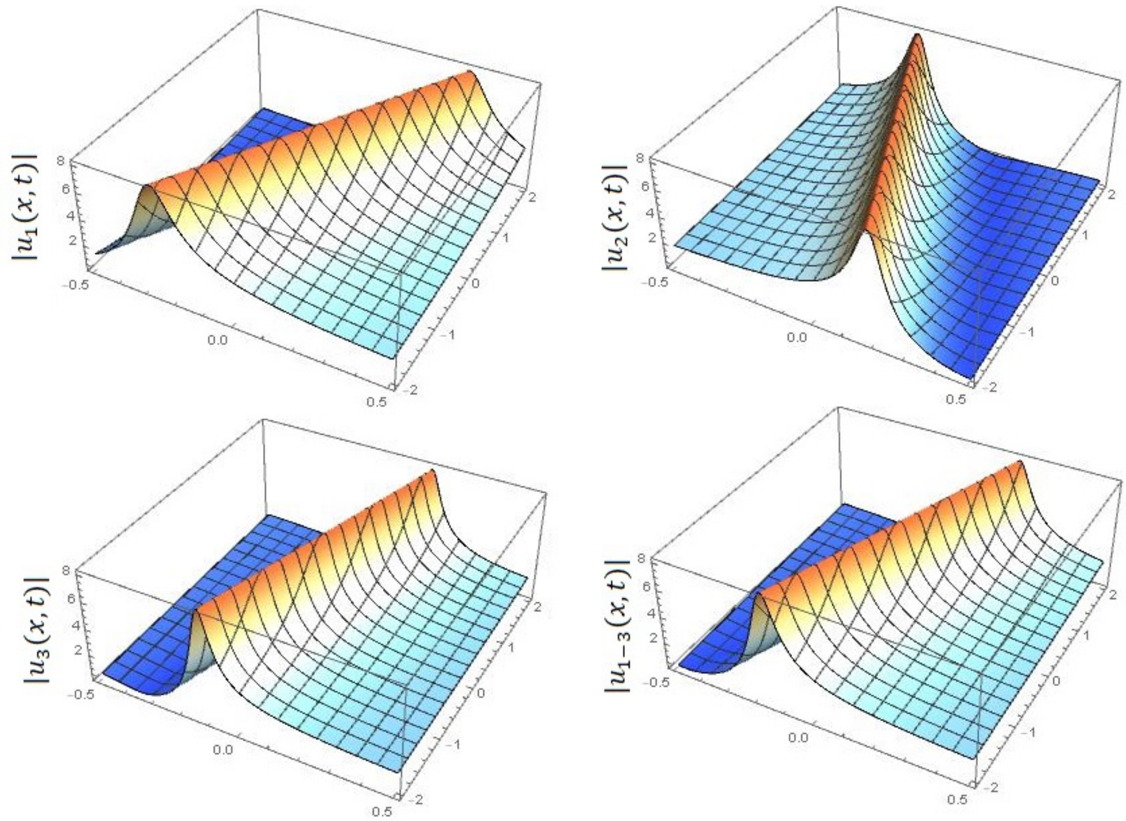

Figure 4.2: *3D plots for the first order rational solution (4.12), $|u_1|$, top left, when $\alpha_1 = 1$ and $\alpha_n = 0$ for $n \neq 1$, $|u_2|$, top right, when $\alpha_2 = 1$ and $\alpha_n = 0$ for $n \neq 2$, $|u_3|$, bottom left, when $\alpha_3 = 1$ and $\alpha_n = 0$ for $n \neq 3$, and $|u_{1-3}|$, bottom right, when $\alpha_1 = \alpha_2 = \alpha_3 = 1$ and $\alpha_n = 0$ for $n > 3$. In all cases, $k = 1.2$ and $c = 1$ are assumed. Clearly, all the solutions have the same amplitude but different velocities.*

Further particular cases up to and including u_7, i.e. up to the equation $KdV-15$, reveal the general solution:

$$u_n = \frac{8}{(2t + p_n x + ic)^2} - k, \tag{4.18}$$

where

$$p_n = \alpha_n \frac{(-k)^n}{2^{n+1}} (4n^2 - 1) b_n,$$

with $b_n = \{16, 8, 8, 10, 14, 21, 33, \cdots\}$ for $n = 1, 2, 3, \cdots, 7, \cdots$ and k is an arbitrary real parameter. Taking into account this form of b_n, we can write the expression for p_n explicitly:

$$p_n = 8\alpha_n \left(-\frac{k}{2}\right)^n \frac{(2n+1)!!}{n!}, \tag{4.19}$$

where the double factorial is defined as $(2n+1)!! = (2n+1)(2n-1)(2n-3)\cdots 1$.

In fact, we can solve the infinitely extended equation (4.2) with

$$u_\infty = \frac{8}{(2t+px+ic)^2} - k$$

, where $p = \sum_{n=1}^{\infty} p_n$, or

$$p = 8\sum_{n=1}^{\infty} \alpha_n (-\frac{k}{2})^n \frac{(2n+1)!!}{n!}.$$

Each of the above solutions is a rational soliton with a fixed velocity v. It has a ridge of height 9 while the background is $|u| = 1$. In order to avoid large numbers in the solution, we replace the independent variables with $X = 12x$ and $T = 2t$. Then, we can write the solution in log-form:

$$u_1(x,t) + k = \frac{8}{R_1^2} = -2\frac{\partial^2}{\partial t^2}(log R_1), \tag{4.20}$$

where $R_1 = 2t - 12\alpha_1 kx + ic$. Hence, $R_1 = T - \alpha_1 kX + ic$. For the arbitrary n,

$$u_n(x,t) + k = \frac{8}{R_n^2} = -2\frac{\partial^2}{\partial t^2}(log R_n), \tag{4.21}$$

where $R_n = 2t + p_n x + ic$. Hence, $R_n = T + p_n X/12 + ic$, with p_n given by Eq.(4.19).

Solutions presented in this section are rational solitons. They have long tails and would not be classified as 'rogue waves' in common parlance. Similar to the soliton, the first rational solutions have the same shape, in terms of width and amplitude, in different extension $K_n(u)$. The first rational solutions for different extension are plotted in figure 4.2.

Rogue waves should have a localized bump that 'appears from nowhere' [16]. Below, we present the higher-order rational solutions that do show the rogue wave features.

4.4 Second order rational solutions as rogue waves

Rational solutions to many integrable evolution equations comprise hierarchies that start with the lowest order and continue to infinitely high order. The infinitely-extended KdV equation and its particular cases have the same property. All of them have higher-order rational solutions. In contrast to solutions of the previous section, they can describe rogue waves.

Higher-order rational solution of the 'defocusing' equation (4.2) with a single nonzero coefficient α_n can be written in general form:

$$u_n^r(x,t) = -2\frac{\partial^2}{\partial t^2}(log G_n) - 1, \tag{4.22}$$

where

$$G_n = (T-X)^3 + 11X - 3T - 3i(T-X)^2 + d, \tag{4.23}$$

with $X = 12\alpha_n x r_n v_n$ and $T = 2tv_n$, as above, and with $v_n = 1/\sqrt{n}$. In the entire of this section, $d = d_r + i d_i$ is a non-zero complex constant with $d_i < 0$. The denominator of u_n can be zero at a

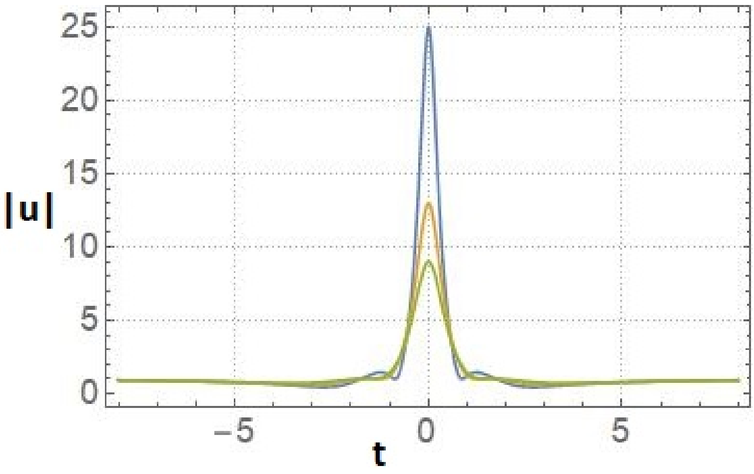

Figure 4.3: *Maximum amplitude for the second order rational solution (rogue wave) at $x = 0$. The blue curve shows the solution for the $KdV-3$ with $\alpha_1 = 1$ and $\alpha_n = 0$ for $n \neq 1$, the orange one for the $KdV-5$, i.e. $\alpha_2 = 1$ and $\alpha_n = 0$ for $n \neq 2$ and the green one is plotted for $KdV-7$, i.e. $\alpha_3 = 1$ and $\alpha_n = 0$ for $n \neq 3$. In all cases, $d_r = 0$, $d_i = -3$ are assumed.*

value of x that depends on $\sqrt{d_i}$. If $d_i > 0$, this occurs at real x (giving a singular solution), but if $d_i < 0$ then no such real value of x exists, and the solution is finite everywhere.

The definition of the variables X and T thus depends on the particular value of n chosen. Namely, when $n = 1$, i.e for KdV-3 equation, we have $r_1 = 1$. Next, when $n = 2$, i.e. for KdV-5, we have $r_2 = -\frac{5}{4}$. Further, for $n = 3$, i.e. in the case of KdV-7, we have $r_3 = \frac{35}{24}$. When $n = 4$, i.e. for KdV-9, we have $r_4 = -\frac{105}{64}$. The highest order for which we explicitly provide this coefficient is $n = 5$. Namely, for KdV-11, we have $r_5 = \frac{231}{128}$. In fact, these coefficients can be written for arbitrary n in the form

$$r_n = (-1)^{n+1}\frac{2^{1-n}}{3n!}(2n+1)!!\ .$$

Unlike the soliton and first-order rational solutions provided previously, these solutions not only have different velocities but also possess different shapes in terms of width and amplitude. The highest amplitude belongs to $|u_1|$. This comparison can be seen in figure 4.3. The shapes of the rogue wave for $KdV-3$ to $KdV-9$ are gathered in figure 4.4.

Let us consider a few examples. The complex polynomial G_n in Eq.(4.23) for KdV-3 is:

$$G_1 \quad = \quad 8(t-6\alpha_1 x)^3 - 12i(t-6\alpha_1 x)^2 + 132\alpha_1 x - 6t + d.$$

Then, if $d_r = 0$, the maximum of the corresponding solution $|u_1|$ is $|u_1(0,0)| = -u_1(0,0) = 1 + \frac{72}{d_i^2} - \frac{48}{d_i}$. So, if $d_i = -3$, this is 25. The polynomial G_n for KdV-5 is:

$$G_2 = \frac{1}{8}[2\sqrt{2}(15\alpha_2 x + 2t)^3 - 12i(15\alpha_2 x + 2t)^2 - 660\sqrt{2}\alpha_2 x - 24\sqrt{2}t + 8d].$$

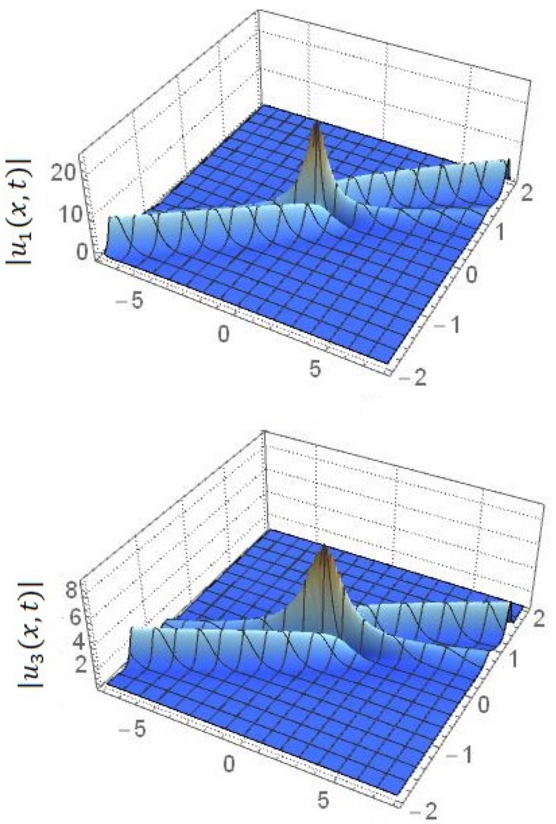

Figure 4.4: *3D plots for the second order rational solution (rogue wave) Eq.(4.22), $|u_1|$, top left, when $\alpha_1 = 1$ and $\alpha_n = 0$ for $n \neq 1$, $|u_2|$, top right, when $\alpha_2 = 1$ and $\alpha_n = 0$ for $n \neq 2$, $|u_3|$, bottom left, when $\alpha_3 = 1$ and $\alpha_n = 0$ for $n \neq 3$, and $|u_4|$, bottom right, when $\alpha_4 = 1$ and $\alpha_n = 0$ for $n \neq 4$. In all cases, $d_r = 1.2$ and $d_i = -3$ are assumed. Clearly, the shapes of rogue waves, amplitude and their velocities are distinct.*

Then, if $d_r = 0$, the maximum of the corresponding solution $|u_2|$ is $|u_2(0,0)| = -u_2(0,0) = 1+\frac{36}{d_i^2}-\frac{24}{d_i}$. So, if $d_i = -3$, this is 13. Finally, the polynomial G_n for KdV-7 is:

$$G_3 \quad = \quad \frac{(4t-35\alpha_3 x)^3}{24\sqrt{3}} - \frac{i}{4}(4t-35\alpha_3 x)^2 + \frac{385\alpha_3 x}{2\sqrt{3}} - 2\sqrt{3}t + d.$$

This leads to the complex solution u_3. Then, if $d_r = 0$, the maximum of the corresponding solution $|u_3|$ is $|u_3(0,0)| = -u_3(0,0) = 1+\frac{24}{d_i^2}-\frac{16}{d_i}$. So, if $d_i = -3$, this is 9. Thus, for $d_r = 0$, we have the maximum of $|u_n|$ being $|u_n(0,0)| = 1+\frac{24}{n d_i^2}(3-2d_i)$, for n=1,2,3. As n increases, the maximum possible value thus decreases.

It has long 'soliton'-like tails but the most prominent feature of this solution is the rogue wave bump at the origin. This feature is present in all solutions considered in this section. As we can see from the above, the highest amplitude is in the case of 'standard' KdV-3. As noted above, its value depends on d_r and d_i.

4.5 Conclusions

In conclusion, an infinitely extended KdV equation that contains an infinite number of arbitrary real coefficients controlling higher-order terms in this extended evolution equation is presented. The higher-order terms are chosen in such a way as to maintain the integrability of the whole equation. Another significant step in this work is that this extended equation admits complex-valued solutions. This generalization allows us to expand the set of solutions and include both solitons and rogue waves in the family. The rogue waves take the form of rational solutions of this equation. Special choices of the arbitrary coefficients in the equation lead to particular cases - the basic KdV and a multiplicity of its higher-order elaborations. Using the extended KdV instead of the basic one may well improve the accuracy of the description of rogue waves in shallow water.

CHAPTER 5

ROGUE WAVES IN PLASMAS

The term '*plasma*' has been applied to the fourth state of matter. When in a confined gas, for example, temperature increases, molecules become more vigorous and try to dissociate to form a gas of atoms. Then this bulk of gas converts to gas of freely moving charged particles, such as electrons, and ions. This state is normally called the plasma state, a term proposed by Langmuir to describe the region of gas discharge [248]. It can be classified by the amount of mixture of electrons, ions, and neutral particles moving in arbitrary directions that, overall, is electrostatically neutral. Moreover, plasmas are perfect examples of electric conductors, even better than some metals such as gold and copper, because of the existence of free-charge carriers [249]. Sometimes plasmas emerge naturally, for example, due to the reaction of sunlight and atmospheric gas molecules, but also can be man-made, created in a laboratory. Generation and stabilization of plasma even in a highly-equipped laboratory are not as straightforward as it may seem, but very worthwhile for many advanced applications, including creating electronic devices and lasers. Most computer hardware is manufactured based on plasma technologies. One example is very large and thin plasma screens [249].

Normally, plasmas consist of a neutral binary mixture of ions and electrons. However, there are non-neutral plasmas, which often can be made in a laboratory [250]. Not surprisingly, they behave in different ways from conventional plasmas. The microwave oscillators and amplifiers, for example, are manufactured by the use of non-neutral plasmas [250].

Non-neutral plasmas have one fewer components than a conventional plasma; however, there is another kind of plasma, called dusty plasma which has one more species [249, 251]. This addition of the third component creates more possibilities and lead to new behaviours as well as distinctive applications. The third component in a dusty plasma is an electrically charged dust grain that normally has a charge to mass ratio significantly higher than the ratio for electrons or ions. Various feasible methods can be used to produce charged dust grains in plasma. In laboratory dusty plasmas, electron bombardment is a conventional method for charging the dust grains. Photoionisation is another mechanism that usually occurs in the upper layers of the atmosphere. The latter mechanism charges positively the dust grains because photoionisation forces electrons to abandon their surface [251].

There has been an intense interest in dusty plasmas for the past three decades because of their presence in a wide variety of physical environments, such as the mid-layer of atmosphere [252], magnetically-confined fusion plasmas [253], comet tails and the space environment [254]. One of the interesting subjects in this respect is the study of dust acoustic waves [255]. Here, the dust is cold but moving due to the pressure exerted by other plasma components [256] or due to the external electric field [257].

Recent development

The subject of rogue waves in both pure and dusty plasmas has been studied widely [258–261]. There are dust-ion acoustic rogue waves [262, 263], plasma surface rogue waves [264], rogue waves in multi-component plasmas [260] and triplet rogue waves in plasmas [265], to name just a few. It has been shown that typical solar winds can excite plasma rogue waves in the interstellar regions [9]. Rogue waves have been investigated in space dusty plasma [259], in a medium with four-component multi-ion plasma [266], in a plasma with positive and negative ion fluids as well as non-extensive pairs of electrons and positrons [267]. Rogue waves appear in relativistic quantum plasma [268], in plasmas with dust grains [257, 269], and in the presence of the superthermal electrons in the earth atmosphere [270].

The theoretical description of rogue waves in all the aforementioned articles, as far as the author is aware, has been based on the nonlinear Schrödinger Equation (NLSE). This equation provides a solution for the envelope of the wave in moderate and high-frequency models.

Although rogue wave solutions of the NLSE are well-studied and have a myriad of applications, they are complex functions, and this might not be universally applicable to the situation where the functions of interest, such as the electrostatic potential, are real. Thus, the physical interpretation of the results could be misleading. For the moment, we just note this, but this issue is discussed in more detail later in this chapter. In addition, in many cases [271–273], rogue wave profiles are found from the solutions of the NLSE, which, in turn, is derived from one of the family of real-valued equations. These are either Korteweg-de Vries equation (KdV), the modified KdV (mKdV) or Gardner equations. Thus, these rogue waves must be originated by these real-valued equations rather than the NLSE itself. This fact has encouraged us to find an alternative, and mathematically much more straightforward, way to to describe rogue wave profiles using these real-function equations rather than NLSE. Another advantage of this approach is finding other interesting solutions. One example is a rational soliton solution which, to the best of the author's knowledge, has never been used in the plasma theory.

Our approach is based on the Gardner equation, which is fully presented in chapter 2, as the modeling tool. Although the Gardner equation has been used in dusty plasmas quite frequently, starting with the pioneering work of Rao, Shukla and Yu [198], the full set of applicable solutions has not yet been revealed. The well-known steady state solutions of the Gardner equation include its soliton solutions. Here, we present three other solutions that are relevant to the subject of rogue waves. These include (i) the lowest order rational soliton, (ii) the first and (iii) the second order rogue waves. The latter two were unknown before and they are the most suitable candidates for description of rogue waves in dust acoustic plasmas in the small-amplitude approximation.

5.1 Model

Following [198], let's consider a dusty plasma consisting of three components: (i) negatively charged, cold heavy dust particles, (ii) electrons and (iii) ions obeying Boltzmann distribution functions with temperatures T_e and T_i, respectively. For a one-dimensional model of low frequency acoustic wave propagation in such a plasma, the dynamics of the dust particles is governed by the following set of equations [198]. The first is the continuity equation for dust particles,

$$\frac{\partial n}{\partial t} + \frac{\partial (nv)}{\partial x} = 0, \tag{5.1}$$

where n is the density of dust particles, v is their velocity, and t and x represent time and space. The second is for the velocity field,

$$\frac{\partial v}{\partial t} + v\frac{\partial v}{\partial x} = \frac{Ze}{m}\frac{\partial \phi}{\partial x}, \tag{5.2}$$

where ϕ is the electrostatic potential, m is mass of the particles and $-Ze$ is their charge. Finally, we have the Poisson equation for the potential ϕ:

$$\frac{\partial^2 \phi}{\partial x^2} = -4\pi e(n_i - n_e - Zn), \tag{5.3}$$

where e is the elementary electron charge; n_i and n_e are the ion and electron densities which obey the Boltzmann distribution function and can be approximated through the functions of equilibrium densities, n_{i0} and n_{e0}:

$$n_i = n_{i0} \exp\left[-\frac{e\phi}{T_i}\right] \tag{5.4}$$

and

$$n_e = n_{e0} \exp\left[\frac{e\phi}{T_e}\right]. \tag{5.5}$$

One can expand the above-mentioned equations assuming the electric potential energy on dust particles is much smaller than the kinetic energy of electrons and ions, viz. T_e and T_i. Equations (5.1) to (5.5), together with the condition of quasi-neutrality of the plasma in equilibrium,

$$n_{i0} = n_{e0} + Zn_0, \tag{5.6}$$

where n_0 is the equilibrium number density of the dust particles, form a closed mathematical system.

The issue of interest here, in this medium, is the propagation of low frequency waves which take the form $\exp(ikx - i\omega t)$, where ω is the frequency and k is the wave-number of the waves. The dispersion relation for these waves in the long wavelength limit $k\lambda_{De} << 1$, where $\lambda_{De} = \sqrt{T_e/4\pi n_0 e^2}$, can be written as

$$\frac{\omega}{k} = \beta V_s$$

where $\beta = \sqrt{Z(\delta-1)/(1+\eta\delta)}$, $\delta = n_{i0}/n_{e0}$, $\eta = T_e/T_i$, and $V_s = (T_e/m)^{(1/2)}$.

After eliminating n_i, n_e and v from equations (5.1)-(5.6), the electrostatic potential in the small-amplitude regime can be found as [198, 274, 275]:

$$\frac{\partial\phi}{\partial t} + \beta V_s \frac{\partial\phi}{\partial x} - \sigma\phi\frac{\partial\phi}{\partial x} + \rho\phi^2\frac{\partial\phi}{\partial x} + \mu\frac{\partial^3\phi}{\partial x^3} = 0, \tag{5.7}$$

where

$$\rho = \frac{1}{4}\left(15\frac{Z^2 V_s}{\beta^3} - \beta V_s \frac{\delta\eta^3 + 1}{1+\eta\delta}\right),$$

$$\sigma = \frac{1}{2}\left(3\frac{ZV_s}{\beta} - \beta V_s \frac{\delta\eta^2 - 1}{1+\eta\delta}\right)$$

and

$$\mu = \frac{1}{2}\frac{\beta V_s}{1+\delta\eta}\lambda^2{}_{De}.$$

This equation can be further transformed using variables in the moving frame:

$$x = x' + \beta V_s t', \qquad t = t'.$$

Normalising these variables:

$$\tau = \frac{\sigma^3}{\rho\sqrt{\mu\rho}}t', \qquad \xi = \frac{\sigma}{\sqrt{\mu\rho}}x', \tag{5.8}$$

and the function:

$$\psi(\tau,\xi) = -\frac{\rho}{\sigma}\phi(\tau,\xi), \tag{5.9}$$

we obtain

$$\psi_\tau + \psi\psi_\xi + \psi^2\psi_\xi + \psi_{\xi\xi\xi} = 0. \tag{5.10}$$

This equation is well known as the Gardner equation.

Rescaling in Eqs.(5.8) requires the condition $\rho\mu > 0$, which is always satisfied since η and $\delta > 1$, thus both ρ and σ are positive and non-zero. Comparison of the nonlinear terms in Eq.(5.7) shows that the coefficient σ responsible for quadratic effects should be much smaller than the cubic coefficient ρ. This can be linked to a plasma phenomenon known as the near-critical plasma composition [276]. This configuration appears at specific densities of plasma components and specific ratio of electron and ion temperatures. Strictly speaking, the critical configuration does not exist in this model since δ and η both are positive. However, the quadratic coefficient σ is small compared to ρ, leading to a near-critical condition.

This relation between the plasma parameters is shown in Fig.5.1. This figure clearly demonstrates that for typical values of δ and η, the quadratic coefficient is very small compared to the cubic coefficient. When η and δ are fixed, the potential ϕ is directly proportional to ψ. Typically, when the density of the dust particles is in the interval from $n_0 = 10^3 m^{-3}$ to $n_0 = 10^5 m^{-3}$, more electrons are absorbed by dust than ions and the value of $\delta \equiv n_{i0}/n_{e0}$ varies from 1 to 1.8.

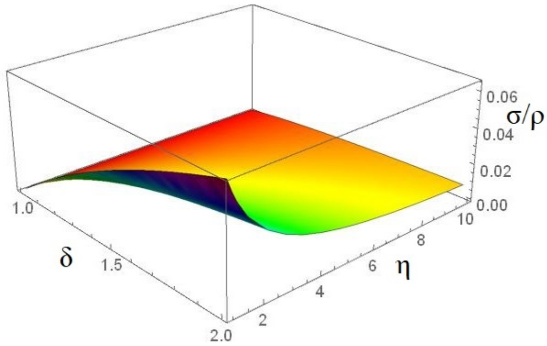

Figure 5.1: *The influence of parameters δ and η on the transformation factor of Eq.(5.9), i.e. $\frac{\sigma}{\rho}$, from ψ to the potential ϕ.*

Below, we present the solutions of the (normalised) Gardner equation (5.10). They are transformed back to the dust potential ϕ, given by the equation (5.7). The latter is then represented in the figures. In all figures provided here, the condition $|\phi_{max}| << 1$ is satisfied in accordance with our approach. Before presenting solutions of the Gardner equation (5.10), we give a general scaling transformation that significantly extends the range of particular solutions.

5.2 The family of soliton solutions

Eq.(5.10) can support a wide range of solutions. One of the most widely-used solutions of this equation is the soliton solution [168, 277–279]. In contrast to these papers, we write the soliton solutions in the form of a family with a free real parameter α:

$$\psi(\tau,\xi) = \frac{1-\alpha^2}{\alpha\left\{\cosh\left[\frac{\sqrt{1-\alpha^2}(\alpha^2(6\xi+\tau)-\tau)}{6\sqrt{6}\alpha^3}\right]+\alpha\right\}}. \tag{5.11}$$

Here, the amplitude and velocity of the soliton are controlled by the arbitrary real parameter α. The range of this parameter is restricted by the condition $|\alpha| \le 1$ and $\alpha \ne 0$. The amplitude of the soliton $((1-\alpha)/\alpha)$ is negative when $\alpha < 0$ and positive when $\alpha > 0$. The background is zero for any

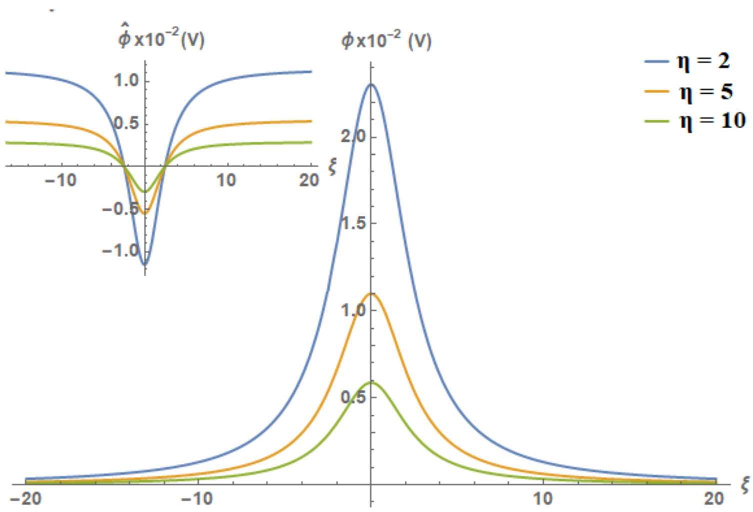

Figure 5.2: *The first order bright (ϕ) and dark ($\hat{\phi}$) (inset) rational soliton solution of the Gardner equation, given by Eq.(5.12) for any t. Here, $\delta = 1.2$ and $\eta = 1$, 5 and 10 are shown by blue, orange and green, respectively. The amplitude of the potential decreases as η increases. The blue curve has highest maximum in the main panel, and lowest minimum in the inset. The green curve has lowest maximum in the main panel, and highest minimum in the inset.*

values of α. The velocity of the soliton, $v_s = (1-\alpha^2)/(6\alpha^2)$, is always positive. It does not depend on the sign of α. Thus, Eq.(5.11) defines a one-parameter family of soliton solutions with the parameter within the interval $-1 < \alpha < +1$. Formally, for very small values of $|\alpha|$, the amplitude of the dust potential, ϕ, may violate the small-amplitude criterion. In order to avoid this, we have to impose the restriction $\sigma/\rho < |\alpha| < 1$. Here, we assumed that $\rho/\sigma >> 1$, which is always valid. Consequently, the maximum soliton velocity is $v_{s(max)} \approx \rho^2/6\sigma^2$. This family can be significantly extended using the scaling transformation (2.4) by adding one more parameter (κ) to the family.

5.3 Rogue waves

Rogue waves are commonly associated with rational solutions of an evolution equation. This is the case for the NLSE, Hirota equation, mKdV and even KdV. Let us begin with the lowest order rational solution of the Gardner equation. It can be found as the limiting case $\alpha \to -1$, of the solution solution (5.11) that reduces to the first order rational solution which can be expressed as [125]:

$$\psi(\tau,\xi) = -\frac{12}{\xi^2+6}. \tag{5.12}$$

This represents a stationary (τ-independent) soliton-type solution of Eq.(5.10). It is not a rogue wave that is localized both in τ and ξ. Solution (5.12) is given in normalized form. Returning to the electric potential $\phi(\tau,\xi)$, this solution, for selected parameters, η and δ, is shown in Fig.5.2.

When the normalized potential ψ is a bright (or dark) solution, the electric potential ϕ, obtained from Eq.(5.9), reverses and becomes a dark (or bright) solution. In the figures presented below, dark and bright solutions of the normalized potential ψ, are transformed to bright and dark solutions ϕ and $\hat{\phi}$, for the dust electric potential, respectively. It can be seen from Fig.5.2 that the amplitude of the electric potential strongly depends on two important factors, η and δ. The amplitude of the solution does satisfy the criterion of its smallness, viz. $|\phi_{max}| \approx 0.023 < 1$.

The second order rogue wave solution is given by [125]

$$\psi_2(\tau,\xi) = -1 - \frac{36(108 - \xi^4 - 36\xi^2 + 24\xi\tau)}{(\xi^3 - 18\xi + 12\tau)^2 + 54(\xi^2 + 6)^2}. \tag{5.13}$$

The method of its derivation has been presented earlier in chapter 2. In contrast to the lowest order solution (5.12), solution (5.13) depends on both τ and ξ variables. The polynomial in the denominator of (5.13) is sixth-order in ξ and second-order in τ, meaning that the fraction on the right-hand-side goes to zero as ξ and τ approach infinity. Consequently, the background of this solution is -1. The minimum, at the origin, is -3. According to Eq.(5.9), ψ (normalized potential) has to be converted to the potential ϕ. Therefore, it is expected that the dust potential will have a maximum, which is localized, three times larger than its background. The shape of the potential, ϕ, calculated using the parameters $\delta = 1.2$ and $\eta = 2$, is shown in Fig.5.3. It clearly shows a rogue wave at the origin with an amplitude around 0.035 , while the background is around 0.01. This maximum value meets the small-amplitude criterion ($|\phi_{max}| < 1$).

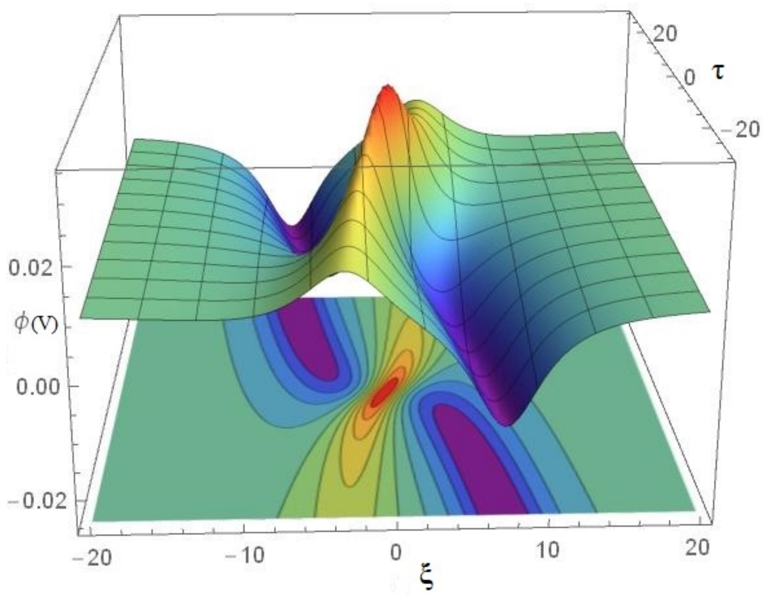

Figure 5.3: *The second order rational solution to the Gardner equation showing a rogue wave at the origin. Potential ϕ is calculated from ψ, Eq.(5.13), using Eq.(5.9) with parameters, $\delta = 1.2$ and $\eta = 2$.*

The third order rational solution is given by [125]:

$$\psi_3(\tau,\xi) = -72\,\frac{G(\tau,\xi)}{D(\tau,\xi)} \tag{5.14}$$

where,

$$\begin{aligned}G(\tau,\xi) &= 5400\left(\tau^2-18\right)\xi^4 - 32400\left(2\tau^2+27\right)\xi^2\\ &+43200\left(\tau^2+54\right)\tau\xi + 194400\left(5\tau^2+27\right)\\ &-4320\tau\xi^5+259200\tau\xi^3+\xi^{10}+90\xi^8+7560\xi^6,\end{aligned}$$

and

$$\begin{aligned}D(\tau,\xi) &= 2160\left(\tau^2+234\right)\xi^6+97200\left(2\tau^2+45\right)\xi^4\\ &-86400\tau\left(\tau^2-108\right)\xi^3-3499200\left(\tau^2-27\right)\xi^2\\ &+777600\left(2\tau^2-135\right)\tau\xi+129600\left(4\tau^4+594\tau^2+729\right)\\ &+120\tau\xi^9-233280\tau\xi^5+\xi^{12}+36\xi^{10}+4860\xi^8.\end{aligned}$$

The minimum of this solution is -4 (at the origin), while the background is -1, as the denominator D is a higher power polynomial than the numerator, G. Again, using Eq.(5.9) allows us to convert the normalized potential to the potential for the dust particles. Thus, the maximum, which is localized, is expected to be around four times larger than the background. The result, for particular values of η and δ, is shown in Fig.5.4. The profile clearly shows a rogue wave at the center with an amplitude of 0.044. This maximum value meets the small-amplitude criterion and it is thus physical and applicable.

The rescaled potential ϕ for the second and third order solutions is shown in figures 5.3 and 5.4. These figures demonstrate the influence of the plasma parameters, η and δ, on the characteristics of these solutions. In each case, the parameter η simply rescales the amplitude of the wave, although the rescaling is nonlinear. The smaller the value of η, the larger is the rogue wave. The maximum values are roughly doubled when the ratio of the electron and ion temperatures is doubled. Interestingly, the scaling transformation (2.4) can be used to reshape a solution in order to adjust it for given initial conditions. Having a free parameter, κ, that can be changed continuously allows us to make the adjustment over a wide range of shapes. It should be remembered that the background also changes with κ. Thus, the background may be the decisive parameter in choosing κ. However, the restriction in choosing this parameter is that the amplitude of rogue waves must satisfy the criterion discussed above.

In order to illustrate the dramatic influence of the parameter κ on rogue wave solutions, we choose two values for it: $\kappa = +1$ and $\kappa = -1$. When changing the sign of κ, the shape of the rogue wave is inverted, i.e. it is transformed from a 'bright' one to a 'dark' one, or *vice versa*. Examples of this conversion are shown in Fig.5.5 and Fig.5.6 for the second and third rational solutions, respectively. They show the rogue wave profiles at $\tau = 0$, i.e. in the middle of the wave evolution when the amplitude is maximal. In the main panel, the parameter $\kappa = +1$. The inset of the same

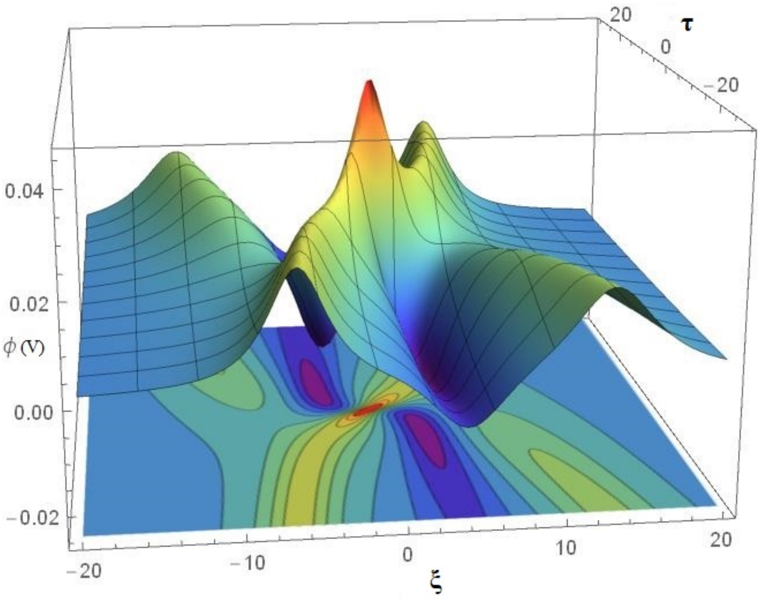

Figure 5.4: *The third order rational solution of the Gardner equation in the form of a rogue wave. Potential, ϕ, is recovered from ψ, Eq.(5.14), using Eq.(5.9) with parameters,* $\delta = 1.2$ *and* $\eta = 2$.

figure shows the rogue wave in the case $\kappa = -1$. The rogue wave here is inverted and becomes a 'dark' rogue wave. These plots also show the influence of the parameter η on the rogue wave shapes.

The wave profiles shown in Figs.5.5 and 5.6 are particular cases. These plots also show the influence of the parameter η on the rogue wave shapes. As can be seen from the three curves, in each case, the parameter η simply rescales the amplitude of the wave, although the rescaling is nonlinear. The smaller the value of η , the larger is the rogue wave.

5.4 Discussion

The sharp localised peaks in the figures presented here can be recognised as rogue waves for the electric potential. Although the profile of the electric potential is relatively small ($10^{-2}V$), these peaks are 3 times the background for the second-order rational solution and 4 times the background for the third-order one. This fact shows that they, indeed, represent real-valued rogue waves in a dust-acoustic plasma.

Mathematically, all solutions provided here have an inversion-reflection symmetry, i.e. $\phi(-t,-x) = \phi(t,x)$, as can be observed in Figs. 5.3 and 5.4. On the other hand, the lowest order solution (5.12) is a stationary 'soliton' with a constant (zero) velocity. A constant velocity could be added to this soliton using the transformation of Eq.(2.4). This transformation changes not only the velocity, but the amplitude and the background of the solution. In this way, the bright soliton can be

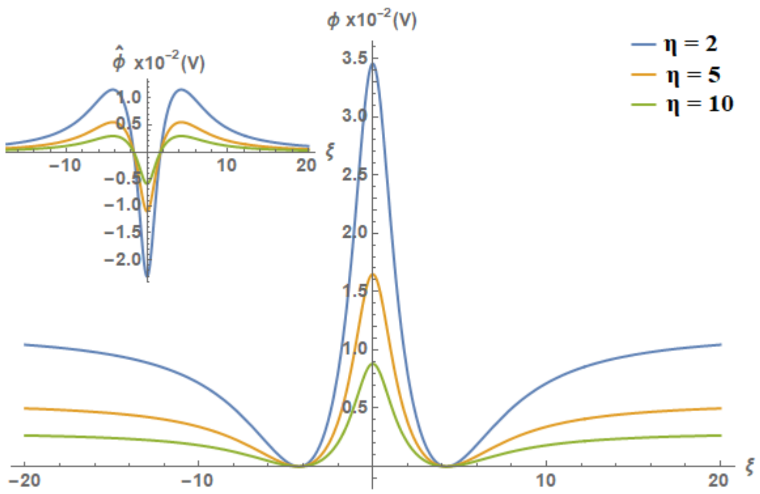

Figure 5.5: *The influence of parameters κ and η on the second order rogue wave profile at $\tau = 0$. The main panel shows the case $\kappa = +1$ while the inset corresponds to the case $\kappa = -1$. The three curves shown by blue, orange and green in each case, correspond to $\eta = 2$, $\eta = 5$ and $\eta = 10$ respectively. In all cases, $\delta = 1.2$. The blue curve has highest maximum in the main panel, and lowest minimum in the inset. The green curve has lowest maximum in the main panel, and highest minimum in the inset.*

converted to dark one and *vice versa*.

Higher order solutions, Eqs.(5.13) and (5.14), may be interpreted as a collision of such 'solitons'. Moreover, rogue waves at the origin can also be converted to dark ones. This conversion simultaneously changes the background. This property is unique for the rogue waves of the Gardner equation. Clearly, the choice of the solution in an experiment is dictated by initial conditions.

The amplitude of the rational solution presented here by equations (5.12), (5.13), and (5.14) depends on the order of the solution (see table 2.1 in chapter 2). As stated above, the scaling transformation in our model should be restricted to meet the small-amplitude criterion. This may impose constrains on the choice of κ, so that roughly $|\kappa| < \rho/\sigma j$, where j is the order of the solution. We also assume that $\rho/\sigma >> 1$ is always true. This limitation still admits a wide range of values for the parameter κ. For example, when $\delta = 1.8$ and $\eta = 2$, κ can be chosen from the interval $(-15, 15)$ for the second rational solution and from the interval $(-10, 10)$ for the third-order one. This restriction may vary from one case to another and this free parameter should be adjusted to particular plasma conditions.

The value of δ typically varies roughly from 1 to 1.8 because more electrons are absorbed by dust than ions when the density of the dust particles is in the range from $10^3 m^{-3}$ to $10^5 m^{-3}$. Thus, the value $\delta = 1.2$ is a reasonable choice, as it is compatible with the experimental observations in [251, 280]. When we choose $\eta = 2$ and $\delta = 1.8$, the amplitude of the potential ϕ increases roughly

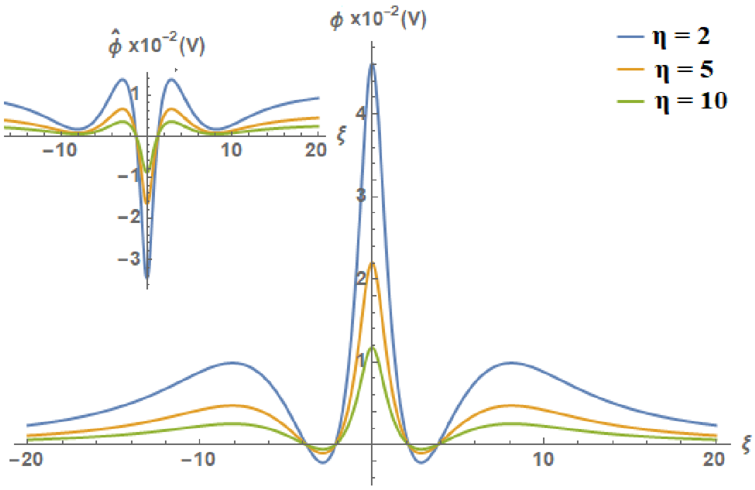

Figure 5.6: *The influence of parameters κ and η on the third order rogue wave profile at $\tau = 0$. The main panel shows the case $\kappa = +1$ while the inset corresponds to the case $\kappa = -1$. The three curves shown by blue, orange and green in each case, correspond to $\eta = 2$, $\eta = 5$ and $\eta = 10$ respectively. In all cases, $\delta = 1.2$. The blue curve has highest maximum in the main panel, and lowest minimum in the inset. The green curve has lowest maximum in the main panel, and highest minimum in the inset.*

by a factor of three. Fig.5.7 shows the potential of the three rogue wave solutions at $\tau = 0$ for a fixed $\eta = 2$ and two different values of δ. This figure illustrates that a change of δ from 1.2 to 1.8 leads to a visible increase in the amplitude.

It can also be seen from Fig.5.7 that the width of the rogue wave at $\tau = 0$ decreases with the order of the solution while the amplitude increases. The second order rogue wave has 1.5 times the amplitude of the first order solution. At the same time, its width shrinks to approximately ≈ 0.6 times its former value. The same scenario also occurs for the third order solution.

The real advance in using the Gardner equation for modeling rogue waves is that its solutions are real. It is directly applicable to the electrostatic potential ϕ which is real by definition. There is no need to employ rogue wave solutions of the NLSE, as these require additional unnecessary assumptions for converting to a real potential from complex ones.

In order to expand on this fact, we can start with the seminal paper written by R. Grimshaw *et al* [281]. In that paper, the authors derived the NLSE from the Gardner equation, substituting real solutions by an addition of a complex function and its complex conjugate, and sometimes a series of infinite complex solutions and their complex conjugates. This method allows one to transform a real equation into the NLSE. Obviously, there is no doubt about this method. However, to interpret the solutions, the shape of a rogue wave appears as the absolute value of the complex solution. Therefore, this may not represent the shape of the real quantity which would have been sought.

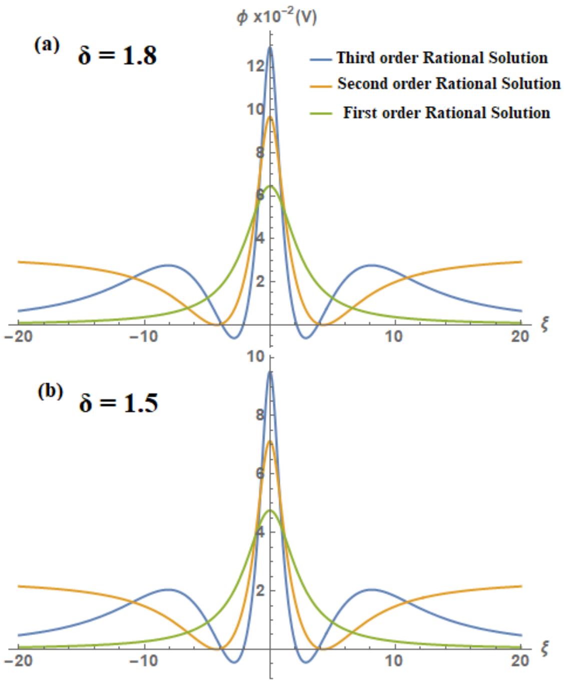

Figure 5.7: *Potential ϕ at $\tau = 0$ for three lowest order rational solutions when $\eta = 2$. The plot at the top (a) is calculated for $\delta = 1.8$ while the lower one (b) is for $\delta = 1.5$. The lowest order solution, in each case, is shown by the light green curve; these have the lowest maxima. The second-order rogue wave is in yellow. The third-order rogue wave is in blue; these have the highest maxima. Increase of δ leads to the increase of rogue wave amplitudes.*

5.5 Conclusion

We have provided a theory for novel rogue wave structures among nonlinear dust-acoustic waves for a long wavelength model in a plasma with cold and heavy dust particles at thermal equilibrium. Our model is based on the Gardner equation, which is a generic model for weakly nonlinear and dispersive wave propagation. New solutions suggest that a considerable amount of energy (or electric charge) could become concentrated in a relatively small volume of space at a certain time. These are features of rogue waves that are similar to those in the ocean or in fibre optics.

Rogue waves in our model have soliton-like precursors before the strong amplitude event and a similar continuation after it. This behaviour is different from the rogue waves of the NLSE which 'appear from nowhere and disappear without a trace' [16]. The presence of a scaling transformation (2.4) is another distinctive feature of rogue waves in our model, and this allows them to vary continuously from 'bright' rogue waves to 'dark' ones. Our approach can also be applied to nonlinear waves in other kinds of plasmas, like ultra-cold [282] and magnetized neutral plasmas [283].

Moreover, we have found that the amplitude, the background and the velocity of these structures can vary over large but finite intervals. This interval varies from one model to another and should be carefully adjusted for the plasma parameters. One of the consequences of this variability is the possibility of a transformation from ‘bright’ to ‘dark’ rogue waves, and this is a unique feature of the waves considered here. It also has been found that the dust electric potential amplitude of these rogue waves strongly depends on the ratio between the ion and electron temperatures η and densities δ in the plasma.

CHAPTER 6

LAGRANGIAN APPROACH TO THE THEORY OF OPTICAL ROGUE WAVES: INTEGRABLE CASES

Total internal reflection is the physical effect behind the long distance light propagation in optical fibres. The first optically transparent glass fibre was made in 1966 [284]. Low loss fibre (20 dB/km) has been first produced in 1970 [285]. The level of loss has been reduced to 0.2 dB/km in later works [286]. At high intensity of optical pulses achievable in fibres, glass becomes a non-linear medium [32, 228]. Hasegawa and Tappert in 1974 discovered that nonlinearity may lead to propagation of solitons [39]. These are pulses that precisely balance the nonlinear and dispersion effects [52] thus preserving their shape. The term 'soliton' has been coined by Zabusky and Kruskal earlier in 1965 [195]. The existence of solitons in optical fibre has been experimentally confirmed by Mollenauer, Stolen and Gordon [40]. It was suggested that optical solitons can be used for transmitting bits of information in optical communication systems [287].

Apart from the application of solitons in optical communication systems, they can be used for information processing. The benefit of using solitons is that they preserve their shapes after collisions. Duration of solitons can be in the time scale of femtoseconds [288, 289]. Generally, the NLSE has an infinite number of solutions. They describe many interesting phenomena including optical rogue waves, i.e. "the waves appear from nowhere and disappear without a trace" [16]. Solli, Ropers, Koonath and Jalali were first to observe rogue waves in an optical fibre [60]. This subject has been quickly growing with many research publications in diverse areas of optics. These include supercontinuum generation [68], pulse generation in passively mode-locked lasers [82, 290], nonlinear waves in fibers as well as optical cavities [81] and the propagation of light in photonic crystal fibers [291].

The propagation of short pulses in a single-mode fiber with reasonable accuracy can be described by the NLSE [52]. This equation models counterbalancing of the nonlinearity and dispersive effects in the lowest orders. However, other higher-order linear and/or nonlinear terms should be added to the NLSE in order to describe the propagation of ultra-short pulses in optical fibres with higher accuracy. These include the third-order dispersion, ψ_{ttt} [230, 292]; fourth-order dispersion, ψ_{tttt} [293]; a "quintic" adjustment to the Kerr nonlinearity [230], $|\psi|^4\psi$; and the Raman downshift effect [38], $\tau_R \psi(|\psi|^2)_t$ to name a few.

Similarly, water wave propagation in "deep" water can be influenced by assorted physical phenomena [294], such as wind [295], viscosity [296], and bottom friction [294]. These higher-order effects might potentially influence the dynamics of rogue waves. Such impacts can significantly change the water wave shapes. Then, finding exact solutions in the form of rogue waves is difficult or impossible. Given this fact, finding approximate solutions can be a good approach.

Scientists have developed several approximate methods such as Lagrangian technique [297], variational method [298], and the method of moments [299]. These approaches have been used to solve practical problems based on the NLSE with higher-order terms. The essence of the Lagrangian technique is finding a trial function, which can be optimised using minimisation of a Lagrangian. The choice of the trial function is crucial. In the case of solitons, this could be a sech function with variable width and amplitude. In the case of rogue waves, it could be a rational solution with variable coefficients in polynomials. The accuracy of representation of the actual solution requires more free parameters in the trial function. However, the difficulty in solving the corresponding Euler-Lagrange equations also increases. Thus, some optimum has to be found.

The Lagrangian approach allows us to reduce dynamical systems from infinite-dimensional to finite-dimensional, thus allowing us to study them, at least at a qualitative level. The early practical use of it in studying solitons dates back three decades, when the variational perturbation method has been developed to analyze the evolution of solitons in the presence of perturbations [298, 300]. Since then, it has been used in a wide variety of physical applications ranging from nonlinear dissipative pulse propagation [301] to correlations in charged polymers [302]. A few examples of the application of this technique are: analyzing the stability of dissipative solitons of the complex cubic-quintic Ginzburg-Landau equation [303], finding the impact of an external magnetic field on dissipative solitons [304], perturbation of solitons of the Ginzburg-Landau equation [305], studying the changes in localized patterns [306], describing dissipative systems in passively mode-locked lasers [307] and analyzing the propagation of a dressed solitary wave in filtered amplification [308].

Another technique is the ‘method of moments’ [309]. The method is based on "integrals of motion". These integrals are invariant when the evolution equation is not perturbed. However, in the presence of the perturbation, they do evolve. This leads to a set of dynamical equations for parameters of a trial function. This technique might give results which are similar to, or in some cases, even the same as those obtained from the minimization of the Lagrangian [107]. The two methods have been compared explicitly when finding solutions to the cubic-quintic complex

Ginzburg-Landau equation in [310]. We expect that the approximate solution should coincide with the exact one when the equation under study is integrable.

Being applied to solitons, the above techniques have never been used for studying rogue wave solutions. Exceptions are the recent works of the author and his colleagues [2, 130] which are presented below. In contrast to solitons, which are localized either in time or in space, rogue waves are solutions of the evolution equations that are localized both in time and in space. Besides, the rational functions involving polynomials may have less mathematical flexibility than functions used in the soliton theory. Consequently, extending the Lagrangian approach to the case of rogue waves is far from being straightforward. The double localisation means that additional efforts are required in applying the formalism. Another downside of using the Lagrangian approach is that finding the Lagrangian density that can handle the extra terms (linear or nonlinear) is not always straightforward. At the end of this chapter, various forms of perturbation terms and the corresponding Lagrangian densities are given. This is also done for the infinitely-extended NLSE. These results might ease the calculations in practical applications of the technique.

Chapter outline

First, a succinct review of using the Lagrangian approach is given. Then, this method will be examined on some integrable equations, including the NLSE without perturbation, the Hirota equation, the Lakshmanan - Porsezian - Daniel (LPD) equation and the Kundu-Eckhaus (KE) equation, to obtain the solutions representing the rogue waves. These solutions have been previously found by other methods; however, this is common practice to do so with this approach.

6.1 Basic equations

We start with the extended nonlinear Schrödinger equation that describes propagation of ultra-short pulses in optical fibres:

$$i\psi_x + \frac{1}{2}\psi_{tt} + |\psi|^2\psi = R, \tag{6.1}$$

where R, for example, indicates the additional terms in the form

$$\begin{aligned} R \;=\; & \tau_R\psi(|\psi|^2)_t - \nu|\psi|^4\psi - \nu_{2n}|\psi|^{2n}\psi \\ & + i\gamma_3\psi_{ttt} - d_4\psi_{tttt} - d_6\psi_{tttttt} - is(\psi|\psi|^2)_t, \end{aligned} \tag{6.2}$$

where n is an integer, $n = 3, 4, \cdots\infty$. Here ν represents a nonlinearity which is of higher order than a Kerr-law response for the system. The first term is the intrapulse Raman scattering with a constant coefficient τ_R, the second and third terms are the quintic and the higher even-order nonlinearities, the fourth, fifth and sixth terms show the effect of the third, fourth and sixth-order dispersions, while the last term is responsible for the self-steepening effect. To start with, we restrict ourselves to these examples of higher-order terms that are commonly studied in the literature. Other types of terms can be considered using the same technique as we discuss here.

Equation (6.1) in general is not integrable and cannot be solved exactly. Therefore, we have a choice of finding approximate solutions. It is less obvious that the Lagrangian approach can be applied to rogue wave solutions which are localized both in space and time, in contrast to soliton solutions that are localized only in either time or space. In this chapter, we show that the technique can be applied to rogue waves when the exact solutions are available. The next chapter will be devoted to the non-integrable cases for which no exact solutions exist. In particular, it is applied to the higher-order extensions of the NLSE.

The use of the variational integral and Euler equations has been explained in [311], where the Lagrange density is introduced and its relation to the Euler-Lagrange equations for the Schrödinger equation and other conservative equations is also given. We employ the Lagrangian

$$L = \int_{-\infty}^{\infty} L_d \, dt \tag{6.3}$$

where L_d is the Lagrangian density and we have

$$L_d = -\frac{i}{2}\left(\psi^* \frac{\partial \psi}{\partial x} - \psi \frac{\partial \psi^*}{\partial x}\right) + \frac{1}{2}\left|\frac{\partial \psi}{\partial t}\right|^2 - \frac{1}{2}|\psi|^4 \tag{6.4}$$

for field $\psi(x,t)$. When dealing with solutions on a constant background, it is common practice to subtract off any constant part of L_d.

If we apply the Euler-Lagrange equations to the above equation, we obtain:

$$-\frac{\partial L_d}{\partial \psi^*} + \frac{\partial}{\partial x}\frac{\partial L_d}{\partial \psi^*_x} + \frac{\partial}{\partial t}\frac{\partial L_d}{\partial \psi^*_t} - \frac{\partial^2}{\partial t^2}\left(\frac{\partial L_d}{\partial \psi^*_{tt}}\right) = R,$$

where a subscript x or t means derivative with respect to that variable, the star * indicates complex conjugate and R indicates the added higher-order terms.

For a trial solution containing several parameters $c^{(j)}, j = 1, 2 \ldots.$, the standard variational approach can be modified to allow for dissipative terms [304, 307, 310, 312]. In this way, we obtain a separate equation

$$\frac{d}{dx}\left(\frac{\partial L}{\partial c_x^{(j)}}\right) - \frac{\partial \, L}{\partial c^{(j)}} = 2Re\left(\int_{-\infty}^{\infty} R \frac{\partial \, \psi^*}{\partial c^{(j)}} dt\right) \equiv J[c^{(j)}; R] \tag{6.5}$$

for each parameter $c^{(j)}$. The set of Eqs.(6.5) comprise the reduced dynamical system for the rogue wave parameters. In other words, the wave profiles and, more generally, the wave evolution are described by the variation of these parameters.

6.2 Peregrine rogue wave

In order to illustrate the application of the above technique to solutions which are localized both in time and space, we first apply it to the simplest case, *viz.* the lowest-order rational solution of the NLSE. Thus, we first consider the case $R = 0$, i. e. the basic nonlinear Schrödinger equation,

$$i\psi_x + \frac{1}{2}\psi_{tt} + |\psi|^2\psi = 0,$$

and illustrate the idea using its known exact solution. Namely, we write the solution in the form of trial function

$$\psi = \left[4\,\frac{1+2ix}{c(x)+4t^2} - 1\right]\exp[ix] \tag{6.6}$$

with the intention of finding the unknown function, $c(x)$.

Following Eq.(6.4), we first write the Lagrangian,

$$L = -\frac{2\pi}{c(x)^{7/2}}\left[-xc(x)^2c'(x) - 14(4x^2+1)c(x) + 2c(x)^3 + 10(4x^2+1)^2\right],$$

where a prime mark denotes a derivative with respect to x. Eq.(6.5) allows us to write the equation relative to the unknown function $c(x)$:

$$-\frac{70\pi(4x^2+1)(-c(x)+4x^2+1)}{c(x)^{9/2}} = 0,$$

which results in

$$c(x) = 1 + 4x^2,$$

giving

$$\psi = \left[4\frac{1+2ix}{1+4x^2+4t^2} - 1\right]\exp[ix]. \tag{6.7}$$

Clearly, this is the well-known rogue wave solution of the NLSE [16]. In this case, the result is exact, as we deal with the integrable NLSE and we knew the form of the solution in advance. In general, the solutions are expected to be approximate.

6.3 General form of the trial function

As a next step, we allow for arbitrary functional R in the trial function. One of the consequences may be resizing of the rogue wave, say, in the x-direction. In order to take this into account, we extend the result of Eq.(6.7) by taking

$$\psi(x,t) = \left[4\,\frac{1+2iBx}{D_m(x,t)} - 1\right]e^{iF_m(x,t)}, \tag{6.8}$$

where

$$D_m(x,t) = r(x) + 4\left[t - t_0(x)\right]^2, \tag{6.9}$$

and

$$F_m(x,t) = x + a(x)[t - t_0(x)] - \theta(x), \tag{6.10}$$

with the function $t_0(x)$, $r(x)$ and $\theta(x)$ being responsible for the lateral motion, amplitude of the wave and change of the phase, respectively. Now, we apply the Euler-Lagrange formalism to the more general trial function (6.8).

For convenience, we split L_d into three parts:

$$L_d = L_{d1} + L_{d2} + L_{d3}$$

where

$$L_{d1} = -\frac{i}{2}\left(\psi^*\frac{\partial\psi}{\partial x} - \psi\frac{\partial\psi^*}{\partial x}\right) + a_1 a(x) t_0'(x) + h_1\theta'(x) - u_1,$$

$$L_{d2} = \frac{1}{2}\left|\frac{\partial\psi}{\partial t}\right|^2$$

and

$$L_{d3} = -\frac{1}{2}\left(|\psi|^4 - 1\right).$$

We need to integrate these terms over an infinite range in $y_1 \equiv t - t_0(x)$. The terms in odd powers of y_1 will integrate out to zero. In the remaining part of L_{d1}, a background is subtracted so that its limit is zero for high $|y_1|$. Then, taking $L_j = \int_{-\infty}^{\infty} L_{dj}\, dt$, we have $L = L_1 + L_2 + L_3$.

Taking the limit $\underset{y_1\to\infty}{lim} L_{d1}$ shows that it equals to

$$(a_1 - 1)a(x)t_0'(x) + (h_1 - 1)\theta'(x) - u_1 + 1,$$

with unknown functions $a(x), t_0'(x), \theta'(x)$. Setting this to zero shows that the constants needed here are $a_1 = h_1 = u_1 = 1$. Now, L_{d2} clearly approaches zero for large t or y_1, and so needs no level adjustment. For L_{d3}, we note that $\underset{y_1\to\infty}{lim}|\psi| = 1$, hence we subtract this background before integrating. We thence find:

$$L\frac{r^{7/2}(x)}{2\pi} = 14Xr(x) - 10X^2 + r(x)^2\left[a^2(x)X - 2a(x)X\, t_0'(x) - 2X\theta'(x) + Bxr'(x) + 4B - 4\right]$$

$$-r(x)^3\left[a^2(x) + 2B - 2a(x)t_0'(x) - 2\theta'(x)\right] \tag{6.11}$$

where $X = 4B^2x^2 + 1$.

Using Eq.(6.5), we define the left-hand-side terms of the equation related to parameter $c^{(j)}$ as:

$$S[c^{(j)}] \equiv \frac{d}{dx}\left(\frac{\partial L}{\partial c_x^{(j)}}\right) - \frac{\partial\, L}{\partial c^{(j)}} \tag{6.12}$$

for each parameter $c^{(j)}$.

So, using Eq.(6.11) above, the $a(x)$ term is

$$\frac{r(x)^{3/2}}{4\pi}\left[\frac{d}{dx}\left(\frac{\partial L}{\partial a'(x)}\right)-\frac{\partial\, L}{\partial\, a(x)}\right]=\frac{r(x)^{3/2}}{4\pi}S[a]=(r(x)-X)\left[a(x)-t_0'(x)\right]. \tag{6.13}$$

The $\theta(x)$ term is

$$\frac{r(x)^{5/2}}{2\pi}\left[\frac{d}{dx}\left(\frac{\partial L}{\partial \theta'(x)}\right)-\frac{\partial\, L}{\partial\, \theta(x)}\right]=\frac{r(x)^{5/2}}{2\pi}S[\theta]=[3X-r(x)]r'(x)-16B^2xr(x), \tag{6.14}$$

while the $t_0(x)$ term is

$$\frac{r(x)^{5/2}}{2\pi}\left[\frac{d}{dx}\left(\frac{\partial L}{\partial t_0'(x)}\right)-\frac{\partial\, L}{\partial\, t_0(x)}\right]=\frac{r(x)^{5/2}}{2\pi}S[t_0]$$

$$=2r(x)a'(x)[r(x)-X]-a(x)\left\{[r(x)-3X]r'(x)+16B^2xr(x)\right\}. \tag{6.15}$$

The $r(x)$ term is

$$\frac{r(x)^{9/2}}{\pi}\left[\frac{d}{dx}\left(\frac{\partial L}{\partial r'(x)}\right)-\frac{\partial\, L}{\partial\, r(x)}\right]=\frac{r(x)^{9/2}}{\pi}S[r]$$

$$=r(x)\left\{r(x)\{(3X-r(x))\left[a^2(x)-2a(x)t_0'(x)-2\theta'(x)\right]+12(B-1)\}+70X\right\}-70X^2. \tag{6.16}$$

Using Eq.(6.5), we define the influence of any functional R on the parameter $c^{(j)}$ as:

$$J[c^{(j)};R]=2Re\left(\int_{-\infty}^{\infty}R\,\frac{\partial\,\psi^*}{\partial\,c^{(j)}}\,dt\right). \tag{6.17}$$

Once R is given, we thus need to solve the four ordinary differential equations (ODEs), $S[c^{(j)}]=J[c^{(j)};R]$, with $c^{(j)}=\{a(x),t_0(x),r(x),\theta(x)\}$.

6.4 'General' Peregrine rogue wave

As a complicated example, we consider a rogue wave with an internal 'velocity' or 'skewness'. From previous experience, we know that this occurs for rogue waves of the Hirota equation [4] and for a multiplicity of extended equations with odd higher-order terms [5]. In order to describe this type of rogue wave, we take the solution in the general form (6.8). Since there are no perturbed terms on the left-hand-side of equation (6.1), i.e. $J[R]=0$, then all functions $S[r]$, viz. equation (6.16); $S[\theta]$, viz. equation (6.14); $S[t_0]$, viz. equation (6.15) and $S[a]$, viz. equation (6.13) should be zero. Thus, we obtain the 4 ODEs, and then solve the $S[a]=0$ equation by setting $a(x)=t_0'(x)$. By setting $S[\theta]=0$, we find:

$$r(x)\left[r'(x)+16x\right]-3\left(4x^2+1\right)r'(x)=0,$$

and we use its simplest solution, $viz.$ $r(x)=4x^2+1$.

Then the only remaining non-zero equation is:

$$[t_0'(x)]^2 + 2\theta'(x) = 0.$$

Now $t_0'(x)$ is a velocity, and the simplest solution is to take it as an arbitrary constant velocity, v, so $t_0'(x) = v$. Hence $t_0(x) = v\,x$ and $\theta(x) = -v^2 x/2$, so we have

$$\psi = \left[4\frac{1+2ix}{1+4x^2+4(t-vx)^2} - 1\right] e^{i\left[vt+\left(1-\frac{v^2}{2}\right)x\right]}. \tag{6.18}$$

The Galilean transformation of the NLSE is well-known (e.g. see Eq.(2.6) of [52]). The solution given by Eq.(6.18) agrees with that found by applying such a transform to the basic rogue wave of Eq.(6.7). It reduces to that lowest-order rogue wave equation (6.7) when $v = 0$. We can see that the Lagrangian approach works well for these simple illustrative cases. This encourages us to move up to more complicated cases, as given below. This moving form of the Peregrine rogue wave can be seen in Fig.6.1.

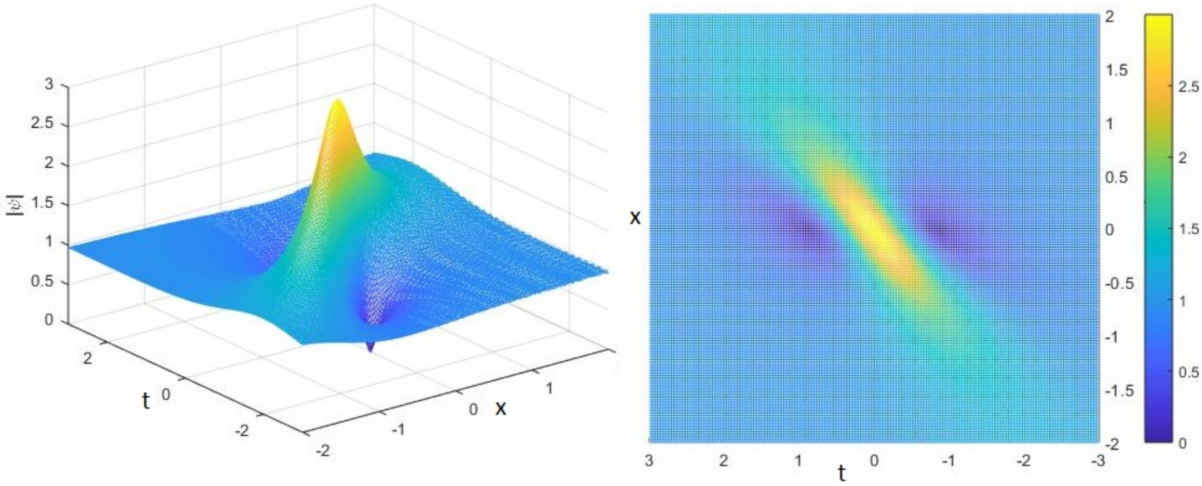

Figure 6.1: *The general form of the Peregrine rogue wave with the constant velocity, i.e. equation (6.18). Here, $v = 1$.*

6.5 Rogue waves of Hirota equation

In the Ultrashort Pulse (USP) regime, when the pulse width is less than 1 picosecond, the NLSE cannot give an accurate prediction. In solid-state lasers, for instance, where the width of solitons is less than 10 fs, the approximation is no longer valid. Thus, the higher-order dispersion terms should be taken into account. When the group velocity dispersion approaches zero, the third-order dispersion must be taken into account. Then, the propagation of nonlinear waves through an optical fiber is governed by:

$$i\phi_x + \frac{1}{2}\phi_{tt} + |\phi|^2\phi = -i\alpha_3\phi_{ttt},$$

where ϕ is the envelope of the nonlinear wave and $\alpha_3 = -\beta_3/(6|\beta_2|t_0)$. β_2, β_3 are, respectively, the second and third-order dispersion terms at the pulse central frequency. t_0 is related to the width of the ultra-short pulse launched into the fiber, $t_0 = L_D|\beta_2|$ and L_D is the dispersion length. Changing the variable in the above-equation as [313, 314]:

$$\psi = \phi - 3i\alpha_3\left(\phi_t + 2\phi\int_{-\infty}^{t}|\phi(t')|^2 dt'\right),$$

allows us to obtain the Nonlinear Schrödinger-Hirota equation or simply Hirota equation as:

$$i\psi_x + \frac{1}{2}\psi_{tt} + |\psi|^2\psi = i\alpha_3(\psi_{ttt} + 6|\psi|^2\psi_t),$$

after ignoring the higher order of α_3. This is a modification of the NLSE with the additional terms responsible for the third-order dispersion effect and time-delay correction to the cubic nonlinearity.

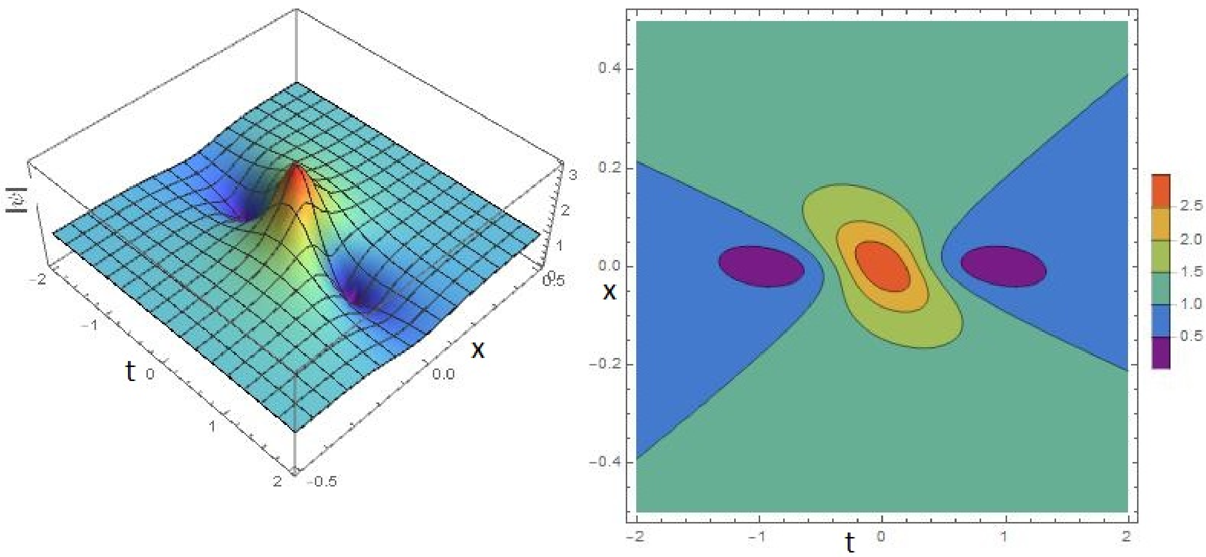

Figure 6.2: *The rogue wave solution for the 'full' Hirota equation with* $\alpha_3 = 1$ *and* $k = 1$*. This is in a good agreement with the result found in [4].*

This equation describes the propagation of nonlinear waves in a single-mode fiber in the presence of the third-order dispersion. The term 'full' is used here to show that this equation only in this form and with these fixed coefficients is integrable. Selecting other parameters may change the features of the equation and it may lose its integrability.
The additional terms in this equations are:

$$R = i\,\alpha_3(\psi_{ttt} + 6|\psi|^2\psi_t) \equiv R_h.$$

The right hand sides of the reduced dynamical system (6.5) for this equation take the form:

$$\frac{r(x)^{7/2}}{12\pi\alpha_3} J[a;R_h] = [X - r(x)]\left\{r(x)\left[\left(a^2(x) - 2\right)r(x) + 4\right] - 10X\right\} \tag{6.19}$$

and

$$\frac{r(x)^{9/2}}{2\pi\alpha_3\, a(x)} J[r;R_h] = 210X^2 + r(x)\{r(x)[a^2(x)(r(x) - 3X) + 6(6 - r(x) + 3X)] - 210X\}, \tag{6.20}$$

while $J[t_0;R_h] = J[\theta;R_h] = 0$.

Setting $r(x) = 1 + 4B^2x^2$ reduces the dynamical system and leaves only the equation for r, *viz.* $S[r] = J[r;R_h]$ to solve. It is straightforward to show that it can be solved with $a(x) = k$, an arbitary constant, $B = 6\alpha_3 k + 1$ and $\theta(x) = xc_0$ and $t_0 = -v_s x$, where $c_0 = k^2(c_1 + c_2\alpha_3 k)$ while

$$v_s = \alpha_3\left(1 - \frac{k^2}{2}\right)v_1 - k.$$

Hence,

$$\alpha_3 k^2(2c_2 + v_1 - 2) - 2\alpha_3(v_1 - 6) + (2c_1 + 1)k = 0.$$

This equation must be valid for all k and all α_3. Consequently, we obtain $c_1 = -\frac{1}{2}$, $v_1 = 6$ and $c_2 = -2$. Then, the functions $t_0(x)$ and $\theta(x)$ in the trial function (6.8) become:

$$\begin{aligned} t_0(x) &= x\left[3\alpha_3\left(k^2 - 2\right) + k\right], \\ \theta(x) &= -\frac{1}{2}k^2 x(4\alpha_3 k + 1). \end{aligned}$$

As it can be seen from the Fig.6.2, this outcome agrees well with the known exact result (with $\alpha_2 = \frac{1}{2}$) found in [5]. The velocity factor, $t_0'(x)$, can be zero for some combinations of k and α_3, thus, cancelling the effect of higher-order terms in the Hirota equation.

6.6 Rogue waves of Lakshmanan - Porsezian - Daniel (LPD) equation

A variety of models can describe the optical pulse propagation across a long-haul telecommunication fiber. One of those models is the LPD equation. This equation was first derived in 1988 and since then has received much attention. In optical fibers, this model explains the pulse propagation both in polarization-maintaining fibers and in birefringent optical fibers.

The LPD equation [3, 315] can be written as:

$$i\psi_x + \frac{1}{2}\psi_{tt} + |\psi|^2\psi = R[\psi(x,t)]$$

where

$$R = -\alpha_4\left(\psi_{tttt} + 6\psi_t^2\psi^* + 4\psi|\psi_t|^2 + 8\psi_{tt}|\psi|^2 + 2\psi_{tt}^*\psi^2 + 6\psi|\psi|^4\right) \equiv R_l.$$

The LPD equation contains the terms describing the fourth-order dispersion, quintic, Kerr and higher-order nonlinear dispersive terms. Hence, it can be used in practice for modelling the propagation of femtosecond USP across transoceanic distances. It can also model the nonlinear excitations in a one-dimensional biquadratic Heisenberg spin chain.

For this equation, the right hand sides of the dynamical system (6.5) are:

$$\frac{r(x)^{7/2}}{16\pi a(x)\alpha_4}J[a;R_l]=[r(x)-X]\Big\{r(x)\left[\left(a^2(x)-6\right)r(x)+12\right]-30X\Big\},$$

and

$$\frac{r(x)^{13/2}}{2\pi\alpha_4}J[r;R_l]=2772X^3+r(x)\Big\{r(x)\big[12a^2(x)(r(x)(r(x)[r(x)-3X-6]+35X)-35X^2)$$
$$+a^4(x)r(x)^2[3X-r(x)]-2r(x)(3r(x)[r(x)-3(X+4)]+70(3X+2))+28X(15X+91)\big]-5040X^2\Big\},$$

while $J[t_0;R_l]=J[\theta;R_l]=0$.

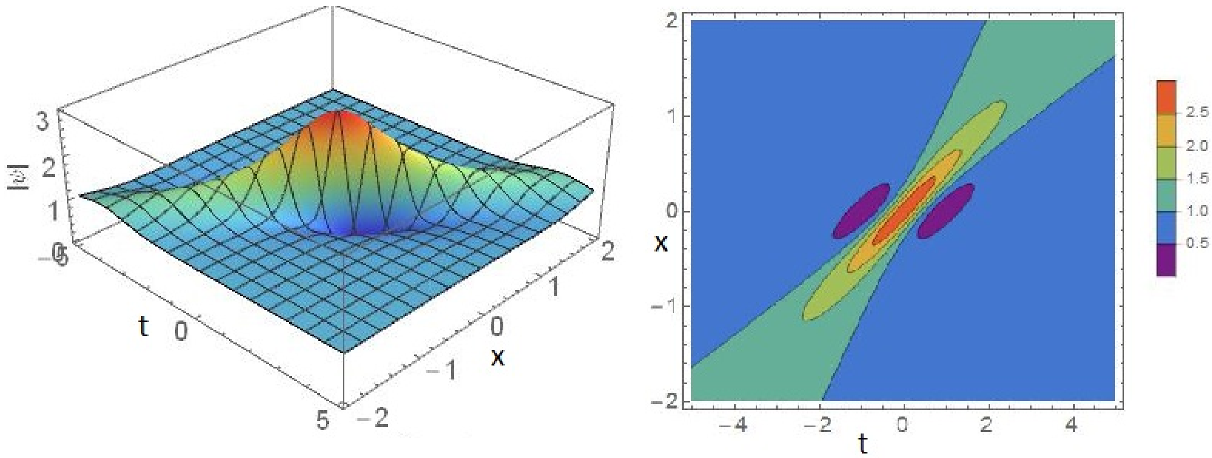

Figure 6.3: *The rogue wave solution of the LPD equation with $\alpha_4=0.05$ and $k=1$. This is in a good agreement with the result found in [5].*

Again, setting $r(x)=1+4B^2x^2$ reduces the system and leaves only the r equation, $S[r]=J[r;R_l]$ to solve. It is straightforward to show that it can be solved with $a(x)=k$, an arbitrary constant, $B=\alpha_4\left(b_1k^2+b_2\right)+b_0$, $\theta(x)=x\{3\alpha_4\left[\left(k^2-2\right)^2+n_2\right]+k^2n_1\}$ and $t_0=-v_e x$, where $v_e=k\left[\alpha_4\left(j_1+j_2k^2\right)-1\right]$.

Expanding $S[r]=J[r;R_l]$, we readily find the constants, $b_0=1, b_1=-12, b_2=12, j_1=-24, j_2=4, n_1=-1/2, n_2=-6$. Hence $B=1-12\alpha_4\left(k^2-1\right)$, and

$$\begin{aligned} t_0(x) &= -v_e\,x=-k\left[4\alpha_4\left(k^2-6\right)-1\right]x, \\ \theta(x) &= \left\{3\alpha_4\left[\left(k^2-2\right)^2-6\right]-\frac{k^2}{2}\right\}x. \end{aligned}$$

As it can be seen from the Fig.6.3, this outcome also agrees with the known exact result (with $\alpha_2=\frac{1}{2}$) found in [5]. Again, the velocity factor, $t_0'(x)$, is zero for some combinations of k and α_4.

6.7 Rogue waves of Kundu-Eckhaus equation

Similar to the NLSE, the Kundu-Eckaus eqaution (KEE) describes the wave propagation in optical fibres but it takes into account additional nonlinear effects [316]. It is a more accurate model for propagation of the USP in optical fibers. This model is also used in the theory of the femtosecond lasers and in chemistry studies in the time scales of femtoseconds.

$$i\psi_x + \frac{1}{2}\psi_{tt} + |\psi|^2\psi = R_K, \tag{6.21}$$

where R_K indicates additional terms in the form

$$R_K \quad = \quad 2ib\psi(|\psi|^2)_t - 2b^2|\psi|^4\psi, \tag{6.22}$$

where the first term is responsible for the Raman delay, while the second term describes the quintic nonlinearity. Each of these two terms added separately leads to a non-integrable equation. However, their combination with an arbitrary choice of the coefficient (b) produces an integrable equation. Thus, its exact solutions can be presented in analytic form. The KEE has been extensively studied in [6, 317, 318]. It is also worth mentioning that the equation,

$$i\psi_x + \psi_{tt} + |\psi|^4\psi + 2\psi(|\psi|^2)_t = 0, \tag{6.23}$$

known as the Eckhaus equation [319], differs from Eqs.(6.21) and (6.22) mainly by lacking the factor i with the $\psi(|\psi|^2)_t$ term. Importantly, the Eckhaus equation (6.23) can be linearized, in contrast to Eq.(6.22). The i factor makes a major mathematical and physical difference.

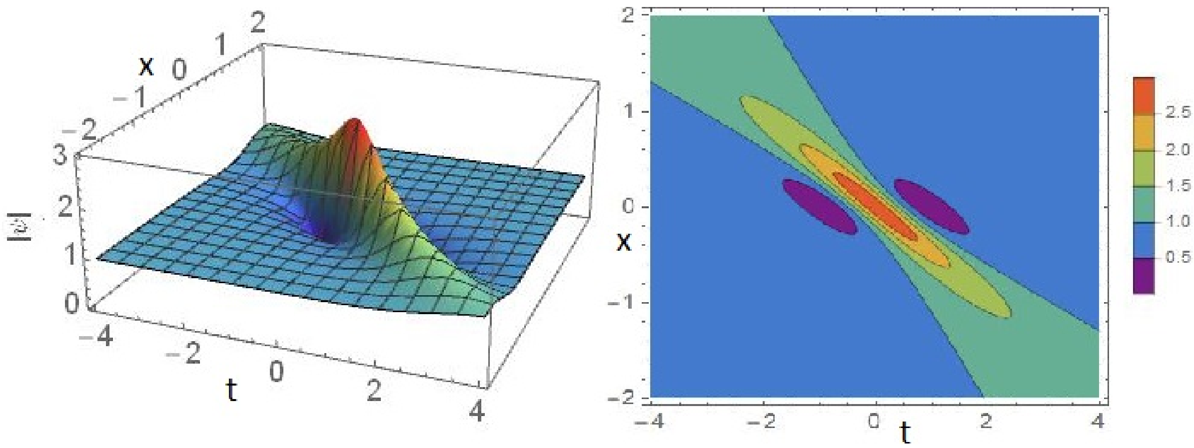

Figure 6.4: *The rogue wave solution of the KEE with $b = 1$. This is in a good agreement with the result found in [6].*

In order to investigate the rogue wave of Eq.(6.21), we need a more involved *ansatz* than that given by Eqs.(6.8) to (6.10). Specifically, we have the form

$$\psi(x,t) = \left[4\,\frac{1+2ix}{D_m(x,t)} - 1\right]e^{iF_m(x,t)}, \tag{6.24}$$

where $D_m(x,t)$ from Eq.(6.9) is retained, but the exponent $F_m(x,t)$ is now more elaborate than Eq.(6.10). Namely:

$$F_m(x,t) = x - \theta(x) + \frac{a(x)[t - t_0(x)]}{D_m(x,t)}, \tag{6.25}$$

with the functions $t_0(x)$, $r(x)$ and $\theta(x)$ being responsible for the lateral motion, amplitude of the wave and change of the phase, respectively. We now need to find a new L and then the 4 unknown functions $a(x), t_0(x), r(x), \theta(x)$. We find:

$$L\frac{r^{7/2}(x)}{2\pi} = r(x)^2\left[xr'(x) - 2X\theta'(x)\right] + \frac{1}{2}a(x)r(x)[r(x) - 2X]t_0'(x) + 2r^3(x)\left[\theta'(x) - 1\right]$$

$$+14Xr(x) - 10X^2 + \frac{1}{32}a(x)^2\left[r^2(x) - 7r(x) + 13X\right], \tag{6.26}$$

where $X = 1 + 4x^2$. We define:

$$S[c^{(j)}] \equiv \frac{d}{dx}\left(\frac{\partial L}{\partial c_x^{(j)}}\right) - \frac{\partial L}{\partial c^{(j)}} \tag{6.27}$$

for each parameter $c^{(j)}$. Then, using Eq.(6.26) above, we find the $a(x)$ term:

$$\frac{8r^{7/2}(x)}{\pi}S[a] = 8r(x)[2X - r(x)]t_0'(x) - a(x)\{[r(x) - 7]r(x) + 13X\}. \tag{6.28}$$

The $\theta(x)$ term is

$$\frac{r^{5/2}(x)}{2\pi}S[\theta] = [3X - r(x)]r'(x) - 16xr(x), \tag{6.29}$$

while the $t_0(x)$ term is

$$\frac{2r^{7/2}(x)}{\pi}S[t_0] = 2r(x)a'(x)[r(x) - 2X] + a(x)\left\{[10X - 3r(x)]r'(x) - 32xr(x)\right\}. \tag{6.30}$$

The $r(x)$ term is

$$\frac{r^{9/2}(x)}{\pi}S[r] = \frac{1}{2}a(x)r(x)[3r(x) - 10X]t_0'(x) + 2r^2(x)[r(x) - 3X]\theta'(x) + \frac{1}{32}a^2(x)\times$$

$$\{r(x)[3r(x) - 35] + 91X\} + 70X[r(x) - X]. \tag{6.31}$$

Using Eq.(6.22), we obtain $J[\theta;R] = 0$, $J[t_0;R] = \frac{6b\pi x}{r^{7/2}(x)}[5X - 2r(x)]$, etc. We find that the simplest solution for the four ODEs, $S[c^j] = J[c^j;R]$, is $r(x) = X$, $a(x) = 16b$, $t_0(x) = -2bx$ and $\theta(x) = -2b^2x$. Substitution into Eqs.(6.21) to (6.25) shows that these expressions indeed provide the exact rogue wave solution of the Kundu-Eckhaus equation for any b, agreeing with other derivation methods. The rogue wave solution of the KEE is shown in Fig.6.4.

6.8 Lagrangian for the extended NLSE

The Lagrangian technique like other methods has its own strengths and weaknesses. One of the deficiencies is the difficulty of finding the Lagrangian density for some equations. When the Lagrangian density is too complicated then tedious algebra is involved in the calculations. When the Lagrangian density cannot be found, the approach cannot be applied. Despite the fact that the Lagrangian density may not exist or be very hard to work with, it still can be useful in a variety of physical and mathematical applications. For example, the change of coordinates may simplify mathematical calculations and even reveal new features of nonlinear waves [297]. Changing coordinates, Osborne *et al* [208] transformed the KdV equation to the 'Lagrangian' Korteweg-de Vries (LKdV) equation. Analogy between a particle motion and the LKdV dynamics has been revealed. Further studies of LKdV and its implications have been provided in [320]. Connection between the nonlinear Schrödinger equation in Lagrangian coordinates (LNLSE) and the LKDV has been found. Lie symmetries have been used for finding approximate solutions of the nonlinear Schrödinger equation. The Lagrangian density is not unique [321, 322]. It may take different forms for the same nonlinear equation. Nutku proposed a generic technique for finding several forms of Lagrangian for fully integrable nonlinear evolution equations [321, 322]. Here, the Lagrangian density is calculated for the extended NLSE including the perturbation terms.

We consider the extended NLSE:

$$i\psi_x \quad + \quad \alpha_2 K_2 - i\alpha_3 K_3 + \alpha_4 K_4 - i\alpha_5 K_5 = 0, \tag{6.32}$$

where $\alpha_2, \alpha_3, \alpha_4$ and α_5 are arbitrary real coefficients. Here, K_2 - K_5 are the four lowest order operators of the infinitely extended integrable NLS equation [230]:

$$i\psi_x + \sum_{j=1}^{\infty}(\alpha_{2j}K_{2j} - i\,\alpha_{2j+1}K_{2j+1}) = 0. \tag{6.33}$$

Namely, these are

$$K_2 = \psi_{tt} + 2|\psi|^2\psi \tag{6.34}$$

$$K_3 = \psi_{ttt} + 6\,|\psi|^2\psi_t \tag{6.35}$$

while K_4 and K_5 operators can be found in [230].

In further analysis, Eq.(6.32) can be considered in two ways. Firstly, we can consider the NLSE $i\psi_x + \alpha_2 K_2 = 0$ as the base equation and other terms as perturbations. Secondly, we can consider the extended integrable NLSE (6.33) as the base equation. Let us start with the second choice.

We employ the Lagrangian

$$L = \int_{-\infty}^{\infty} L_d\, dt$$

where L_d is the Lagrangian density. Its form depends on the terms in the generalized NLSE that we want to take into account. We define operator F through the variational derivative:

$$F[L_d] = -\frac{\partial L_d}{\partial \psi^*} + \frac{\partial}{\partial x}\frac{\partial L_d}{\partial \psi_x^*} + \frac{\partial}{\partial t}\frac{\partial L_d}{\partial \psi_t^*} - \frac{\partial^2}{\partial t^2}\left(\frac{\partial L_d}{\partial \psi_{tt}^*}\right) + \cdots,$$

where, the star * indicates complex conjugate.

The first few invariant densities of the NLSE are given by [230, 323]:

$$\begin{aligned} L_1 &= \psi\psi_t^*, \\ L_2 &= |\psi|^4 + \psi\psi_{tt}^*, \\ L_3 &= \psi\left[\psi_t(\psi^*)^2 + 4\psi_t^*|\psi|^2 + \psi_{ttt}^*\right], \\ L_4 &= \psi[6|\psi_t|^2\psi^* + \psi_{tt}(\psi^*)^2 \\ &+ \psi\left(5\psi_t^{*2} + 6\psi^*\psi_{tt}^*\right) + \psi_{tttt}^*] + 2|\psi|^6. \end{aligned} \tag{6.36}$$

With this formulation, all signs are positive.

Let us start with

$$L_s = i\left[g\psi_x\psi^* + (1+g)\psi\psi_x^*\right] \tag{6.37}$$

for finding the left hand side of Eq.(6.33) for any real g. For example, using $g = -1/2$ gives

$$L_s = -\frac{i}{2}\left(\psi_x\psi^* - \psi\psi_x^*\right)$$

while using $g = -1$ gives

$$L_s = -i\psi_x\psi^*$$

and hence, in either case, we find:

$$F[L_s] = i\psi_x.$$

This is the evolution term in any equation that we consider. For the next order, $j = 2$, we can use $L_2 = |\psi_t|^2 + |\psi|^4$ instead of $L_2 = |\psi|^4 + \psi\psi_{tt}^*$ above. As shown in [107], their equivalence in this regard follows from the fact that:

$$\int_{-\infty}^{\infty} |\psi_t|^2\,dt = -\int_{-\infty}^{\infty} \psi^*\,\psi_{tt}\,dt = -\int_{-\infty}^{\infty} \psi\,\psi_{tt}^*\,dt.$$

Then, we have

$$F[L_2] = -\psi_{tt} - 2\psi|\psi|^2 = -K_2.$$

Similarly, for the third order, $j = 3$, we have

$$F[L_3] = \psi_{ttt} + 6|\psi|^2\psi_t = K_3.$$

In general, $F[L_j] = (-1)^{j+1}K_j$, so

$$L_d = L_s - \alpha_j L_j$$

leads to $i\psi_x + \alpha_j K_j = 0$ if j is even, and

$$L_d = L_s - i\,\alpha_j L_j$$

leads to $i\psi_x - i\,\alpha_j K_j = 0$ if j is odd.

To summarize, for j=2, we obtain the NLSE, $i\psi_x + \alpha_2 K_2 = 0$, and for j=3, we get the Hirota equation, $i\psi_x - i\,\alpha_3 K_3 = 0$. Overall, the total Lagrangian is:

$$\begin{aligned} L_{tot} &= L_s - \sum_{n=1}^{\infty} (\alpha_{2n} L_{2n} + i\,\alpha_{2n+1} L_{2n+1}) \\ &= L_s - \alpha_2 L_2 - i\,\alpha_3 L_3 - \alpha_4 L_4 - i\,\alpha_5 L_5 - \cdots \end{aligned} \tag{6.38}$$

So

$$\begin{aligned} F[L_{tot}] &= i\psi_x + \sum_{n=1}^{\infty} (\alpha_{2n} K_{2n} - i\,\alpha_{2n+1} K_{2n+1}) \\ &= i\psi_x + \alpha_2 K_2 - i\,\alpha_3 K_3 + \alpha_4 K_4 - i\,\alpha_5 K_5 + \cdots \\ &= 0, \end{aligned} \tag{6.39}$$

which is the extended NLSE found in [230]. In principle, the whole infinite number of terms can be taken into account if we need them for any particular reason.

6.9 Lagrangian for perturbed terms in the NLSE

Now, let us consider the standard NLSE as the base equation and other terms as perturbations. Let us consider, as an example, the Lagrangian component

$$\bar{L}_2 = -\frac{\nu_4}{3}\,|\psi|^6,$$

which yields

$$F[\bar{L}_2] = -\frac{\partial \bar{L}_2}{\partial \psi^*} = \nu_4\,\psi|\psi|^4,$$

and, hence, the full equation

$$i\psi_x + \alpha_2 K_2 = R_q,$$

where $R_q = -\nu_4\,\psi|\psi|^4$. This equation is the NLSE with quintic term. More generally, if we use the Lagrangian component

$$\bar{L}_n = -\frac{\nu_{2n}}{n+1}\,|\psi|^{2n+2},\ n>1,$$

which gives

$$F[\bar{L}_n] = -\frac{\partial \bar{L}_n}{\partial \psi^*} = \nu_{2n}\,\psi|\psi|^{2n},$$

the general equation can be obtained as follows:

$$i\psi_x + \alpha_2 K_2 = R_n,$$

where $R_n = -\nu_{2n}\psi|\psi|^{2n}$ and n is integer.

Now, we consider the Lagrangian component

$$L_{4OD} = -d_4|\psi_{tt}|^2,$$

which gives

$$F[L_{4OD}] = -\frac{\partial^2}{\partial t^2}\left(\frac{\partial L_{4OD}}{\partial \psi^*_{tt}}\right) = d_4\psi_{tttt},$$

and hence full equation

$$i\psi_x + \alpha_2 K_2 = R_{4OD},$$

where $R_{4OD} = -d_4\psi_{tttt}$, with '4OD' indicating 4-th order dispersion. This equation is the NLSE with 4-th order dispersion term.

Next, the Lagrangian component

$$L_{6OD} = +d_6|\psi_{ttt}|^2$$

gives

$$F[L_{6OD}] = \frac{\partial^3}{\partial t^3}\left(\frac{\partial L_{6OD}}{\partial \psi^*_{ttt}}\right) = d_6\psi_{6t},$$

and hence full equation

$$i\psi_x + \alpha_2 K_2 = R_{6OD},$$

with '6OD' indicating 6-th order dispersion, and $R_{6OD} = -d_6\psi_{6t}$ is the 6-th order dispersion term in the NLSE with perturbation. For several effects acting simultaneously, the components can be added one by one, e.g.

$$L_f = -i\psi_x\psi^* - d_4|\psi_{tt}|^2 + d_6|\psi_{ttt}|^2$$
$$-\frac{\nu_{2n}}{n+1}|\psi|^{2n+2} - \alpha_2 L_2 - i\alpha_3 L_3 - \alpha_4 L_4 - i\alpha_5 L_5 + \cdots.$$

This way, we obtain the desired form of equation. The crucial point here is that terms in the Lagrangian can be added. This allows us to consider each term separately or all of them simultaneously. The coefficients are arbitrary, but in most cases, we set $\alpha_2 = 1/2$. A summary of forms of L_j for various components in Eq.(6.32) is given in the table below. It can serve as a database when considering any particular equation that we wish to analyze.

As an another example, the Lagrangian density for the Hirota equation can be written in the form

$$L_h = L_s + c_1\left[p\psi\psi^*_{ttt} + (p-1)\psi^*\psi_{ttt}\right] + c_2\frac{3}{4b-1}|\psi|^2(\psi_t\psi^* + 4b\psi\psi^*_t), \tag{6.40}$$

where c_1, c_2, p and $b \neq 1/4$ are arbitrary real numbers and L_s is given by Eq.(6.37). When $b = 1$ and $p = 1$, Eq.(6.40) gives the form provided in the table, while $b = -1/4$ and $p = 1/2$ give the form presented in [324], where the last part is $-\frac{3}{2}|\psi|^2(\psi_t\psi^* - \psi\psi^*_t)$. Thus, this shows that the Lagrangian density is not unique, as it may have various forms that produce a given perturbed term in the equation.

effect	math form of R	Equivalent Lagrangian density for (-R)
evolution term	$i\psi_x$	$-i(\psi_x\psi^*)$
2OD	$-\alpha_2\psi_{2t}$	$+\alpha_2\|\psi_t\|^2$
3OD	$ic_1\alpha_3\psi_{3t}$	$ic_1\alpha_3\psi\psi^*_{ttt}$
4OD	$-d_4\psi_{4t}$	$-d_4\|\psi_{tt}\|^2$
6OD	$-d_6\psi_{6t}$	$+d_6\|\psi_{ttt}\|^2$
(2n)OD	$-d_{2n}\psi_{(2n)t}$	$(-1)^{n+1}d_{2n}\|\psi_{nt}\|^2$
(2n+1)OD	$d_{2n+1}\psi_{(2n+1)t}$	$d_{2n+1}\psi\psi^*_{(2n+1)t}$
5^{th} order	$3(4b-1)\|\psi\|^4\psi_t$	$\|\psi\|^4[\psi_t\psi^*+4b\psi^*_t\psi]$
Kerr	$-2\alpha_2\psi\|\psi\|^2$	$-\alpha_2\|\psi\|^4$
quintic	$-\nu_4\psi\|\psi\|^4$	$-\frac{\nu_4}{3}\|\psi\|^6$
n	$-\nu_{2n}\psi\|\psi\|^{2n}$	$-\frac{\nu_{2n}}{n+1}\|\psi\|^{2n+2}$
NLS	$\psi_{2t}+2\psi\|\psi\|^2$	$-\|\psi_t\|^2-\|\psi\|^4$
Hirota	K_3	L_3
general Hirota	$c_1\psi_{3t}+6c_2\|\psi\|^2\psi_t$	$c_1\psi\psi^*_{ttt}+c_2\|\psi\|^2[\psi_t\psi^*+4\psi^*_t\psi]$
LPD	K_4	$-L_4$

Table 6.1: *List of Lagrangian components for various physical effects. For dispersion of order 2n, viz. $R_{2nOD}=-d_{2n}\psi_{2nt}$. Here '2nOD' indicates (2n)-th order dispersion and '(2n+1)OD' indicates (2n+1)-th order dispersion. See Eq.(6.36) for L_3,L_4. Here 'LPD' means the Lakshmanan-Porsezian-Daniel equation [3], which is of 4th order. 'Kerr' indicates cubic nonlinearity in a system, while 'quintic' means fifth order nonlinearity, relating to the overall power of ψ.*

6.10 Conclusions

In this chapter, we have developed a Lagrangian approach for finding rogue wave solutions of the extended NLSE. Only integrable equations have been considered. These include nonlinear Schrödinger, Hirota, LPD and KE equations. Approximate rogue wave solutions in all these cases coincide with the exact solutions. The latter have been found earlier by other methods. Thus, the Lagrangian approach passed the test: it can be used to obtain rogue wave solutions.

A useful outcome of this analysis is the list of Lagrangian components calculated for a variety of commonly used higher-order terms in the extended NLSE. Using these components turns the analysis of any particular equation into a simple and straightforward exercise.

Another important finding is the following. There is a flexibility in including the higher-order dispersion and nonlinear terms either in the base part of the equation modifying the Lagrangian in Eq.(6.32), or placing them at the right-hand-side of the equation, thus, considering them as a perturbation R. Remarkably, the results are not influenced by this choice. This conclusion is valid no matter whether the equation we are dealing with is integrable or not.

Approximate rogue wave solutions for non-integrable equations are presented in the next chapter. The absence of exact solutions in these cases makes the Lagrangian approach an irreplaceable tool for analysing rogue waves.

CHAPTER 7

Lagrangian Approach To The Theory Of Optical Rogue Waves: Non-Integrable Cases

Using femtosecond pulses in optical communication systems might lead to significant increase of transmission rates [325]. In the linear regime, one of the basic barriers in reaching this aim is fibre dispersion. The dispersion can be reduced when the laser frequency is close to the zero dispersion point [326, 327]. Even in this case, the higher-order dispersion terms cannot be avoided [328]. They have to be included in the evolution equation [30, 329].

The cubic dispersion as well as the fourth-order dispersion terms do affect propagation of femtosecond pulses at the distances less than a kilometer [330, 331]. Even sixth-order dispersion can be important as the experiments of Singh *et al* have shown [332]. In fact, ignoring higher-order dispersion terms may lead to significant errors in modelling the short pulse propagation [333]. They influence the shapes of bright and dark optical solitons [334, 335]. Triangular and flat-top solitons may appear in studies of parabolic pulse propagation in a single-mode fiber with fourth-order dispersion [336]. Higher-order dispersion terms are also important in modelling pulse generation in dissipative optical cavities [334]. The higher-order dispersion terms influence physical effects such as modulation instability (MI) [337]. Namely, two pairs of the MI sidebands become unstable [338]. This happens when the second-order dispersion coefficient is negative while the fourth-order dispersion one is positive. This leads to the emergence of new MI peaks [339]. These examples show that the higher-order dispersion terms should be included in the NLSE for improved accuracy [30, 332, 333, 339].

Another important physical effect in optical fibres is Raman scattering [30, 32, 340]. It causes so-called soliton self-frequency shift [341]. This means that the pulse energy moves from the higher-frequency components of the pulse spectrum to the lower-frequency components upon the pulse propagation [32]. This physical phenomenon was first observed in 1986 [342]. This effect becomes stronger for shorter pulses [30, 32]. Self-frequency shift in a birefringent fiber is studied in [343] and experimentally observed in [344]. The impact of Raman scattering in dispersion-shifted fibers is studied in [345]. Raman effect on pulse propagation is quite similar to self-steepening effect. However, they are different and, in practice, the Raman effect is stronger [30, 32]. The Raman response function in silica fibers is studied in detail in [346].

Generally, the Raman term added to the NLSE does not maintain the integrability of the equation. However, conserved quantities do exist and they can be used in the analysis [347]. The Raman term can preserve the soliton shape [347]. As another example, a kink-type topological soliton has been found in [348]. Bright and dark soliton solutions can be found in special cases [340].

An addition of higher-order dispersion terms and the Raman term to the NLSE transforms this equation into non-integrable form. Therefore, the best way for finding the rogue wave solutions of these equations is their approximation by trial functions and using the Lagrangian approach.

Chapter outline

All above-mentioned studies are related to a soliton propagation in an optical fibre. However, the higher-order effects must have a significant impact on optical rogue waves as well. Below, we show how a rogue wave shape changes in presence of the higher-order dispersion terms, such as the fourth and sixth order ones as well as the Raman term. First, we have found approximate solutions for rogue waves using the Lagrangian approach in presence of the fourth-order and the sixth-order dispersion terms. Next, a generalised solution describing an arbitrary even higher-order dispersion term is given in terms of a hypergeometric function. The effect of Raman delay on soliton is considered first in order to show how it influences the pulse propagation in a fibre. The Lagrangian approach is used for finding an approximate solution in this model. Then, we revealed the effect of the Raman delayed response on rogue waves. A numerical scheme is employed to verify the solution. A reasonable agreement has been found between an approximate analytical solution and numerical results.

7.1 Effect of fourth-order dispersion perturbation on rogue waves

Let's start with the extended NLSE (6.1) and set all the coefficients in equation (6.2) to zero except d_4. The term describes the effect of the $4-th$ order dispersion and can be written as [30, 32, 337–339]:

$$R[\psi(x,t)] = -d_4\left(\psi_{tttt}\right) \equiv R_4 \tag{7.1}$$

where $d_4 << 1$ is an arbitrary positive constant. We take the trial function from the previous chapter, i.e. Eqs.(6.8)-(6.10), and then use equation (6.17) to find $J[c^j; R_4]$ for $c^j = \{a(x), t_0(x), \theta(x), r(x)\}$. We find:

$$\frac{r^{5/2}(x)}{16\pi a(x) d_4} J[a; R_4] = a^2(x) r(x)[r(x) - X] - 6X, \tag{7.2}$$

and

$$\frac{r^{9/2}(x)}{2\pi d_4} J[r; R_4] = a^4(x) r^2(x)[3X - r(x)] + 60 X a^2(x) r(x) + 168X, \tag{7.3}$$

while $J[t_0; R_4] = J[\theta; R_4] = 0$.

Therefore, it follows, from equations (6.14) and (6.15), that $S[t_0]$ and $S[\theta]$ should be zero and we will find that $a(x)$ is a *constant* and $t_0'(x) = a(x)$. Without loss of generality, setting $a(x) = 0, t_0(x) = 0$ reduces Eq.(7.2) to $J[a; R_4] = 0$ and Eq.(7.3) to

$$r^{9/2}(x) J[r; R_4] = 336\pi d_4 X \tag{7.4}$$

leaving only the θ and r functions in equations (6.13) and (6.16), $S[\theta] = 0$ and $S[r] = J[r; R_4]$, to solve. The former equation can be written as:

$$3\left(4x^2 + 1\right) r'(x) - r(x)\left[r'(x) + 16x\right] = 0.$$

We can solve this, to order d_4 with:

$$r(x) = 1 + 4x^2 - c_4 d_4 (1 + 4x^2)^{3/2}, \tag{7.5}$$

where c_4 is a constant. The approximation becomes more accurate if the higher order terms are included; however, this makes algebra more lengthy and complicated. So long as keeping d_4 small, the effect of higher order terms is negligible. The curve differs little from $r(x) = 1 + 4x^2$, since d_4 is small, e. g. 10^{-3}. The value of c_4 is specified by the initial condition for $r(0)$, viz. $r(0) = 1 - c_4 d_4$.

$$S[r] = \frac{2\pi (r(x) - 3X)\theta'(x)}{r^{5/2}(x)} - \frac{70\pi X (X - r(x))}{r^{9/2}(x)}$$

and

$$J[r; R_4] = \frac{336 d_4 \pi X}{r^{9/2}(x)}$$

Then, setting $S[r] - J[r; R_4] = 0$ and expanding to order d_4 gives

$$r^2(x)\,[r(x) - 3X]\,\theta'(x) - 7X\,\{24 d_4 + 5\,[X - r(x)]\} = 0. \tag{7.6}$$

Using $r(x)$ from Eq.(7.5), we find

$$2X^2(3 c_4 d_4 \sqrt{X} + 1)\theta'(x) + 7 d_4 (5 c_4 X^{3/2} + 24) \ = \ 0. \tag{7.7}$$

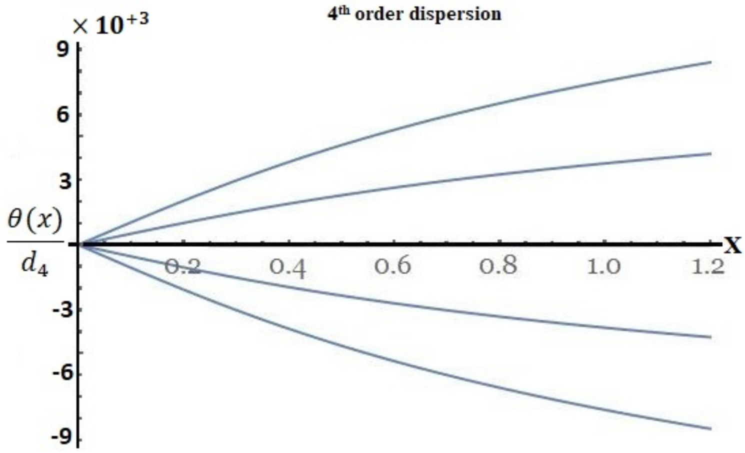

Figure 7.1: *Plot of $\theta(x)/d_4$, the analytic form of Eq.(7.8), for 4-th order dispersion. The curves are, from the upper one going down: $c_4 = -600, -300, 0, 300, 600$. The curve for $c_4 = 0$ is close to the horizontal axis, so it can hardly be seen.*

and it is straightforward to show that

$$\theta(x) = -7d_4\Big[\frac{6x}{4x^2+1} + 3\arctan(2x) + \frac{5}{4}c_4 \operatorname{arcsinh}(2x)\Big]. \tag{7.8}$$

It is again correct to order d_4.

Fig.7.1 shows $\theta(x)$ as a function of c_4. It is clear that small changes in c_4 can cause large changes in $\theta(x)$. Therefore, if c_4 is not very small, then the '*arcsinh*' term is the most important, and $\theta(x)/d_4 \approx -14c_4 x$. We reiterate that this corresponds to an initial offset of $r(0) = 1 - c_4 d_4$. Indeed, the numeric result for the Partial Differential Equation (PDE) is close to the $c_4 = 200$ curve here. For c_4 large, the '*arcsinh*' term is the dominant one. Then,

$$\frac{\theta(x)}{d_4 c_4} = -\frac{35}{4}\operatorname{arcsinh}(2x). \tag{7.9}$$

Figure 7.2 compares the numeric results with the analytic forms Eq.(7.9) and Eq.(7.5), respectively. They clearly show a close agreement between them. As expected, the numerical result showed that there is no transverse movement and hence $t_0(x) = 0$.

A physical term that we consider can be included either in the base part of the equation, thus by modifying the Lagrangian (as for the term $d_4\psi_{tttt}$ in Eq.(6.32)), or it can be included on the right, thus by modifying the perturbation R as it has been shown in secion 6.9, chapter 6. Remarkably, both approaches give the same final answer. Using the example below, we explain the reason for this. Suppose, we include the d_4 term on the left, as in Eq.(6.32). This adds a term

$$\frac{96\pi d_4 X}{r^{7/2}(x)}$$

to the Lagrangian. Then $S[\theta]$ can be written in the form:

$$3Xr'(x) - r(x)\left[r'(x) + 16x\right] = 0,$$

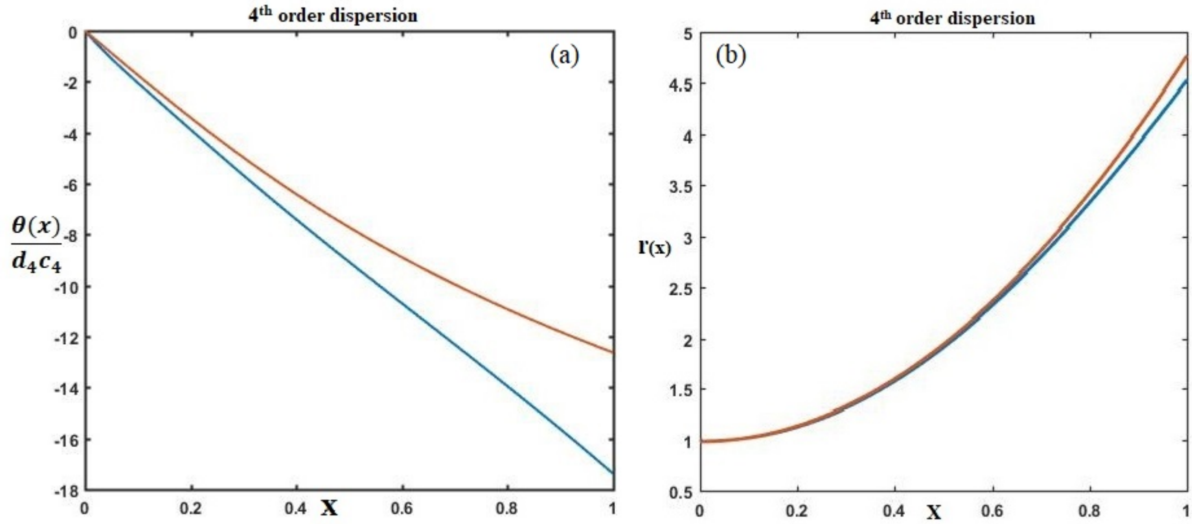

Figure 7.2: *Comparison of numeric solution of PDE giving, (a):* $\frac{\theta(x)}{d_4 c_4}$ *(blue) with its analytic form,* $\frac{\theta(x)}{d_4 c_4} = -\frac{35}{4}\,\mathrm{arcsinh}(2x)$ *(red) and (b): r(x) (blue curve) with analytic form, Eq.(7.5) (red curve). Here* $d_4 = 0.0001, c_4 = 200$.

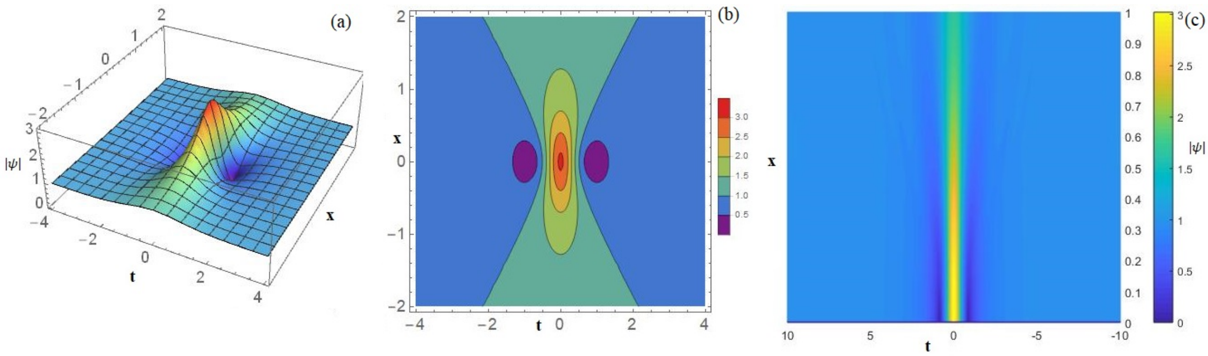

Figure 7.3: *Comparison between the analytical solution and numerical analysis. (a) a 3D plot and (b) a contour plot of the rogue wave in the presence of the fourth-order dispersion in an analytical form. (c) The numeric contour plot of the rogue wave with influence of the fourth-order dispersion. This shows a good agreement between numerical and analytical results. Here* $d_4 = 0.0001$ *and* $c_4 = 200$.

so this (θ) equation is unchanged. However, the (r) equation is changed to:

$$7X(24d_4 + 5r(x) - 5X) + r^2(x)(r(x) - 3X)\theta'(x) = 0.$$

Now, from Eq.(7.3) above, the 4OD term (using $a(x) = 0$) adds $(2\pi)168Xd_4/r^{9/2}(x)$ to J. So, the resultant ODEs are the same.

7.2 Effect of sixth-order dispersion perturbation on rogue wave

The next even perturbation that we consider here is 6-th order dispersion. It becomes important when describing propagation of femtosecond pulses in optical fibers [332, 349]. It can be written as:

$$R[\psi(x,t)] = -d_6\left(\psi_{6t}\right) \equiv R_6, \tag{7.10}$$

where d_6 is a small constant. We thence find:

$$\frac{r^{7/2}(x)}{24\pi a(x) d_6} J[a;R_6] = a^2(x)r(x) \times \{a^2(x)r(x)[X - r(x)] + 20X\} + 120X, \tag{7.11}$$

and

$$\frac{r^{11/2}(x)}{2\pi d_6} J[r;R_6] = a^6(x)r^3(x)[r(x) - 3X] - 150Xa^4(x)r^2(x) - 2520Xa^2(x)r(x) - 6480X, \tag{7.12}$$

while $J[t_0;R_6] = J[\theta;R_6] = 0$.

Similar to the case in section 7.1, setting $a(x) = 0$ and $t_0(x) = 0$ reduces Eq.(7.11) to $J[a;R_6] = 0$ while Eq.(7.12) is transformed to

$$r^{11/2}(x) J[r;R_6] = -12960\pi d_6 X. \tag{7.13}$$

This reduces the system and leaves only the θ and r equations, i.e. $S[\theta] = J[\theta;R_6]$ and $S[r] = J[r;R_6]$ to solve. The former one is

$$3\left(4x^2+1\right)r'(x) - r(x)\left[r'(x) + 16x\right] = 0, \tag{7.14}$$

as before, and

$$J[r;R_6] = -\frac{12960 d_6 \pi \left(4x^2+1\right)}{r^{11/2}(x)}.$$

Then, setting $S[r] - J[r;R_6] = 0$ and expanding to order d_6 gives

$$r^3(x)\,[r(x) - 3X]\theta'(x) + 35Xr(x)[r(x) - X] + 6480 d_6 X = 0. \tag{7.15}$$

By solving Eq.(7.14), correct to order d_6, we have:

$$r(x) = X - c_6 d_6 X^{3/2}, \tag{7.16}$$

where the extra constant, c_6, is specified by the initial condition for $r(0)$, viz. $r(0) = 1 - c_6 d_6$.

Next, using $r(x)$ from Eq.(7.15) and expanding to order d_6, we obtain the equation

$$5d_6\left[1296 - 7c_6 X^{5/2}\right] - 2X^3\left(1 + 3c_6 d_6\sqrt{X}\right)\theta'(x) = 0, \tag{7.17}$$

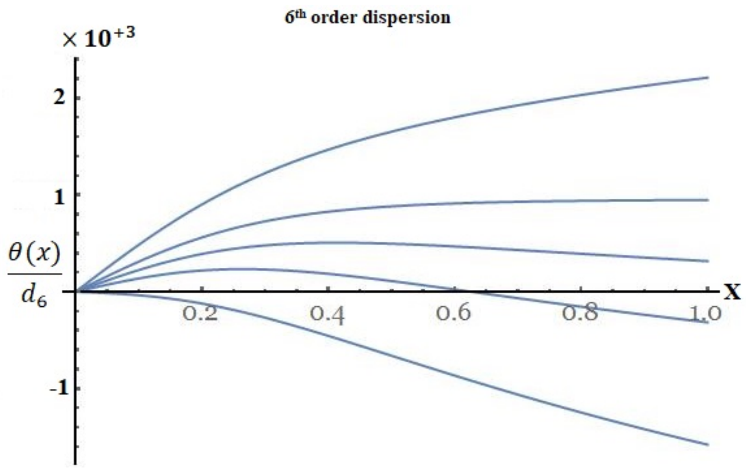

Figure 7.4: *Plot of $\theta(x)/d_6$, the analytic form of Eq.(7.18), for 6-th order dispersion, Eq.(7.10). The top curve is for $c_6 = -100$, the next lower is for $c_6 = 0$, the third curve is for $c_6 = 50$, the fourth curve is for $c_6 = 100$, while the lowest curve is for $c_6 = 200$.*

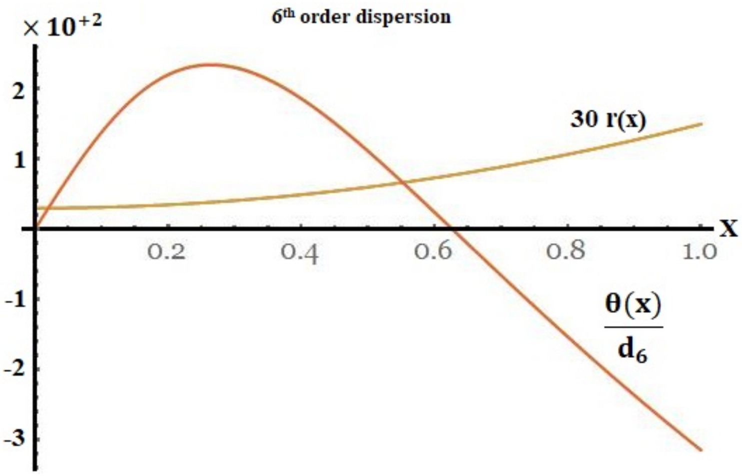

Figure 7.5: *Comparison of numeric solution of ODEs giving $\theta(x)/d_6$ with its analytic form from Eq.(7.18), for 6-th order dispersion, Eq.(7.10). Here $\theta(x)$ features a maximum. We also plot $30\,r(x)$ and its analytic form from Eq.(7.16). Here $r(x)$ increases monotonically. We use $c_6 = 100$, and $d_6 = 10^{-5}$, and the initial values used are $r(0) = 1 - c_6 d_6$ and $\theta(0) = 0$. In each case, the numeric curve is indistinguishable from the analytic one.*

which has a solution:

$$\theta(x)/d_6 = \frac{5}{4}\Big[\frac{324x(12x^2+5)}{(4x^2+1)^2} + 486\ \arctan(2x) - 7c_6\ \operatorname{arcsinh}(2x)\Big], \tag{7.18}$$

where c_6 is a constant.

Fig.7.4 shows $\theta(x)$ for several values of c_6. It is obvious that a small change in c_6 results in a large difference in this function. Therefore, for c_6 large, the '$arcsinh$' term is the dominant one. Then

$$\frac{\theta(x)}{d_6 c_6} = -\frac{35}{4}\,\mathrm{arcsinh}(2x). \tag{7.19}$$

Fig.7.5 illustrates $\theta(x)$ and $r(x)$ obtained from numerical solution of Eq.(7.14) and Eq.(7.15) and compares their solutions with the analytic forms, Eq.(7.16) and Eq.(7.18). The curves are indistinguishable from the analytic forms.

Figs.7.6 and 7.7 also show a good agreement between numerically-found results from Eq.(7.15) and Eq.(7.14) and analytic solutions from Eq.(7.19) and Eq.(7.16), respectively. As we expected, the numerical result shows the absence of any transverse movement, and hence $t_0(x) = 0$.

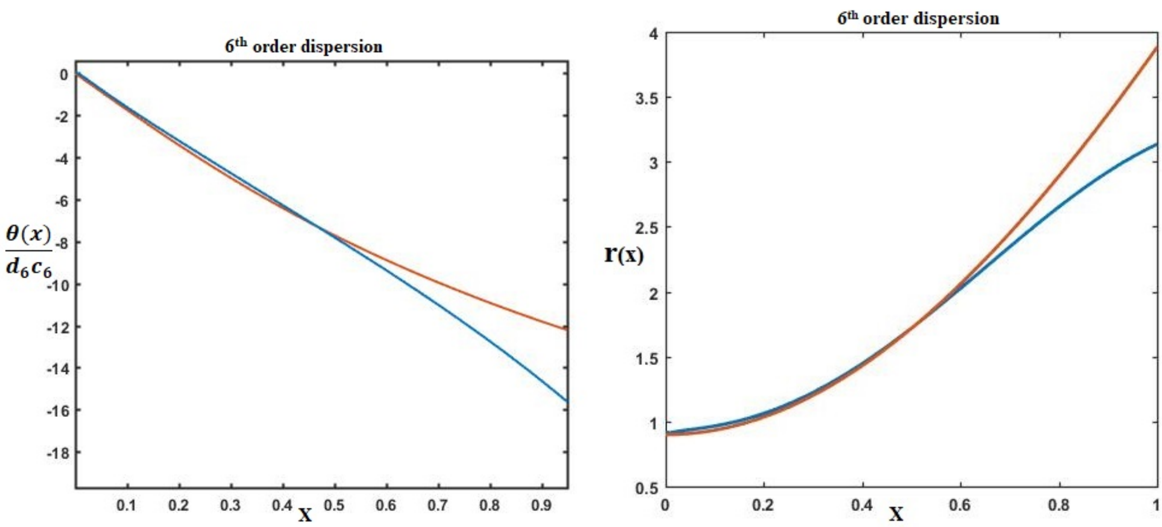

Figure 7.6: *Comparison of numeric solution of partial differential equation (PDE) giving (a) $\frac{\theta(x)}{d_6 c_6}$ (blue) with its analytic form, $\frac{\theta(x)}{d_6 c_6} = -\frac{35}{4} arcsinh(2x)$, Eq.(7.19)(red) and (b) numerical solution for r(x) (blue) with its analytic form, Eq.(7.16) (red). Here $d_6 = 0.0001$, $c_6 = 1000$.*

Here, we assumed the sixth-order dispersion as a perturbation term and considered it in the left-hand-side R of the NLSE, i.e. Eq.(6.1). Let's check if it is added to the Lagrangian form and not considered as a perturbation. As it has been previously shown, additional terms can be included either in the base part of the equation, modifying the Lagrangian in Eq.(6.32), or they can be included on the right-side, considered as perturbation R. Suppose we now include the d_6 term in the base equation, as in Eq.(6.32). This adds a term

$$-\frac{2880\pi d_6 X}{r^{9/2}(x)}$$

to the Lagrangian. Then finding $S[\theta]$ leads to:

$$3Xr'(x) - r(x)\left(r'(x) + 16x\right) = 0,$$

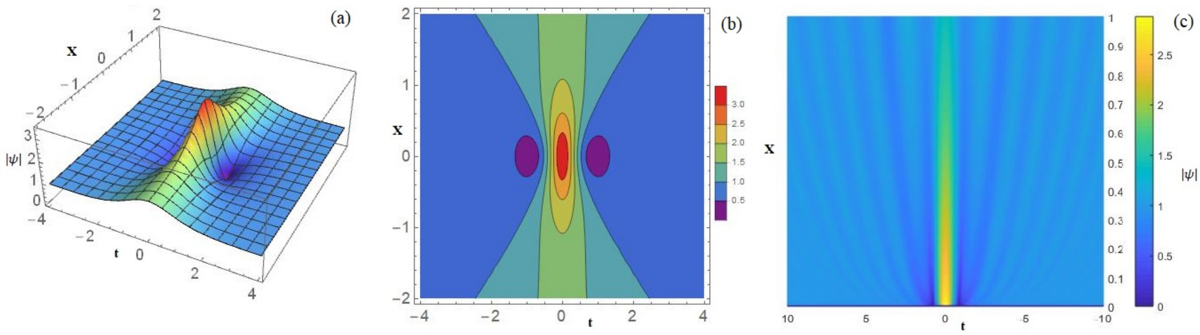

Figure 7.7: *Comparison between the analytical solution and numerical analysis. (a) A 3D plot and (b) a contour plot of the analytic solution for the rogue wave in the presence of the sixth-order dispersion. (c) The numeric contour plot of the rogue wave with influence of the sixth-order dispersion. This shows a good agreement between numerical and analytical results. Here* $c_6 = 1000$*,* $d_6 = 0.0001$.

so this (θ) equation is the same as Eq.(7.14), as expected, since it does not include d_6. However, the (r) equation is changed to:

$$r^3(x)[r(x) - 3X]\theta'(x) - 5X\{1296d_6 + 7r(x)[X - r(x)]\} = 0.$$

Now, from Eq.(7.12) above, the 6OD term (using $a(x) = 0$) adds $-(2\pi)6480X\,d_6/r^{11/2}(x)$ to J. So the resultant ODEs are the same in each case.

7.3 General case: Dispersion term of any order

For integer n, we now consider n^{th} order derivative terms. For higher order dispersion, for the (2n)OD term, $R_{(2n)OD} = -d_{2n}\psi_{(2n)t}$, we need Lagrangian density

$$L_{(2n)OD} = (-1)^{n+1} d_{2n} |\psi_{nt}|^2.$$

For $(2n+1)OD$ term, $R_{(2n+1)OD} = d_{2n+1}\psi_{(2n+1)t}$, the Lagrangian density becomes

$$L_{(2n+1)OD} = p\psi\psi^*_{(2n+1)t} + (p-1)\psi^*\psi_{(2n+1)t}$$

for arbitrary real p. The $n = 1$ case is given in the first part of Eq.(6.40). For the even order ($R_{(2n)OD} = -d_{2n}\psi_{(2n)t}$) dispersion case, we find:

$$d_{2n}(-1)^{n+1}(2n+3)X(2n)! + r^n(x)[r(x) - 3X]\theta'(x) + 35Xr^{n-2}(x)[r(x) - X] = 0. \tag{7.20}$$

By putting in $r(x) = X - c_{2n}d_{2n}X^{3/2}$ for integer n, and taking terms to order d_{2n} only, we get:

$$-d_{2n}\left[(-1)^n(2n+3)X(2n)! + 35c_{2n}X^{n+\frac{1}{2}}\right] - 2X^{n+1}\left(3c_{2n}d_{2n}\sqrt{X} + 1\right)\theta'(x) = 0. \tag{7.21}$$

This reduces to earlier forms found for n=2, 3. The solution is:

$$\theta(x) = -\frac{1}{4}d_{2n}\left[2(-1)^n(2n+3)x(2n)!\,{}_2F_1\left(\frac{1}{2},n;\frac{3}{2};-4x^2\right)+35c_{2n}\operatorname{arcsinh}(2x)\right]. \tag{7.22}$$

Here, ${}_2F_1$ stands for the Gaussian hypergeometric function. If c_{2n} is large, then the solution is accurately given by:

$$\theta(x) = -\frac{35}{4}d_{2n}c_{2n}\operatorname{arcsinh}(2x),$$

thus explaining the identical forms of results given by Eqs.(7.9) and (7.19).

For example, for $n=2$, we have fourth order dispersion and Eq.(7.20) gives

$$-168d_4X+(r(x)-3X)r^2(x)\theta'(x)+35X(r(x)-X)=0,$$

which matches Eq.(7.6). Then Eq.(7.21) reduces to Eq.(7.7). For this $n=2$ case, its solution, from Eq.(7.22), reduces to Eq.(7.8), to first order in d_4. If c_4 is large, then the solution is approximated by:

$$\theta(x) = -\frac{35}{4}d_4c_4\ \operatorname{arcsinh}(2x).$$

This could be a confirmation of the general solution, i.e. Eq.(7.22).

As another example, let's take $n=3$. Then we have the sixth-order dispersion and Eq.(7.20) gives

$$r^3(x)[r(x)-3X]\theta'(x)+5X\{1296d_6+7r(x)[r(x)-X]\}=0,$$

which is equivalent to Eq.(7.15). For $n=3$ case, the solution reduces to:

$$\theta(x) = \frac{5}{4}d_6\left[-7c_6\operatorname{arcsinh}(2x)+\frac{324x\left(12x^2+5\right)}{\left(4x^2+1\right)^2}+486\operatorname{arctanh}(2x)\right],$$

which is equivalent to Eq.(7.18). If c_6 is large, then the solution is approximated by:

$$\theta(x) = -\frac{35}{4}d_6c_6\ \operatorname{arcsinh}(2x).$$

This can confirm Eq.(7.22) as well.

7.4 Soliton under influence of Raman delay

We consider a soliton solution under the influence of Raman delay. This has been done earlier using other methods [347, 350, 351]. Suppose, $R=\tau_R\psi(|\psi|^2)_t\equiv R_r$ is the only nonzero term in Eq.(6.2). Various approximations have been used to estimate the soliton shape for small delay, τ_R, [347, 351, 352]. The delay makes the soliton solution non-symmetric in t, and this requires a new trial function. Here we take

$$\psi(x,t)=\sqrt{\frac{Q(x)}{2w(x)}}\operatorname{sech}\left(\frac{y_1}{w(x)}\right)\exp\{i[a(x)y_1-\theta(x)]\} \tag{7.23}$$

where $Q(x)$ is the energy, $w(x)$ is the pulse width, and $y_1 = t - t_0(x)$, with $t_0(x)$ being the time delay offset. The Lagrangian form of the soliton-like trial function, i.e. Eq.(7.23) can be found by the same procedure explained in chapter 6. The Lagrangian density is:

$$L_d(8w^3(x)) = -Q(x)\operatorname{sech}^2\left(\frac{t-t_0(x)}{w(x)}\right)[-4tw^2(x)a'(x) + 4t_0(x)w^2(x)a'(x) + 4a(x)w^2(x)t_0'(x)$$

$$-2a^2(x)w^2(x) + Q(x)w(x)\operatorname{sech}^2\left(\frac{t-t_0(x)}{w(x)}\right) - 2\tanh^2\left(\frac{t-t_0(x)}{w(x)}\right) + 4w^2(x)\theta'(x)]$$

which leads to the average Lagrangian (over t) Eq.(6.3) as:

$$L(12w^2(x)) = Q(x)[-12t_0(x)w^2(x)a'(x) + \pi^2 w^4(x)a'(x) - 12a(x)w^2(x)t_0'(x)$$

$$+6a^2(x)w^2(x) - 2Q(x)w(x) - 12w^2(x)\theta'(x) + 2].$$

The approximating procedure leads to 5 ODEs (recall Eq.(6.5)). We use:

$$S[a] = \frac{1}{12}\left(\pi^2 w(x)\left(w(x)Q'(x) + 2Q(x)w'(x)\right) - 12t_0(x)Q'(x)\right) - a(x)Q(x),$$

$$S[t_0] = -a(x)Q'(x),$$

$$S[w] = -\frac{Q(x)\left(\pi^2 w^4(x)a'(x) + Q(x)w(x) - 2\right)}{6w^3(x)},$$

$$S[Q] = \mathrm{t0}(x)a'(x) - \frac{1}{12}\pi^2 w^2(x)a'(x) + a(x)t_0'(x) - \frac{1}{2}a^2(x) + \frac{Q(x)}{3w(x)} + \theta'(x) - \frac{1}{6w^2(x)},$$

and

$$S[\theta] = -Q'(x).$$

The corresponding functions $J[c^j;R]$ with $c = \{a(x), t_0(x), w(x), Q(x), \theta(x)\}$ for the above trial function can be found as:

$$J[Q;R_r] = \frac{\tau_R Q(x)}{6w(x)},$$

$$J[w;R_r] = \frac{4\tau_R Q^2(x)t_0(x)}{15w^4(x)},$$

and

$$J[t_0;R_r] = -\frac{4\tau_R Q^2(x)}{15w^3(x)},$$

while $J[a;R_r] = J[\theta;R_r] = 0$. The $\theta(x)$ equation is:

$$Q'(x) = 0, \tag{7.24}$$

showing that $Q(x) = Q_0$ is a constant. The $a(x)$ equation is:

$$Q(x)[a(x) - t_0'(x)] = 0 \tag{7.25}$$

showing that $a(x) = t_0'(x)$. The $w(x)$ equation is:

$$\frac{Q(x)}{6w^3(x)}[w(x)Q(x) - 2] \tag{7.26}$$

showing that $w(x) = 2/Q_0 = w_0$. Finally, the $t_0(x)$ equation is:

$$\frac{8\tau_R}{15w_0^4} - t_0''(x) = 0, \tag{7.27}$$

showing that

$$t_0'(x) = a(x) = \frac{4\tau_R Q(x)}{15w_0^3}x = \frac{8\tau_R}{15w_0^4}x, \tag{7.28}$$

as in [350] (where $w_0 = 1/\eta$, $t_0 = -\bar{t}$ and $a = -\omega$). Thus,

$$t_0(x) = \frac{4\tau_R x^2}{15w_0^4}. \tag{7.29}$$

This result for time shift is in agreement with Eqs.(5b) and (13) in [351]. Plainly, $t_0(x)$ is a close analogue of vertical projectile motion under gravity, where the velocity $t_0'(x)$ changes sign at $x = 0$, but the acceleration, $t_0''(x) = \frac{8\tau_R}{15w_0^4}$, does not. This is expected, since the acceleration is caused by the Raman delay and this does not change sign.

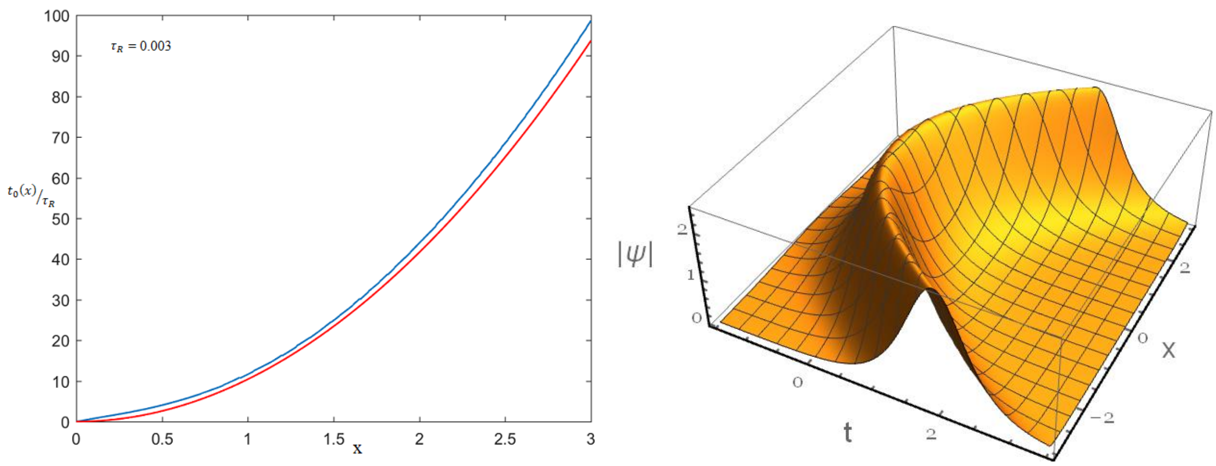

Figure 7.8: Plot of the relative soliton offset, t_0/τ_R, showing the effect of Raman delay. We compare the numerically-found result (blue curve) with the analytic result of Eq.(7.29), (red curve). Plot of the soliton, Eq.(7.23), under the effect of Raman delay, using Eqs.(7.24) to (7.30). Here, delay is given by $\tau_R = 0.02$, and width $w_0 = 0.4$.

The remaining $Q(x)$ equation is:

$$\frac{1}{w_0^2} + t_0'(x)^2 + 2\theta'(x) = 0, \tag{7.30}$$

showing that the rate of change of phase is $\theta'(x) = -\frac{1}{2w_0^2} - \frac{1}{2}\left(\frac{8\tau_R x}{15w_0^4}\right)^2$, as in [350] (where $\theta = -\phi$). If $\tau_R = 0$, we obtain

$$\psi(x,t) = \frac{1}{w_0}\text{sech}\left(\frac{t}{w_0}\right)\exp\left\{\frac{ix}{2w_0^2}\right\} = \frac{Q_0}{2}\text{sech}\left(\frac{Q_0 t}{2}\right)e^{\frac{1}{8}iQ_0^2 x}, \tag{7.31}$$

which is the NLSE soliton of width w_0 with the energy Q_0. An example of the solution, showing the parabolic path, is given in Fig.7.8.

Our numerical propagation studies of this soliton, as exemplified in Fig.7.8, verify the above analytic results, and thus give confidence in the approach.

7.5 Rogue wave under influence of Raman delay

Now, instead of a soliton, we consider a rogue wave solution which is localized in time. For this, we use the same trial function that we took in Eqs.(6.8), (6.9) and (6.10). The ODEs will naturally differ from the previous cases. The $\theta(x)$ equation is:

$$r(x)\left[r'(x) + 16x\right] = 3(4x^2+1)r'(x). \tag{7.32}$$

To solve it, we set $z = \sqrt{X} = \sqrt{1+4x^2}$ and $r(z) = s^2(z)$. This gives:

$$\left[3z^2 - s^2(z)\right]s'(z) = 2zs(z). \tag{7.33}$$

We find that the solution is:

$$s(z) = \frac{1}{6c}\left(F^{1/3} + F^{-1/3} - 1\right) \tag{7.34}$$

where

$$F = 54c^2z^2 - 1 + 6cz\sqrt{3}\sqrt{27c^2z^2-1}, \tag{7.35}$$

where c is an arbitrary real solution parameter.

Note that this remains real even when c is small. In fact $\lim_{c\to 0} s(z) = z$, so $\lim_{c\to 0} r(z) = z^2$. Also, $r(x)$ is even in c, so we only need to use $c \geq 0$. This means that $r(0) \leq 1$ for any c. We plot the function $r(x)$ in Fig.7.9(a).

Since c is generally small ($c < 0.1$), it is convenient to expand this result. For $c \geq 0$:

$$r(z) = z^2\left(1 - 2cz + 6c^2z^2 - 21c^3z^3 + 80c^4z^4 + \cdots\right), \tag{7.36}$$

or,

$$r(x) = (1+4x^2)\left[1 - 2c\sqrt{1+4x^2} + 6c^2(1+4x^2)\right.$$
$$\left. - 21c^3\left(1+4x^2\right)^{3/2} + 80c^4\left(1+4x^2\right)^2 + \cdots\right]. \tag{7.37}$$

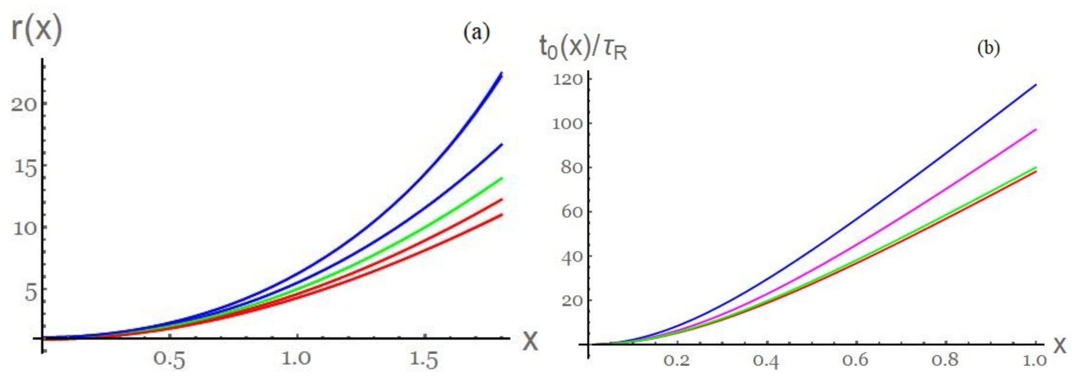

Figure 7.9: (a) Plot of function $r(x)$ for various c values. The blue curves are for $c < 0$. This solution corresponds to the expansion in Eq.(7.36) with $c = -0.04$ (top blue curve) and $c = -0.02$ (next blue curve). The green curve, *viz.* $r(x) = z^2 = 1 + 4x^2$ is for $c = 0$. The two red curves are plots of Eqs.(7.34) and (7.35). The upper red curve is for $c = 0.02$. The lower red curve is for $c = 0.04$. In each case, the expansion, Eq.(7.36), is superimposed on the exact result. The curves are indistinguishable. (b) Plot of function $t_0(x)/\tau_R$, from Eq.(7.45) for various c: $c = 0.04$ (blue curve), $c = 0.4$ (magenta), $c = 0.2$ (red), and $c = 0.1$ (green).

So, when $c = 0$, the solution reduces to the known NLSE result, $r(x) = (1 + 4x^2)$. In solving the 4 ODEs, we take c to be arbitrary but larger than τ_R. Using, Eq.(6.5) with $S[t_0]$ from Eq.(6.15) and $J[t_0;R_r]$ from Eq.(6.17), for $t_0(x)$, we find:

$$\frac{r(x)^{9/2}}{32\pi} J[t_0;R_r] = \tau_R\{r(x)[5X - r(x)] - 7X^2\},$$

so the $t_0(x)$ equation is:

$$16\tau_R \{r(x)[r(x) - 5X] + 7X^2\} + r(x)^2 \Big\{2r(x)\big(a'(x)[r(x) - X] - 8xa(x)\big) + a(x)[3X - r(x)]r'(x)\Big\} = 0, \tag{7.38}$$

where $X = 1 + 4x^2$. The other factors, i.e. $J[r;R_r]$, $J[a;R_r]$, $J[\theta;R_r]$ are zero.

The $r(x)$ equation is:

$$r(x)\{r(x)[r(x) - 3X]\left[a^2(x) - 2a(x)t_0'(x) - 2\theta'(x)\right] - 70X\} + 70X^2 = 0. \tag{7.39}$$

and the $a(x)$ equation is:

$$[X - r(x)][a(x) - t_0'(x)] = 0 \tag{7.40}$$

Now, if we take $r(x) = 4x^2 + 1$ to solve the last equation, then the 2-nd one cannot be solved. So, we need to take $a(x) = t_0'(x)$ to solve it. This reduces Eq.(7.38) to:

$$r(x)\Big\{r(x)[-t_0'(x)\big((r(x) - 3X)r'(x) + 16xr(x)\big) + 2r(x)(r(x) - X)t_0''(x) + 16\tau_R] - 80\tau_R X\Big\} + 112\tau_R X^2 = 0, \tag{7.41}$$

and Eq.(7.39) to:

$$r(x)\{r(x)[3X-r(x)]\left[t_0'(x)^2+2\theta'(x)\right]-70X\}+70X^2 \quad = \quad 0. \tag{7.42}$$

We can solve the resultant ODEs, i.e. Eqs.(7.32), (7.41) and (7.42), to various orders in τ_R. We take c and τ_R, to be small and have similar order (around 10^{-3}). We assume that the offset, c, is not much smaller than τ_R, so we cannot have $\tau_R/c >> 1$. This excludes $c = 0$. In fact, we expect $c > \tau_R$.

Using Eq.(7.37), we have:

$$r(x) = X\left[1-2cX^{1/2}+6c^2X-21c^3X^{3/2}+80c^4X^2+\cdots\right], \tag{7.43}$$

Then:

$$a(x) = t_0'(x) = \frac{2\tau_R x}{cX^{3/2}}\left[2(8x^2+3)+33cX^{1/2}+215c^2X\right]+33\tau_R\arctan(2x). \tag{7.44}$$

Now, taking $t_0(0) = 0$ we obtain:

$$t_0(x) = \tau_R\left\{\tfrac{1}{c}\left(\tfrac{8x^2+1}{X^{1/2}}-1\right)+33x\arctan(2x)+\tfrac{215}{2}c\left[X^{1/2}-1\right]\right\}. \tag{7.45}$$

So, for small x, we have

$$\frac{t_0(x)}{\tau_R} \quad \approx \quad \left(215c+\frac{6}{c}+66\right)x^2-\left(215c+\frac{10}{c}+88\right)x^4+\cdots.$$

The shape of this function is plotted in figure 7.9 (b). In the soliton case, we also found that $t_0(x)$ varied as $\tau_R x^2$. If c is small, say $c < 0.1$, then:

$$t_0(x) \approx 6\frac{\tau_R}{c}x^2(1-\frac{5}{3}x^2+\cdots). \tag{7.46}$$

Hence, we obtain the following simple form for the acceleration:

$$\frac{t_0''(x)}{\tau_R} = \frac{2}{c}\left[6X^{-5/2}+66cX^{-2}+215c^2X^{-3/2}\right]. \tag{7.47}$$

Thus, the acceleration, $t_0''(x)$ of the ridge takes the same sign as that for the soliton case found in Eq.(7.27), and is also an even function, but it has a more complicated form. As for the soliton case, it is proportional to τ_R. The estimates for the function $t_0(x)$ are shown in Fig.7.10 along with the results of numerical simulations for the same set of parameters. As can be seen from this figure, numeric solution of the 4 ODEs give results which are reasonably close to the above approximate solutions for small τ_R, say $\tau_R < 0.002$.

The Raman effect causes a delay, so we expect deceleration. It is analogous to the deceleration found for the Raman soliton in Eq.(7.28). Examples of evolution are shown in Figs.7.11. Acceleration here is clearly seen.

Now, $\frac{t_0''(0)}{\tau_R} = \frac{2}{c}(6+66c+215c^2)$, and we define this to be c_0. On plotting the acceleration, we see that it plainly has a gaussian-type form. We find that it can be approximated by:

$$\frac{t_0''(x)}{\tau_R} \approx c_0 e^{-6x^2}. \tag{7.48}$$

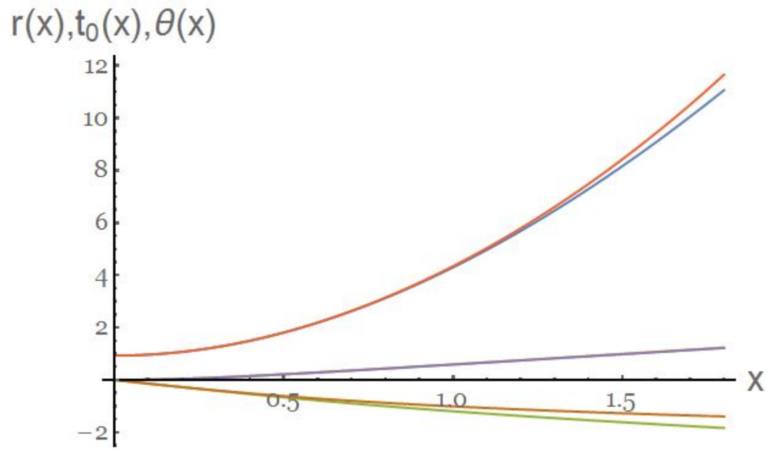

Figure 7.10: Plot of functions $t_0(x)$, Eq.(7.45), $r(x)$, using the results of section 7.4, including Eq.(7.37), and $\theta(x)$, using Eq.(7.52), together with the same functions found numerically by solving Eqs.(7.32) to (7.40). Here, $c = 0.04$, and the delay is given by $\tau_R = 0.005$. The two upper curves give $r(x)$, while the two lower positive ones give $t_0(x)$ and the two negative ones show $\theta(x)$. In each case, the exact numeric solution and the approximation for it is very close.

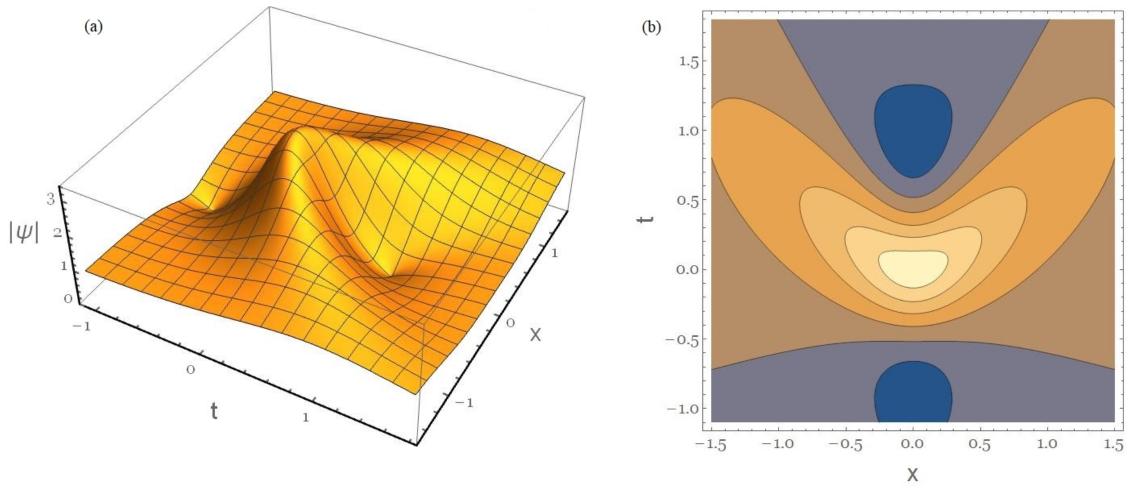

Figure 7.11: (a) Plot of the rogue wave and (b) Contour plot of the rogue wave, Eq.(6.8), using Eqs.(7.45) to (7.52) for delay given by $\tau_R = 0.005$. Here $c = 0.04$.

Integrating shows that:

$$\frac{t_0'(x)}{\tau_R} \approx c_0 \sqrt{\frac{\pi}{6}}\, \mathrm{erf}\left(\sqrt{6}x\right), \tag{7.49}$$

where 'erf' indicates the error function. So the final expression for velocity is $t_0'(\pm\infty)/\tau_R \approx$

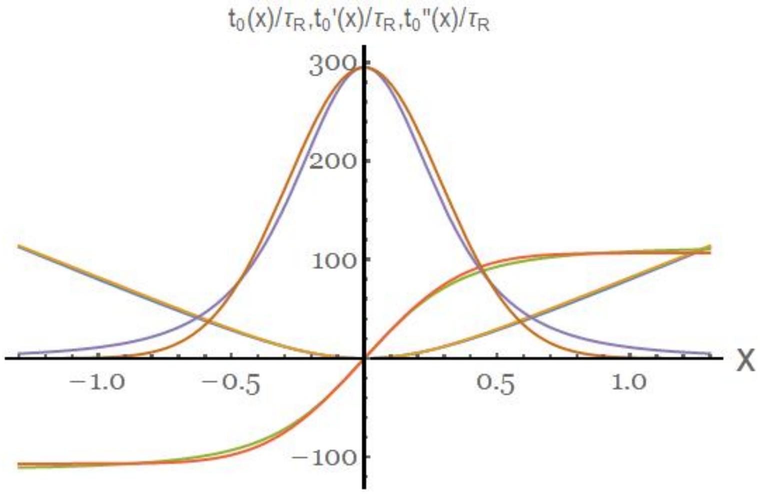

Figure 7.12: Plot of functions $t_0''(x)/\tau_R$ (even function of x with $t_0(0) \approx c_0 = 300$ here), $t_0'(x)/\tau_R$ (odd function of x) and $t_0(x)/\tau_R$ (even function of x with $t_0(0) = 0$) from original Eqs.(7.45), (7.44) and (7.47), respectively, together with a comparison with the gaussian-based approximations for them, given by Eqs.(7.48)-(7.50), all for $c = 0.1$. Here, $c_0 = \frac{2}{c}\left(6+66c+215c^2\right)$.

$\pm\frac{c_0}{2}\sqrt{\frac{\pi}{6}}$. Then

$$\frac{t_0(x)}{\tau_R} \approx \frac{c_0}{2}\sqrt{\frac{\pi}{6}}\left[x\,\mathrm{erf}(\sqrt{6}x) - \frac{1-e^{-6x^2}}{\sqrt{6x}}\right]. \tag{7.50}$$

The comparison of the curves in Fig.7.12 show that this is a convenient and accurate approximation, giving a simple view of the ridge offset during propagation.

So, for small x,

$$\frac{t_0(x)}{\tau_R} \approx \frac{c_0}{2}x^2\left[1 - x^2 + \frac{6x^4}{5}\cdots.\right]$$

For $c_0 = \frac{2}{c}\left(6+66c+215c^2\right)$, we find that c_0 reaches its minimum of 275 when c=0.17, and $275 < c_0 < 295$ for $0.1 < c < 0.28$. For $c_0 = \frac{2}{c}(6+66c)$, we find that $c_0 = 250$ when c=0.1, and then c_0 decreases monotonically as c increases. Now $t_0(x) \approx \frac{c_0}{2}\tau_R x^2$, so we need $\tau_R < c$ to be realistic, i.e. not too high. For typical values of c, say $c = 0.2$, we have c_0 around 250, and hence

$$t_0(x) \approx 125\tau_R x^2 \tag{7.51}$$

for small x.

Eqs.(7.45) to (7.47) are valid for all x; thus the position $t_0(x)$ and acceleration $t_0''(x)$ are even functions of x, while velocity $t_0'(x)$ is an odd function in x. It thus corresponds to a more complicated dynamics than the motion under gravity considered in section 7.4, as here the analogous particle would be subject to a force proportional to $\frac{2\tau_R}{c}\left[6X^{-5/2} + 66cX^{-2} + 215c^2X^{-3/2}\right]$. From Eq.(7.48), this force varies roughly as $c_0\tau_R e^{-6x^2}$. It approaches zero for large $|x|$ but does not change sign.

Now, let us turn to the exponent term $\theta(x)$. Setting $\theta(0) = 0$, we have:

$$\theta(x) = -\frac{35c}{2}\operatorname{arcsinh}(2x) \tag{7.52}$$

Expansion

$$\theta(x) = -35cx\left(1 - \frac{2}{3}x^2 + \cdots\right),$$

agrees with the results from the PDE simulations. Now

$$\theta'(x) = -\frac{35c}{\sqrt{X}}, \tag{7.53}$$

where $X = 1 + 4x^2$. Plainly, this is almost constant for small x.

In the next section, we plot $t_0(x)/\tau_R$ for various c on the same diagram. We also plot $\theta(x)/c$ and $(r(x) - 1 - 4x^2)/c$ to estimate the next term in $r(x)$.

7.6 Comparison with numerical simulations of PDE

For $x = 0$, we have $a(x) = \theta(x) = 0$, so ψ is real. Its maximum value, ψ_m occurs when $t = 0$, and is given by $\psi_m = \frac{4}{r(0)} - 1 \approx 3 + 8c$. As noted earlier, this is a function of c only, as $r(0) = 1 - 2c$. The intensity $I \equiv |\psi|^2$, can be written as:

$$I = \frac{\left\{r(x) + 4[t - t_0(x)]^2 - 4\right\}^2 + 64x^2}{\left(r(x) + 4[t - t_0(x)]^2\right)^2}$$

We note that $r(x)$ is close to $1+4x^2$ for small c. By setting $\frac{\partial I}{\partial t} = 0$, we find that there are 3 stationary points. The first one is at $t = t_0(x)$, and it is a maximum since $\frac{\partial^2 I}{\partial t^2} < 0$, as $4 + 16x^2 >> r(x)$. Either hand, we have $t = t_0(x) \pm \frac{1}{2}\sqrt{16x^2 + 4 - r(x)}$. These are minima, since $\frac{\partial^2 I}{\partial t^2} > 0$ for each.

In the simulations of the PDE we can start with initial conditions with $r(0)$ close to 1 and $t_0(0) = \theta(0) = 0$. At each x, the value of t_0 giving the maximum intensity is then labelled as $t_0(x)$. This shows up the dependence of $t_0(x)$ on c. At this point, we use the intensity maximum, $I_m = \frac{[r(x)-4]^2+64x^2}{r(x)^2}$, to find $r(x)$ by solving the quadratic equation. This shows up the dependence of $r(x)$ on c. At each such point, we have x and $r(x)$, and the complex number $\psi(x, t = t_0(x)) = \left[\frac{4(1+2ix)}{r(x)} - 1\right] e^{i[x-\theta(x)]}$, we directly find $\theta(x)$. So we can compare the PDE results with the results found by solving the 4 ODEs approximately. Using the numerical PDE runs, we now find how $r(x)$, $t_0(x)$ and $\theta(x)$ depend on c and τ_R.

From numerics, we can plot $r(x) - 1 - 4x^2$ for various values of c, and then observe if it can be expressed as $c^n f(x)$ for some integer n, i.e. whether the dependence on c and x can be separated for a suitably chosen value of n. Results show that $n = 1$ with $f(x) = -2(1+4x^2)^k$ works well for $k = 1.865$, thus roughly supporting the result of Eq.(7.37), which had $k = 3/2$. Here, c is arbitrarily chosen, and it determines how much $r(0)$ differs from 1.

Similarly, we can plot $t_0(x)/\tau_R$ for various values of c, and then observe if it can be expressed as

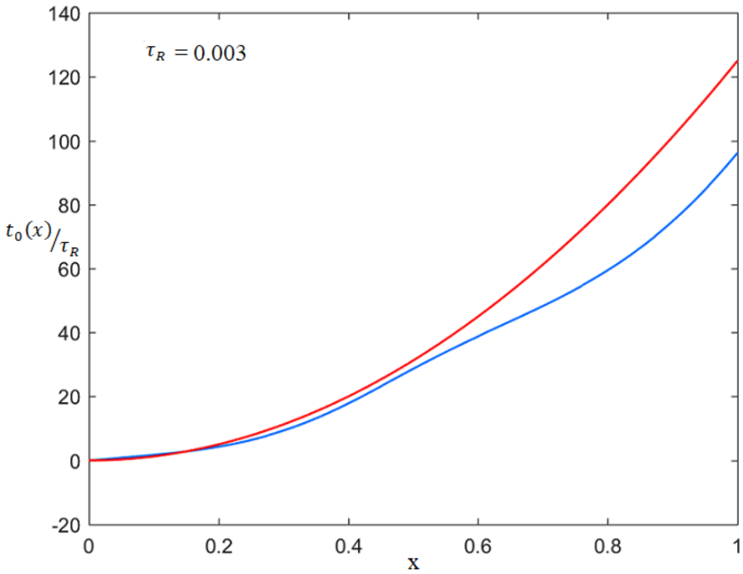

Figure 7.13: Plot of function $t_0(x)/\tau_R$, from numerics (blue curve) for $c = 0.1$. The magenta curve is from the analytic prediction of Eq.(7.51). It is in fairly good agreement with the numeric curve. Thus, the reduced model has provided a reasonably good description of the rogue wave dynamics.

$j[c]g(x)$. Similarly, we plot $\theta(x)$ for various values of c, and then observe if it can be expressed as $c\,h(x)$. For small x, we find that $t_0(x)/\tau_R \equiv x^2$, agreeing with the analytic form.

For small c, the numeric data shows that:

$$t_0(x) \approx 25\,\tau_R x^2(1 + 14.7c),$$

for offset c. So, when c is not too small, $t_0(x)$ is of the same order as the analytic form, Eq.(7.51), found earlier. An example, with $c = 0.1$ is given in Fig.7.13.

7.7 Numerical determination of functions

Suppose $\theta(x) = -c^n y(x)$ and $r(x) = 4x^2 + 1 + c^n r_1(x)$ for some unknown n. Then we find, in this model, that, on the 'ridge' formed by the maxima at each x:

$$\psi[x, t = t_0(x); c] =$$

$$\left(-1 + \frac{4(1+2ix)}{c^n r_1(x) + 4x^2 + 1}\right) e^{i(x + c^n y(x))}$$

while NLSE result is:

$$\psi[x, t = 0] = \left(-1 + \frac{4(1+2ix)}{4x^2 + 1}\right) e^{i(x)}$$

Using numerics, we subtract one from the other. Suppose, the difference Δ is:

$$\Delta = -c^n e^{ix}[f(x) + in(x)].$$

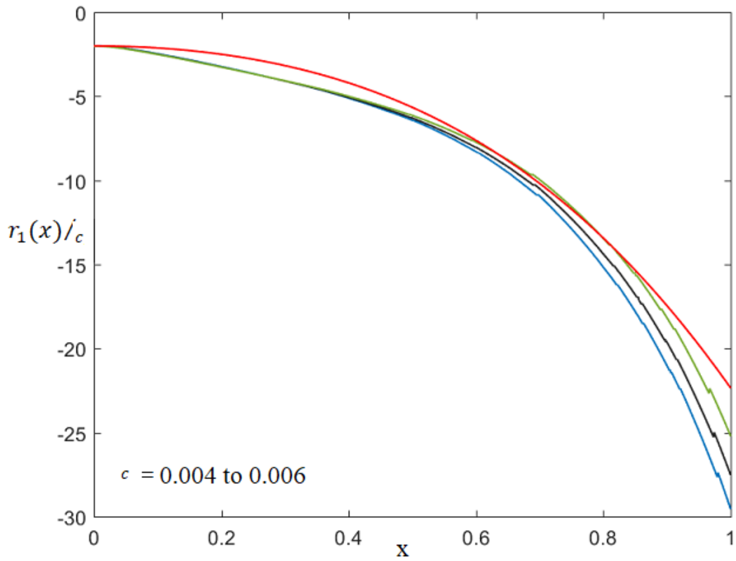

Figure 7.14: The function $r_1(x)$ found from numerical solution of the PDE. Three values of c, from (blue curve) 0.004 to (green curve) 0.006 are used and the initial value is $r(0) = 1-2c$. The analytic form, $r_1(x) = (r(x)-1-4x^2)/c \approx -2(1+4x^2)^{3/2}$, shown by red curve is close to the numerical results.

Along the 'ridge', we measure this Δ as a complex function of x. So, by finding a few values of Δ, we determine the dependence on c, and immediately find the value of n, which turns out to be 1.

Then, expanding $e^{ix}(\psi[x,t=t_0(x);c]-\psi[x,t]-\Delta)$ for small c gives the first non-zero term. Equating it to zero gives

$$f(x)+in(x)+\frac{\frac{4ir_1(x)}{i-2x}+(1-2ix)(2x-3i)y(x)}{(2x+i)^2}=0.$$

Solving this equation, we obtain $r_1(x), y(x)$ explicitly:

$$r_1(x)=\frac{1}{12}\left(4x^2+1\right)\left[\left(3-4x^2\right)f(x)+8xn(x)\right],$$

and

$$y(x)=\frac{1}{3}\left[2xf(x)-n(x)\right].$$

We use this procedure to produce curves for $r_1(x)$ and $y(x)$ for various values of c. From Fig.7.14 and curves for other c values, we find $r_1(x) \approx -2\left(4x^2+1\right)^{1.865}$. This can be compared with $-2\left(4x^2+1\right)^{3/2}$ found from the analytic result, so the approximate result is reasonably accurate.

From Fig.7.15 and curves for other c values, we find $y(x) \approx 35x$ and hence $\theta(x) \approx -35cx$ for $x<1$. For small x, we find:

$$y(x) \equiv -\theta(x)/(c) = 35x+2\left(96+\frac{35}{3}\right)x^3+\cdots.$$

Plainly, for small x, which is the main region of interest for the localized rogue wave, we have $\theta(x) \approx -35\,cx$, which is in good agreement with the value from the expression found numerically.

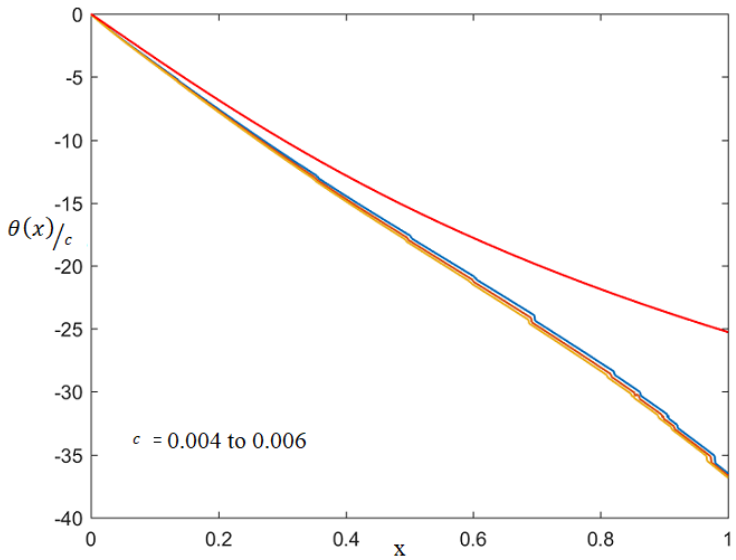

Figure 7.15: Numerical PDE solution giving $\theta(x)/c$. Various values of c are used and the initial value is $r(0) = 1-2c$. The analytic result is plotted by the magenta line, $\theta(x)/c = -(35/2)\,\mathrm{arcsinh}(2x) \approx -35x$ for x small, using Eq.(7.52). The numerically found curve for $\theta(x)/c$ is quite close to $-35x$ over this range, $0 < x < 1$.

7.8 Conclusion

In this chapter, we have found rogue wave solutions of higher-order extensions of the NLSE. It is found that our approach can be useful when exact solutions of the evolution equation do not exist. The applicability of the technique has been confirmed in the previous chapter when we tested it on a few integrable equations and compared the results with the exact solutions. The NLSE equation with extra terms for the intrapulse Raman delay, the fourth and sixth order dispersion is an example of a non-integrable evolution equations for which the exact solution cannot be found. Therefore, as a more complicated example of application of this technique, we used the Lagrangian approach to evaluate the effects of fourth and sixth order dispersion on rogue waves. Besides, approximate solutions in the forms of solitons and rogue waves have been obtained and analyzed for an optical fiber with a Raman delay term. The results were compared with solutions found by numerical simulations of the original equations. Reasonably good agreements were found, confirming the usefulness of the approach. A generalization to even higher-order dispersive terms shows that the phase function for the rogue wave can be written in terms of well-known functions. This approach is not too lengthy for additional dispersion terms (see sections 7.1 and 7.2), whilst it becomes more complicated for the extra nonlinear term like the Raman delay response. In the former case, we have a choice to pick non-lateral movement ($t_0(x) = 0$); however, in the latter case, a bent trajectory is expected due to the nature of this kind of physical effect.

The approach presented here can also be used to study other optical systems that are described by non-integrable equations. One example is wave propagation in nonlinear quadratic media.

CHAPTER 8

Conclusion And Prospective

Conclusions

In this thesis, a detailed study of rogue waves in various nonlinear systems has been presented. Rogue waves are localized structures in both space and time. The formation of these phenomena can vary from a subject to another one. The existence and emergence of these structures in the context of nonlinear dynamics have been discussed.

In this thesis, we investigated rogue waves in various nonlinear systems, such as shallow water waves, internal waves, plasma, and optical fibers. New solutions in the form of localised waves with high-amplitude peaks have been discovered. Important properties of these structures found in these studies are listed below.

- Internal waves have been studied in the frame of the Gardner equation which is a generic model for waves in multi-layer structures. 'Bright' and 'dark' rogue waves of this equation have been found. For each of them, a set of four exact rational solutions with increasing order of polynomials has been given. These are the lowest-order examples which belong to the corresponding hierarchies of rogue-wave solutions of Gardner equation. The maximal (and minimal) amplitudes and the background levels of these solutions for arbitrary order were deduced, based on the lowest-order examples. These solutions can be useful for explanation of extremely large amplitude internal waves in the ocean. They can be used also in other areas of nonlinear physics, such as optics and dusty plasmas.

- The formation of rogue waves in shallow water was modelled by providing the three lowest-order exact rational complex-valued solutions of the Korteweg-de Vries (KdV) equation. It was found that the amplitude amplification factor of such waves is much larger than the amplitude amplification factor of rogue waves occurring in deep water. These results clearly demonstrate a potential hazard for coastal areas. These solutions imply the existence of shallow water rogue waves with amplitudes exceeding the soliton collision amplitudes of the real KdV equation. Namely, they are proportional to the square of the order of the solution. The significance of our findings is not restricted to water rogue waves only. Our findings can be used in optics, where the ideas of shallow water rogue waves are applicable to few-cycle pulses.

- The formation of rogue waves has been studied also in the case of an infinitely-extended KdV equation. This evolution equation contains an infinite number of arbitrary real coefficients controlling higher-order terms. The latter are chosen in a way that maintains the integrability of the whole equation. This extended equation admits complex-valued solutions expressed in terms of hyperbolic and rational functions that model solitons and rogue waves.

- A theory for novel rogue wave structures (called real-valued rogue waves) appearing in nonlinear dust-acoustic waves for a long wave-length model in a plasma with cold and heavy dust particles at thermal equilibrium has been investigated. The model is based on the Gardner equation, which is an accurate model for weakly nonlinear and dispersive wave propagation in the regime of small amplitude waves. A discrete set of rational solutions suggests that a considerable amount of energy (or electric charge) could become concentrated in a relatively small area of space at a certain time. These are features of rogue waves that are similar to those in the ocean or in fiber optics. Furthermore, it was shown that the dust electric potential amplitude of these rogue waves strongly depends on the ratio between the ion and electron temperatures and densities in the plasma.

- The Lagrangian approach has been developed for finding rogue wave solutions of the extended nonlinear Schrödinger equation (NLSE). A list of Lagrangian components for a variety of terms in the extended equation has been presented. Having this list turns the finding and analysis of approximate solutions of any equations into a simple and straightforward exercise. With higher-order terms in the equation, the solution becomes distorted, but it remain localised both in space and time. If the equation of interest is integrable, its trial function solutions naturally coincide with the exact rogue wave solutions. This fact has been demonstrated for several well-known equations. These include Hirota, Lakshmanan-Porsezian- Daniel (LPD), and the Kundu-Echkaus equations.

- Most importantly, the Lagrangian approach has been used for finding approximate solutions of non-integrable equations when finding exact solutions is not possible. One example is the equation with the Raman term. It does not have an exact solution in the form of a rogue wave but an approximation can be found. The accuracy of this approximation has been evaluated using numerical simulations. The approach presented here can also be useful in studies of rogue waves in other optical systems which are modelled by non-integrable equations. This is the case when the pulse duration is in femtosecond time scale.

Future challenges

We are experiencing a new era of living conditions with extremes occurring more frequently. Thus, understanding the reasons for appearance of rogue waves in nature is highly important. Such understanding can be reached using mathematical modelling of wave dynamics.

The goal of this thesis is to apply mathematical formalism to practical needs rather than just solving differential equations. This aspect of research was the major incentive in the choice of problems to consider. One of the consequences of this strategy is the wide range of areas of physics where the results can be used. Although potential extensions and future challenges are countless, the following examples may keep the author busy in future.

- The next step in the problem of shallow water rogue waves can be the variable depth and wave breaking as the most common effects influencing wave dynamics in coastal areas. Taking these effects into account will bring more practical outcomes. Continuing research in this direction is important as rogue waves in the coastal areas constitute nearly 70% of the total number of extreme water wave events.

- Applying the Lagrangian approach to higher-order rogue waves is another challenge to meet. Their deformation in the presence of a perturbations is still an unsolved problem. One example would be the study of the rogue wave triplets when the NLSE has perturbations in the form the fourth, sixth order dispersion or the Raman delay effect.

- The number of parameters in the trial function is the factor that influences the accuracy of the Lagrangian approach. Increasing this number provides more realistic dynamics. However, complexity of the resulting dynamical system with reduced dimensionality requires more efforts to resolve. The potential extension of possibilities in this direction is endless.

- The Lagrangian technique like other methods has its own strengths and weaknesses. One of these difficulties is finding the Lagrangian density for various evolution equations. As this quantity plays a central role in the technique, its calculation is critical. Most common Lagrangian density components for an extended NLSE are given. Their calculation can be tedious and lengthy for other equations leading to complicated results or impossibility of finding the Lagrangian density. Modifications of our present approach to tackle these situations could be the next step.

- In plasmas, rogue waves can be studied for many other component compositions. Significant step of considering the real-valued quantities like electrostatic potential may provide more insight into plasma dynamics at its extremes.

- Propagation of large-amplitude internal waves can be expanded beyond the standard Gardner equation (5.10) with the constant coefficients. Since the coefficients in Gardner equation depend on the depth of the ocean, the variable-coefficient Gardner equation can be a better approximation. Upgrading the three-layer stratification model or considering the two-layer fluid may reveal other important features of these waves.

Chapter 9

Appendix

9.1 Bilinear Hirota method and rational solutions to the Gardner equation

We consider the Gardner equation in the form:

$$\psi_x + \psi\psi_t + 6\psi^2\psi_t + \psi_{ttt} = 0. \tag{9.1}$$

If we have a solution of Eq.(5.10), then we can obtain the corresponding solution of Eq.(9.1) by using $\psi \to \psi/6, t \to t/\sqrt{6}, x \to x/(6\sqrt{6})$. Using Bilinear Hirota method [353], we obtain [354]:

$$(D_x + D_t^3)G(x,t) \diamond F(x,t) = 0,$$

$$iD_t G(x,t) \diamond F(x,t) + 6D_t^2 G(x,t) \diamond F(x,t) = 0.$$

The functions $G(x,t)$ and $F(x,t)$ are related to the solution of the Eq.(9.1) through the mapping:

$$\psi(x,t) = (-i\log(\frac{G(x,t)}{F(x,t)}))_t.$$

Here the Hirota operator D_z^n is:

$$D_z^n F \diamond G = (\frac{\partial}{\partial z} - \frac{\partial}{\partial z'})^n G(x,t)F(x',t'),$$

where z can be x or t.

By defining the real-valued functions f and g, where $F = f - ig$ and $G = f + ig$, we can obtain the Bilinear Hirota equations as:

$$6(f_{tt}f - f_t^2 + g_{tt}g - g_t^2) - (g_t f - f_t g) = 0, \tag{9.2}$$

and

$$g_x f - f_x g + g_{ttt} f - 3g_{tt} f_t + 3g_t f_{tt} - g f_{ttt} = 0. \tag{9.3}$$

For the various orders of the rational solutions, we now seek low order polynomials f and g to satisfy Eqs.(9.2) and (9.3).

9.2 Analysis of functions

We now need to specify the forms for $g(x,t)$ and $f(x,t)$ used in deriving the n^{th} order rogue wave. We set

$$g_n = \sum_{j=0}^{n-1} h_j^{[n]}(t) x^j,$$

$$f_n = \sum_{j=0}^{n-1} s_j^{[n]}(t) x^j. \tag{9.4}$$

We set the leading order coefficient to be positive.

9.2.1 Functions for the first order rational solution

for the 1st order, we can set one of the functions constant and find another one independent of variable x. It is straightforward to show that:

$$\begin{aligned} g_1 &= h_0^{[1]} = 6, \quad &(9.5)\\ f_1 &= s_0^{[1]}(t) = t. \quad &(9.6) \end{aligned}$$

We find the known soliton-like form as:

$$\psi_1 = -\frac{12}{t^2 + 36}. \tag{9.7}$$

This solution is a stationary solution for the Gardner equation as it does not depend on the evolution value x.

9.2.2 Functions for the second order rational solution

For the second order, again we set one of the function $f(x,t)$ and $g(x,t)$ constant respect to the propagation axis, viz. x, and another one as a linear function respect to x. So, for 2nd order, we can write:

$$g_2(x,t) = h_0^{[2]}(t),$$

$$f_2(x,t) = s_0^{[2]}(t) + x s_1^{[2]}.$$

It is easy to show that:

$$\begin{aligned} s_0^{[2]}(t) &= t\left(t^2-108\right), \\ s_1^{[2]} &= 12, \\ h_0^{[2]}(t) &= 18\left(t^2+36\right). \end{aligned} \tag{9.8}$$

So

$$\psi_2 = -\frac{36(t^4+216t^2-24tx-3888)}{t^6+108t^4+24t^3x+34992t^2-2592tx+144(x^2+2916)}. \tag{9.9}$$

9.2.3 Functions for the third order rational solution

The same scenario patterns can be followed for the third and fourth-order sub-functions. A similar pattern can be retained for the 3rd order, and we can write:

$$g_3 = h_0^{[3]}(t) + h_1^{[3]}(t)x$$

$$f_3 = s_0^{[3]}(t) + s_1^{[3]}(t)x + s_2^{[3]}x^2.$$

After some algebraic calculations, we will find:

$$\begin{aligned} s_0^{[3]}(t) &= \frac{t^6}{720} - \frac{3t^4}{4} - 81t^2 - 2916, \\ s_1^{[3]}(t) &= \frac{1}{12}t\left(t^2-108\right), \\ h_0^{[3]}(t) &= t\left(\frac{t^4}{20}+972\right), \\ h_1^{[3]}(t) &= \frac{3}{2}\left(t^2-108\right), \end{aligned} \tag{9.10}$$

and $s_2^{[3]} = -1$ is a constant only. We note that the polynomials have positive terms of highest order.

Using the 'arctan' expression, we now find $\psi_3 = G_3/D_3$ with:

$$G_3 = -72[t^{10}+540t^8+272160t^6-25920t^5x$$

$$+5400t^4\left(x^2-3888\right)+9331200t^3x-388800t^2\left(x^2+2916\right)$$

$$+43200tx\left(x^2+11664\right)+6998400\left(5x^2+5832\right)],$$

and

$$D_3 = t^{12}+216t^{10}+120t^9x+174960t^8$$

$$+2160t^6\left(x^2+50544\right)-8398080t^5x$$

$$+1166400t^4\left(x^2+4860\right)-86400t^3x\left(x^2-23328\right)$$

$$-125971200t^2\left(x^2-5832\right)+9331200tx\left(x^2-14580\right)$$

$$+518400\left(x^4+32076x^2+8503056\right). \tag{9.11}$$

The coefficients differ from those provided in Chapter 2 because a factor of 6 has been put into the equation here.

It is straightforward to show that this satisfies the Gardner equation, i.e. Eq.(9.1).

9.2.4 Functions for the fourth order rational solution

We now need to extend the *ansatz* for g_4 and f_4:

$$g_4 = h_0^{[4]}(t)+xh_1^{[4]}(t)+x^2h_2^{[4]}(t)+x^3h_3^{[4]}, \tag{9.12}$$
$$f_4 = s_0^{[4]}(t)+xs_1^{[4]}(t)+x^2s_2^{[4]}+x^3s_3^{[4]}(t).$$

Now

$$h_0^{[4]}(t) = 60t\left[t^8-216t^6+29393280(t^2-54)\right],$$
$$s_0^{[4]}(t) = t^{10}-1620t^8-272160t^6-146966400(1944+162t^2+t^4),$$

while

$$h_1^{[4]}(t) = 7560\left[t^6-180t^4+58320(84-t^2)\right],$$
$$s_1^{[4]}(t) = 180t\left[t^6-756t^4+45360(108+t^2)\right].$$

Then $h_2^{[4]}(t) = 65318400t$ and $s_2^{[4]} = -391910400$, and $h_3^{[4]} = 1814400$ and $s_3^{[4]}(t) = 302400t$.

With these functions, g_4, f_4 satisfy Eqs.(9.2) and (9.3).

The resulting

$$\psi_4(x,t) = 2[\arctan(\frac{g_4(x,t)}{f_4(x,t)})]_t \tag{9.13}$$

satisfies the Gardner equation, i.e. Eq.(9.1).

9.2.5 Polynomials: even and odd

By looking at these functions for various orders, we observe some patterns by using results given in equations (9.5), (9.8), (9.10) and (9.12).

When the highest power in t in $h_j^{[n]}(t)$ is even, then the whole polynomial $h_j^{[n]}(t)$ is even. When the highest power in t in $h_j^{[n]}(t)$ is odd, then the whole polynomial $h_j^{[n]}(t)$ is odd. For example, in the 3rd order example of the previous section, Eq.(9.10), $h_0^{[3]}(t)$ and $s_1^{[3]}(t)$ are fully odd, while $h_1^{[3]}(t)$ and $s_0^{[3]}(t)$ are fully even. This can reveal the inversion-reflection symmetry, as an important feature, for the solutions of the Gardner equation. If we use the general polynomials for these functions, then we can import arbitrary parameters which can show the dynamics for these waves.

The 4 lowest order Gardner rogues all have zero background in the formulation here. The centre values for $n = 1,2,3,4$ are respectively $-\frac{1}{3}, \frac{1}{3}, -\frac{2}{3}, \frac{2}{3}$. So, in terms of earlier notation, $n = 1,3$ forms are 'dark', while $n = 2,4$ forms are 'bright'. The extrema take values one-sixth of those found with the other normalization [125].

BIBLIOGRAPHY

[1] N. Akhmediev, A. Ankiewicz, and J. M. Soto-Crespo, “Rogue waves and rational solutions of the nonlinear Schrödinger equation,” *Physical Review E*, vol. 80, no. 2, p. 026601, 2009.

[2] A. Ankiewicz and N. Akhmediev, “Rogue wave-type solutions of the mKdV equation and their relation to known NLSE rogue wave solutions,” *Nonlinear Dynamics*, vol. 91, no. 3, pp. 1931–1938, 2018.

[3] M. Lakshmanan, K. Porsezian, and M. Daniel, “Effect of discreteness on the continuum limit of the Heisenberg spin chain,” *Physics Letters A*, vol. 133, no. 9, pp. 483–488, 1988.

[4] A. Ankiewicz, J. Soto-Crespo, and N. Akhmediev, “Rogue waves and rational solutions of the Hirota equation,” *Physical Review E*, vol. 81, no. 4, p. 046602, 2010.

[5] A. Ankiewicz and N. Akhmediev, “Rogue wave solutions for the infinite integrable nonlinear Schrödinger equation hierarchy,” *Physical Review E*, vol. 96, no. 1, p. 012219, 2017.

[6] C. Bayindir, “Rogue waves of the Kundu-Eckhaus equation in a chaotic wave field,” *Physical Review E*, vol. 93, no. 3, p. 032201, 2016.

[7] C. Gasparotti and E. Rusu, “A review concerning the rogue waves and their impact on navigation conditions,” *Mechanical Testing and Diagnosis*, vol. 6, no. 3, pp. 10–21, 2016.

[8] N. Akhmediev, J. M. Dudley, D. R. Solli, and S. Turitsyn, “Recent progress in investigating optical rogue waves,” *Journal of Optics*, vol. 15, no. 6, p. 060201, 2013.

[9] M. Bacha, L. A. Gougam, and M. Tribeche, “Ion-acoustic rogue waves in magnetized solar wind plasma with nonextensive electrons,” *Physica A: Statistical Mechanics and its Applications*, vol. 466, pp. 199–210, 2017.

[10] Y. Zhen-Ya, “Financial rogue waves,” *Communications in Theoretical Physics*, vol. 54, no. 5, p. 947, 2010.

[11] G. A. El, E. G. Khamis, and A. Tovbis, “Dam break problem for the focusing nonlinear Schrödinger equation and the generation of rogue waves,” *Nonlinearity*, vol. 29, no. 9, p. 2798, 2016.

[12] A. Chabchoub and M. Fink, "Time-reversal generation of rogue waves," *Physical Review Letters*, vol. 112, no. 12, p. 124101, 2014.

[13] M. Onorato, S. Residori, U. Bortolozzo, A. Montina, and F. Arecchi, "Rogue waves and their generating mechanisms in different physical contexts," *Physics Reports*, vol. 528, no. 2, pp. 47–89, 2013.

[14] V. Ruban, Y. Kodama, M. Ruderman, J. Dudley, R. Grimshaw, P. McClintock, M. Onorato, C. Kharif, E. Pelinovsky, T. Soomere, *et al.*, "Rogue waves–towards a unifying concept?: Discussions and debates," *The European physical journal special topics*, vol. 185, no. 1, pp. 5–15, 2010.

[15] L.-L. Feng, S.-F. Tian, X.-B. Wang, and T.-T. Zhang, "Rogue waves, homoclinic breather waves and soliton waves for the (2+ 1)-dimensional B-type Kadomtsev-Petviashvili equation," *Applied Mathematics Letters*, vol. 65, pp. 90–97, 2017.

[16] N. Akhmediev, A. Ankiewicz, and M. Taki, "Waves that appear from nowhere and disappear without a trace," *Physics Letters A*, vol. 373, no. 6, pp. 675–678, 2009.

[17] H. Chien, C.-C. Kao, and L. Z. Chuang, "On the characteristics of observed coastal freak waves," *Coastal Engineering Journal*, vol. 44, no. 04, pp. 301–319, 2002.

[18] P. C. Liu, "A chronology of freauqe wave encounters," *Geofizika*, vol. 24, no. 1, pp. 57–70, 2007.

[19] P. Müller, C. Garrett, and A. Osborne, "Rogue waves," *Oceanography*, vol. 18, no. 3, p. 66, 2005.

[20] N. Haritos, "Modelling ocean waves and their effects on offshore structures," Australian Earthquake Engineering Society 2010 Conference, pp. 1–7, 2010.

[21] S. Haver, "A possible freak wave event measured at the Draupner Jacket January 1 1995," in *Rogue waves*, vol. 2004, pp. 1–8, 2004.

[22] E. Didenkulova, "Catalogue of rogue waves occurred in the world ocean from 2011 to 2018 reported by mass media sources," *Ocean and Coastal Management*, p. 105076, 2019.

[23] C. Kharif and E. Pelinovsky, "Physical mechanisms of the rogue wave phenomenon," *European Journal of Mechanics - B/Fluids*, vol. 22, pp. 603–634, 2003.

[24] R. Grimshaw, E. Pelinovsky, T. Taipova, and A. Sergeeva, "Rogue internal waves in the ocean: Long wave model," *The European Physical Journal Special Topics*, vol. 185, no. 1, pp. 195–208, 2010.

[25] A. Porubov, H. Tsuji, I. Lavrenov, and M. Oikawa, "Formation of the rogue wave due to non-linear two-dimensional waves interaction," *Wave Motion*, vol. 42, no. 3, pp. 202–210, 2005.

[26] C. H. Wu and A. Yao, "Laboratory measurements of limiting freak waves on currents," *Journal of Geophysical Research: Oceans*, vol. 109, no. C12, 2004.

[27] A. Chabchoub, N. Hoffmann, and N. Akhmediev, "Rogue wave observation in a water wave tank," *Physical Review Letters*, vol. 106, no. 20, p. 204502, 2011.

[28] N. Akhmediev and E. E. Pelinovsky, "discussion & debate: Rogue waves–towards a unifying concept?," *The European Physical Journal Special Topics*, vol. 185, no. 1, 2010.

[29] A. Chabchoub, N. Hoffmann, M. Onorato, and N. Akhmediev, "Super rogue waves: observation of a higher-order breather in water waves," *Physical Review X*, vol. 2, no. 1, p. 011015, 2012.

[30] G. P. Agrawal, "Nonlinear fiber optics: its history and recent progress," *JOSA B*, vol. 28, no. 12, pp. A1–A10, 2011.

[31] D. Axelrod, T. P. Burghardt, and N. L. Thompson, "Total internal reflection fluorescence," *Annual Review of Biophysics and Bioengineering*, vol. 13, no. 1, pp. 247–268, 1984.

[32] Y. S. Kivshar and G. Agrawal, *Optical solitons: from fibers to photonic crystals, Academic press, 2003*.

[33] D. H. Jundt, "Temperature-dependent Sellmeier equation for the index of refraction in congruent lithium niobate," *Optics Letters*, vol. 22, no. 20, pp. 1553–1555, 1997.

[34] G. P. Agrawal, "Nonlinear fiber optics third edition," *Optics And Photonics*, vol. 2, 2001.

[35] M. F. Ferreira, *Nonlinear effects in optical fibers*, vol. 2, John Wiley & Sons, 2011.

[36] M. Yasin, S. W. Harun, and H. Arof, *Recent progress in optical fiber research, InTech, 2012*.

[37] L. F. Mollenauer and R. H. Stolen, "Solitons in optical fibers," *Laser Focus*, vol. 18, no. 4, p. 196, 1982.

[38] K. J. Blow and D. Wood, "Theoretical description of transient stimulated Raman scattering in optical fibers," *IEEE Journal of Quantum Electronics*, vol. 25, no. 12, pp. 2665–2673, 1989.

[39] A. Hasegawa and F. Tappert, "Transmission of stationary nonlinear optical pulses in dispersive dielectric fibers. I. Anomalous dispersion," *Applied Physics Letters*, vol. 23, no. 3, pp. 142–144, 1973.

[40] L. F. Mollenauer, R. H. Stolen, and J. P. Gordon, "Experimental observation of picosecond pulse narrowing and solitons in optical fibers," *Physical Review Letters*, vol. 45, no. 13, p. 1095, 1980.

[41] F. M. Mitschke and L. F. Mollenauer, "Experimental observation of interaction forces between solitons in optical fibers," *Optics Letters*, vol. 12, no. 5, pp. 355–357, 1987.

[42] M. Peccianti, K. A. Brzdakiewicz, and G. Assanto, "Nonlocal spatial soliton interactions in nematic liquid crystals," *Optics Letters*, vol. 27, no. 16, pp. 1460–1462, 2002.

[43] J. S. Aitchison, A. Weiner, Y. Silberberg, M. Oliver, J. Jackel, D. Leaird, E. Vogel, and P. Smith, "Observation of spatial optical solitons in a nonlinear glass waveguide," *Optics Letters*, vol. 15, no. 9, pp. 471–473, 1990.

[44] C. Conti, M. A. Schmidt, P. S. J. Russell, and F. Biancalana, "Highly noninstantaneous solitons in liquid-core photonic crystal fibers," *Physical Review Letters*, vol. 105, no. 26, p. 263902, 2010.

[45] T. Marchant and N. Smyth, "Soliton interaction for the extended korteweg-de vries equation," *IMA Journal of Applied Mathematics*, vol. 56, no. 2, pp. 157–176, 1996.

[46] D. Guo, S. Mazumdar, S. Dixit, F. Kajzar, F. Jarka, Y. Kawabe, and N. Peyghambarian, "Role of the conduction band in electroabsorption, two-photon absorption, and third-harmonic generation in polydiacetylenes," *Physical Review B*, vol. 48, no. 3, p. 1433, 1993.

[47] A. Peleg, M. Chertkov, and I. Gabitov, "Interchannel interaction of optical solitons," *Physical Review E*, vol. 68, no. 2, p. 026605, 2003.

[48] S. G. Evangelides, L. F. Mollenauer, J. P. Gordon, and N. S. Bergano, "Polarization multiplexing with solitons," *Journal of Lightwave Technology*, vol. 10, no. 1, pp. 28–35, 1992.

[49] R. Noone, "Marconi wins contract for domestic Australian fibre." www.computerworld.com/au, 2001.

[50] C. Gu, *Soliton theory and its applications, Springer Science and Business Media, 2013*.

[51] A. P. Sheppard, *Polarisation effects in the theory of optical solitons, PhD thesis, The Australian National University, 1995*.

[52] N. N. Akhmediev and A. Ankiewicz, *Solitons: nonlinear pulses and beams, Chapman and Hall, 1997*.

[53] A. Armaroli, D. Eeltink, M. Brunetti, and J. Kasparian, "Nonlinear stage of Benjamin-Feir instability in forced/damped deep-water waves," *Physics of Fluids*, vol. 30, no. 1, p. 017102, 2018.

[54] J. Marburger and E. Dawes, "Dynamical formation of a small-scale filament," *Physical Review Letters*, vol. 21, no. 8, p. 556, 1968.

[55] A. Hasegawa and W. Brinkman, "Tunable coherent IR and FIR sources utilizing modulational instability," *IEEE Journal of Quantum Electronics*, vol. 16, no. 7, pp. 694–697, 1980.

[56] K. Tai, A. Hasegawa, and A. Tomita, "Observation of modulational instability in optical fibers," *Physical Review Letters*, vol. 56, no. 2, p. 135, 1986.

[57] N. Akhmediev and V. Korneev, "Modulation instability and periodic solutions of the nonlinear Schrödinger equation," *Theoretical and Mathematical Physics*, vol. 69, no. 2, pp. 1089–1093, 1986.

[58] C. Liu, Y. Ren, Z.-Y. Yang, and W.-L. Yang, "Superregular breathers in a complex modified Korteweg-de Vries system," *Chaos: An Interdisciplinary Journal of Nonlinear Science*, vol. 27, no. 8, p. 083120, 2017.

[59] J. M. Dudley, G. Genty, F. Dias, B. Kibler, and N. Akhmediev, "Modulation instability, Akhmediev Breathers and continuous wave supercontinuum generation," *Optics express*, vol. 17, no. 24, pp. 21497–21508, 2009.

[60] D. R. Solli, C. Ropers, P. Koonath, and B. Jalali, "Optical rogue waves," *Nature*, vol. 450, no. 7172, pp. 1054–1057, 2007.

[61] K. B. Dysthe and K. Trulsen, "Note on breather type solutions of the NLS as models for freak-waves," *Physica Scripta*, vol. 1999, no. T82, p. 48, 1999.

[62] L. Ling, B.-F. Feng, and Z. Zhu, "Multi-soliton, multi-breather and higher order rogue wave solutions to the complex short pulse equation," *Physica D: Nonlinear Phenomena*, vol. 327, pp. 13–29, 2016.

[63] R. Grimshaw, A. Slunyaev, and E. Pelinovsky, "Generation of solitons and breathers in the extended Korteweg–de Vries equation with positive cubic nonlinearity," *Chaos: An Interdisciplinary Journal of Nonlinear Science*, vol. 20, no. 1, p. 013102, 2010.

[64] H. Xiong and Y. Wu, "Optomechanical Akhmediev Breathers," *Laser & Photonics Reviews*, vol. 12, no. 7, p. 1700305, 2018.

[65] B. Frisquet, B. Kibler, and G. Millot, "Collision of Akhmediev breathers in nonlinear fiber optics," *Physical Review X*, vol. 3, no. 4, p. 041032, 2013.

[66] F. Baronio, “Akhmediev breathers and Peregrine solitary waves in a quadratic medium,” *Optics letters*, vol. 42, no. 9, pp. 1756–1759, 2017.

[67] R. Schiek and F. Baronio, “Spatial Akhmediev breathers and modulation instability growth-decay cycles in a quadratic optical medium,” *Physical Review Research*, vol. 1, no. 3, p. 032036, 2019.

[68] D. Solli, C. Ropers, and B. Jalali, “Active control of rogue waves for stimulated supercontinuum generation,” *Physical Review Letters*, vol. 101, no. 23, p. 233902, 2008.

[69] D. H. Peregrine, “Water waves, nonlinear schrödinger equations and their solutions,” *The ANZIAM Journal*, vol. 25, no. 1, pp. 16–43, 1983.

[70] N. K. Vitanov, A. Chabchoub, and N. Hoffmann, “Deep-water waves: on the nonlinear schrödinger equation and its solutions,” *Journal of Theoretical and Applied Mechanics*, vol. 43, no. 2, pp. 43–54, 2013.

[71] B. Kibler, J. Fatome, C. Finot, G. Millot, F. Dias, G. Genty, N. Akhmediev, and J. M. Dudley, “The Peregrine soliton in nonlinear fibre optics,” *Nature Physics*, vol. 6, no. 10, pp. 790–795, 2010.

[72] A. Chabchoub, N. Hoffmann, M. Onorato, A. Slunyaev, A. Sergeeva, E. Pelinovsky, and N. Akhmediev, “Observation of a hierarchy of up to fifth-order rogue waves in a water tank,” *Physical Review E*, vol. 86, no. 5, p. 056601, 2012.

[73] A. Ankiewicz, D. J. Kedziora, and N. Akhmediev, “Rogue wave triplets,” *Physics Letters A*, vol. 375, no. 28-29, pp. 2782–2785, 2011.

[74] D. J. Kedziora, A. Ankiewicz, and N. Akhmediev, “Classifying the hierarchy of nonlinear-schrödinger-equation rogue-wave solutions,” *Physical Review E*, vol. 88, no. 1, p. 013207, 2013.

[75] D. J. Kedziora, A. Ankiewicz, and N. Akhmediev, “Circular rogue wave clusters,” *Physical Review E*, vol. 84, no. 5, p. 056611, 2011.

[76] U. Bandelow and N. Akhmediev, “Persistence of rogue waves in extended nonlinear Schrödinger equations: Integrable Sasa-Satsuma case,” *Physics Letters A*, vol. 376, no. 18, pp. 1558–1561, 2012.

[77] A. Ankiewicz, N. Akhmediev, and J. Soto-Crespo, “Discrete rogue waves of the Ablowitz-Ladik and Hirota equations,” *Physical Review E*, vol. 82, no. 2, p. 026602, 2010.

[78] B.-G. Zhai, W.-G. Zhang, X.-L. Wang, and H.-Q. Zhang, “Multi-rogue waves and rational solutions of the coupled nonlinear Schrödinger equations,” *Nonlinear Analysis: Real World Applications*, vol. 14, no. 1, pp. 14–27, 2013.

[79] S. Residori, U. Bortolozzo, A. Montina, F. Lenzini, and F. Arecchi, "Rogue waves in spatially extended optical systems," *Fluctuation and Noise Letters*, vol. 11, no. 01, p. 1240014, 2012.

[80] S. Residori, M. Onorato, U. Bortolozzo, and F. Arecchi, "Rogue waves: a unique approach to multidisciplinary physics," *Contemporary Physics*, vol. 58, no. 1, pp. 53–69, 2017.

[81] A. Montina, U. Bortolozzo, S. Residori, and F. Arecchi, "Non-gaussian statistics and extreme waves in a nonlinear optical cavity," *Physical Review Letters*, vol. 103, no. 17, p. 173901, 2009.

[82] J. Soto-Crespo, P. Grelu, and N. Akhmediev, "Dissipative rogue waves: extreme pulses generated by passively mode-locked lasers," *Physical Review E*, vol. 84, no. 1, p. 016604, 2011.

[83] C. Lecaplain, P. Grelu, J. Soto-Crespo, and N. Akhmediev, "Dissipative rogue waves generated by chaotic pulse bunching in a mode-locked laser," *Physical Review Letters*, vol. 108, no. 23, p. 233901, 2012.

[84] C. Lecaplain, P. Grelu, J. Soto-Crespo, and N. Akhmediev, "Dissipative rogue wave generation in multiple-pulsing mode-locked fiber laser," *Journal of Optics*, vol. 15, no. 6, p. 064005, 2013.

[85] J. He, S. Xu, and K. Porsezian, "New types of rogue wave in an erbium-doped fibre system," *Journal of the Physical Society of Japan*, vol. 81, no. 3, p. 033002, 2012.

[86] C. Bonazzola, A. Hnilo, M. Kovalsky, and J. R. Tredicce, "Optical rogue waves in an all-solid-state laser with a saturable absorber: importance of the spatial effects," *Journal of Optics*, vol. 15, no. 6, p. 064004, 2013.

[87] M. Erkintalo, G. Genty, and J. Dudley, "Rogue-wave-like characteristics in femtosecond supercontinuum generation," *Optics Letters*, vol. 34, no. 16, pp. 2468–2470, 2009.

[88] J. M. Dudley, G. Genty, and B. J. Eggleton, "Harnessing and control of optical rogue waves in supercontinuum generation," *Optics Express*, vol. 16, no. 6, pp. 3644–3651, 2008.

[89] S. Wabnitz, "Nonlinear guided wave optics; A testbed for extreme waves," *IOP Publishing, ISBN: 978-0-7503-1460-2, (Bristol, UK)*, 2017.

[90] D. Buccoliero, H. Steffensen, H. Ebendorff-Heidepriem, T. M. Monro, and O. Bang, "Midinfrared optical rogue waves in soft glass photonic crystal fiber," *Optics Express*, vol. 19, no. 19, pp. 17973–17978, 2011.

[91] K. Hammani and C. Finot, "Experimental signatures of extreme optical fluctuations in lumped Raman fiber amplifiers," *Optical Fiber Technology*, vol. 18, no. 2, pp. 93–100, 2012.

[92] V. Thomée, "From finite differences to finite elements a short history of numerical analysis of partial differential equations," in *Numerical Analysis: Historical Developments in the 20th Century*, pp. 361–414, Elsevier, 2001.

[93] H. Wang, "Numerical studies on the split-step finite difference method for nonlinear Schrödinger equations," *Applied Mathematics and Computation*, vol. 170, no. 1, pp. 17–35, 2005.

[94] M. Delfour, M. Fortin, and G. Payr, "Finite-difference solutions of a non-linear Schrödinger equation," *Journal of Computational Physics*, vol. 44, no. 2, pp. 277–288, 1981.

[95] J. Shao, X. Liang, and S. Kumar, "Comparison of split-step Fourier schemes for simulating fiber optic communication systems," *IEEE Photonics Journal*, vol. 6, no. 4, pp. 1–15, 2014.

[96] C. Bayindir, "Compressive split-step Fourier method," *arXiv:1512.03932*, 2015.

[97] W. Chang, J. M. Soto-Crespo, P. Vouzas, and N. Akhmediev, "Spiny solitons and noise-like pulses," *JOSA B*, vol. 32, no. 7, pp. 1377–1383, 2015.

[98] O. V. Sinkin, R. Holzlohner, J. Zweck, and C. R. Menyuk, "Optimization of the split-step Fourier method in modeling optical-fiber communications systems," *Journal of Lightwave Technology*, vol. 21, no. 1, pp. 61–68, 2003.

[99] W. Chang, *Dissipative solitons and their applications, PhD thesis, The Australian National University, 2009*.

[100] B. Siwicki, A. Filipkowski, R. Kasztelanic, M. Klimczak, and R. Buczyński, "Nanostructured graded-index core chalcogenide fiber with all-normal dispersion-design and nonlinear simulations," *Optics Express*, vol. 25, no. 11, pp. 12984–12998, 2017.

[101] C. Bao, W. Chang, C. Yang, N. Akhmediev, and S. T. Cundiff, "Observation of coexisting dissipative solitons in a mode-locked fiber laser," *Physical Review Letters*, vol. 115, no. 25, p. 253903, 2015.

[102] T. R. Taha and X. Xu, "Parallel split-step Fourier methods for the coupled nonlinear Schrödinger type equations," *The Journal of Supercomputing*, vol. 32, no. 1, pp. 5–23, 2005.

[103] S. K. Turitsyn, N. N. Rosanov, I. A. Yarutkina, A. E. Bednyakova, S. Fedorov, O. V. Shtyrina, and M. P. Fedoruk, “Dissipative solitons in fiber lasers,” *Physics-Uspekhi*, vol. 59, no. 7, p. 642, 2016.

[104] W. Chang and N. Akhmediev, “Exploding solitons and rogue waves in optical cavities,” *Nonlinear Optical Cavity Dynamics: From Microresonators to Fiber Lasers*, pp. 263–276, 2016.

[105] T. J. Kippenberg, A. L. Gaeta, M. Lipson, and M. L. Gorodetsky, “Dissipative Kerr solitons in optical microresonators,” *Science*, vol. 361, no. 6402, 2018.

[106] N. Akhmediev and A. Ankiewicz, *Dissipative solitons: from optics to biology and medicine*, vol. 751, Springer Science & Business Media, 2008.

[107] P. Grelu and N. Akhmediev, “Dissipative solitons for mode-locked lasers,” *Nature photonics*, vol. 6, no. 2, p. 84, 2012.

[108] N. N. Rosanov, S. V. Fedorov, and N. A. Veretenov, “Laser solitons in 1d, 2d and 3d,” *The European Physical Journal D*, vol. 73, no. 7, p. 141, 2019.

[109] N. Veretenov, N. Rosanov, and S. Fedorov, “Rotating and precessing dissipative-optical-topological-3d solitons,” *Physical Review Letters*, vol. 117, no. 18, p. 183901, 2016.

[110] S. Vergeles and S. K. Turitsyn, “Optical rogue waves in telecommunication data streams,” *Physical Review A*, vol. 83, no. 6, p. 061801, 2011.

[111] A. Klein, G. Masri, H. Duadi, K. Sulimany, O. Lib, H. Steinberg, S. A. Kolpakov, and M. Fridman, “Ultrafast rogue wave patterns in fiber lasers,” *Optica*, vol. 5, no. 7, pp. 774–778, 2018.

[112] F. Baronio, B. Frisquet, S. Chen, G. Millot, S. Wabnitz, and B. Kibler, “Observation of a group of dark rogue waves in a telecommunication optical fiber,” *Physical Review A*, vol. 97, no. 1, p. 013852, 2018.

[113] S. Chen, J. M. Soto-Crespo, and P. Grelu, “Dark three-sister rogue waves in normally dispersive optical fibers with random birefringence,” *Optics Express*, vol. 22, no. 22, pp. 27632–27642, 2014.

[114] S. Chen, Y. Ye, J. M. Soto-Crespo, P. Grelu, and F. Baronio, “Peregrine solitons beyond the threefold limit and their two-soliton interactions,” *Physical Review Letters*, vol. 121, no. 10, p. 104101, 2018.

[115] J. K. Duan, Y. L. Bai, Q. Wei, and M. H. Fan, “Super rogue waves in coupled electric transmission lines,” *Indian Journal of Physics*, pp. 1–5, 2019.

[116] S. Chen, Y. Zhou, L. Bu, F. Baronio, J. M. Soto-Crespo, and D. Mihalache, “Super chirped rogue waves in optical fibers,” *Optics Express*, vol. 27, no. 8, pp. 11370–11384, 2019.

[117] V. E. Zakharov and A. Gelash, “Nonlinear stage of modulation instability,” *Physical Review Letters*, vol. 111, no. 5, p. 054101, 2013.

[118] B. Kibler, A. Chabchoub, A. Gelash, N. Akhmediev, and V. E. Zakharov, “Superregular breathers in optics and hydrodynamics: omnipresent modulation instability beyond simple periodicity,” *Physical Review X*, vol. 5, no. 4, p. 041026, 2015.

[119] C. Liu and N. Akhmediev, “Super-regular breathers in nonlinear systems with self-steepening effect,” *Physical Review E*, vol. 100, no. 6, p. 062201, 2019.

[120] S. Coulibaly, M. Taki, A. Bendahmane, G. Millot, B. Kibler, and M. G. Clerc, “Turbulence-induced rogue waves in Kerr resonators,” *Physical Review X*, vol. 9, p. 011054, 2019.

[121] P. Walczak, S. Randoux, and P. Suret, “Optical rogue waves in integrable turbulence,” *Physical Review Letters*, vol. 114, no. 14, p. 143903, 2015.

[122] J. M. Soto-Crespo, N. Devine, and N. Akhmediev, “Integrable turbulence and rogue waves: breathers or solitons?,” *Physical Review Letters*, vol. 116, no. 10, p. 103901, 2016.

[123] N. Akhmediev, J. Soto-Crespo, and N. Devine, “Breather turbulence versus soliton turbulence: Rogue waves, probability density functions, and spectral features,” *Physical Review E*, vol. 94, no. 2, p. 022212, 2016.

[124] A. Chabchoub and N. Akhmediev, “Observation of rogue wave triplets in water waves,” *Physics Letters A*, vol. 377, no. 38, pp. 2590–2593, 2013.

[125] M. Bokaeeyan, A. Ankiewicz, and N. Akhmediev, “Bright and dark rogue internal waves: The Gardner equation approach,” *Physical Review E*, vol. 99, no. 6, p. 062224, 2019.

[126] I. Nikolkina, I. Didenkulova, E. Pelinovsky, and P. Liu, “Rogue waves in 2006-2010,” *Natural Hazards and Earth System Sciences*, vol. 11, no. 11, pp. 2913–2924, 2011.

[127] A. Ankiewicz, M. Bokaeeyan, and N. Akhmediev, “Shallow-water rogue waves: An approach based on complex solutions of the Korteweg-de Vries equation,” *Physical Review E*, vol. 99, no. 5, p. 050201, 2019.

[128] A. Ankiewicz, M. Bokaeeyan, and N. Akhmediev, “Infinitely extended complex KdV equation and its solutions: solitons and rogue waves,” *Physica Scripta*, vol. 95, no. 3, p. 035201, 2020.

[129] A. Ankiewicz, M. Bokaeeyan, and N. Akhmediev, “Rogue waves under influence of Raman delay,” *JOSA B*, vol. 35, no. 4, pp. 899–908, 2018.

[130] M. Bokaeeyan, A. Ankiewicz, and N. Akhmediev, “Rogue waves in higher-order systems: Lagrangian approach,” *Physica Scripta*, vol. 94, no. 3, p. 035203, 2019.

[131] L. Pomar, M. Morsilli, P. Hallock, and B. Badenas, “Internal waves, an under-explored source of turbulence events in the sedimentary record,” *Earth-Science Reviews*, vol. 111, pp. 56–81, 2012.

[132] R. Grimshaw, E. Pelinovsky, T. Talipova, and O. Kurkina, “Internal waves, an under-explored source of turbulence events in the sedimentary record,” *Nonlin. Processes Geophys.*, vol. 17, pp. 633–649, 2010.

[133] P. Maurer, S. Joubaud, and P. Odier, “Generation and stability of inertia-gravity waves,” *Journal of Fluid Mechanics*, vol. 808, pp. 539–561, 2016.

[134] J. Metz, D. R. Durran, and P. N. Blossey, “Unusual trapped mountain Lee waves with deep vertical penetration and significant stratospheric amplitude,” *Journal of the Atmospheric Sciences*, vol. 77, no. 2, pp. 633–646, 2020.

[135] K. R. Helfrich and W. K. Melvillei, “Long nonlinear internal waves,” *Annu. Rev. Fluid Mech*, vol. 38, pp. 395 – 425, 2006.

[136] C. E. Lennert-Cody and P. J. Franks., “Plankton patchiness in high-frequency internal waves,” *Marine Ecology Progress Series*, vol. 186, pp. 59–66, 1999.

[137] M. White and B. Dorschel, “The importance of the permanent thermocline to the cold water coral carbonate mound distribution in the NE Atlantic,” *Earth and Planetary Science Letters*, vol. 296, pp. 395–402, 2010.

[138] D. A. Segar and E. S. Segar, *Introduction to ocean sciences, 551.46 SEG, Wadsworth Pub, 1998*.

[139] M. Tulin and G. Zilman, “Dead-water effects of a ship moving in stratified seas,” vol. 1 of *Proc llth Int Conf Offshore Mech and Arctic Engg*, 1992.

[140] D. Hambling, “Weatherwatch: ’dead water’ makes ships seem dead in the water.” www.theguardian.com, 2018.

[141] R. B. Perry and G. R. Schimke, “Large-amplitude internal waves observed off the northwest coast of Sumatra,” *Journal of Geophysical Research*, vol. 70, no. 10, pp. 2319–2324, 1965.

[142] A. Osborne and T. Burch, “Internal solitons in the Andaman sea,” *Science*, vol. 208, no. 4443, pp. 451–460, 1980.

[143] J. S. Weisberg and H. I. Parish, *Introductory oceanography, McGraw-Hill Companies, 1974*.

[144] J. Ziegenbein, "Short internal waves in the Strait of Gibraltar," in *Deep Sea Research and Oceanographic Abstracts*, vol. 16, pp. 479–487, Elsevier, 1969.

[145] D. M. Farmer, "Observations of long nonlinear internal waves in a lake," *Journal of Physical Oceanography*, vol. 8, no. 1, pp. 63–73, 1978.

[146] R. Robertson, J. Dong, and P. Hartlipp, "Diurnal critical latitude and the latitude dependence of internal tides, internal waves, and mixing based on Barcoo Seamount," *Journal of Geophysical Research: Oceans*, vol. 122, no. 10, pp. 7838–7866, 2017.

[147] C. R. Jackson, "An empirical model for estimating the geographic location of nonlinear internal solitary waves," *Journal of Atmospheric and Oceanic Technology*, vol. 26, no. 10, pp. 2243–2255, 2009.

[148] J. R. Apel, L. A. Ostrovsky, Y. A. Stepanyants, and J. F. Lynch, "Internal solitons in the ocean and their effect on underwater sound," *The Journal of the Acoustical Society of America*, vol. 121, no. 2, pp. 695–722, 2007.

[149] J. Grue, "Very large internal waves in the ocean-Observations and nonlinear models," in *Waves in Geophysical Fluids*, pp. 205–270, Springer, 2006.

[150] R. Clarke, R. Smith, and D. Reid, "The morning glory of the Gulf of Carpentaria: An atmospheric undular bore," *Monthly Weather Review*, vol. 109, no. 8, pp. 1726–1750, 1981.

[151] M. H. Alford, T. Peacock, J. A. MacKinnon, J. D. Nash, M. C. Buijsman, L. R. Centurioni, S.-Y. Chao, M.-H. Chang, D. M. Farmer, O. B. Fringer, *et al.*, "The formation and fate of internal waves in the South China Sea," *Nature*, vol. 521, no. 7550, pp. 65–69, 2015.

[152] B. Liu, "Investigate the effect of tides on the internal wave mophorlogy and generation sites in the Sulu Sea using satellite images," in *IEEE International Geoscience and Remote Sensing Symposium (IGARSS)*, pp. 3986–3988, 2016.

[153] K. Sabinin and A. Serebryany, "'hot spots' in the field of internal waves in the ocean," *Acoustical Physics*, vol. 53, no. 3, pp. 357–380, 2007.

[154] L. Boegman and M. Stastna, "Sediment resuspension and transport by internal solitary waves," *Annual Review of Fluid Mechanics*, vol. 51, pp. 129–154, 2019.

[155] M. R. Khalilabadi, M. Sadrinassab, V. Chegini, and M. Akbarinassab, "Internal wave generation in the Gulf of Oman (outflow of Persian Gulf)," *Indian Journal of Geo-Marine Sciences*, vol. 44, pp. 371–375, 2015.

[156] P. Baines, "Satellite observations of internal waves on the Australian North-West Shelf," *Marine and Freshwater Research*, vol. 32, no. 3, pp. 457–463, 1981.

[157] L. Cavaleri, F. Barbariol, A. Benetazzo, L. Bertotti, J.-R. Bidlot, P. Janssen, and N. Wedi, "The Draupner wave: A fresh look and the emerging view," *Journal of Geophysical Research: Oceans*, vol. 121, no. 8, pp. 6061–6075, 2016.

[158] R. Grimshaw, E. Pelinovsky, and T. Talipova, "The modified Korteweg-de Vries equation in the theory of large-amplitude internal waves," 1997.

[159] R. Grimshaw, E. Pelinovsky, and T. Talipova, "Modelling internal solitary waves in the coastal ocean," *Surveys in Geophysics*, vol. 28, no. 4, pp. 273–298, 2007.

[160] S. Mohapatra, R. B. Fonseca, and C. Guedes Soares, "Comparison of analytical and numerical simulations of long nonlinear internal solitary waves in shallow water," *Journal of Coastal Research*, vol. 34, no. 4, pp. 928–938, 2018.

[161] T. Talipova, O. Kurkina, E. Rouvinskaya, and E. Pelinovsky, "Propagation of solitary internal waves in two-layer ocean of variable depth," *Izvestiya, Atmospheric and Oceanic Physics*, vol. 51, no. 1, pp. 89–97, 2015.

[162] M. Hooi, W. Tiong, K. Tay, S. Sze, and K. Chiew, "Simulation of internal solitary waves with negative polarity in slowly varying medium," in *AIP Conference Proceedings*, vol. 2013, p. 020006, AIP Publishing LLC, 2018.

[163] M. H. Hooi, W. K. Tiong, K. G. Tay, K. L. Chiew, *et al.*, "Numerical simulation of shoaling internal solitary waves in two-layer fluid flow," *Matematika*, vol. 34, no. 2, pp. 333–350, 2018.

[164] K. Terletska, K. T. Jung, T. Talipova, V. Maderich, I. Brovchenko, and R. Grimshaw, "Internal breather-like wave generation by the second mode solitary wave interaction with a step," *Physics of Fluids*, vol. 28, no. 11, p. 116602, 2016.

[165] M. Carr, P. Sutherland, A. Haase, *et al.*, "Laboratory experiments on internal solitary waves in ice-covered waters," *Geophysical Research Letters*, vol. 46, no. 21, pp. 12230–12238, 2019.

[166] E. Shurgalina, "Mechanism of the emergence of rogue waves as a result of the interaction between internal solitary waves in a stratified basin," *Fluid Dynamics*, vol. 53, no. 1, pp. 59–64, 2018.

[167] E. Didenkulova, "Numerical modeling of soliton turbulence within the focusing Gardner equation: Rogue wave emergence," *Physica D: Nonlinear Phenomena*, vol. 399, pp. 35–41, 2019.

[168] M. A. Rehman and M. Mishra, "Ion-acoustic Gardner solitons in electron-positron-ion plasma with two-electron temperature distributions," *Physics of Plasmas*, vol. 23, no. 1, p. 012302, 2016.

[169] A. Kamchatnov, Y.-H. Kuo, T.-C. Lin, T.-L. Horng, S.-C. Gou, R. Clift, G. El, and R. H. Grimshaw, “Undular bore theory for the Gardner equation,” *Physical Review E*, vol. 86, no. 3, p. 036605, 2012.

[170] E. Pelinovsky, O. Polukhina, A. Slunyaev, and T. Talipova, “Internal solitary waves,” in *Solitary Waves in Fluids*, vol. 47, p. 85, WIT Press Southampton, 2007.

[171] T. Kakutani and N. Yamasaki, “Solitary waves on a two-layer fluid,” *Journal of the Physical Society of Japan*, vol. 45, no. 2, pp. 674–679, 1978.

[172] R. Grimshaw, “Evolution equations for weakly nonlinear, long internal waves in a rotating fluid,” *Studies in Applied Mathematics*, vol. 73, no. 1, pp. 1–33, 1985.

[173] O. Kurkina, A. Kurkin, E. Rouvinskaya, and T. Soomere, “Propagation regimes of interfacial solitary waves in a three-layer fluid,” *Nonlinear Processes in Geophysics*, vol. 22, no. 1, 2015.

[174] L. Ostrovsky, E. Pelinovsky, V. Shrira, and Y. Stepanyants, “Beyond the KdV: Post-explosion development,” *Chaos: An Interdisciplinary Journal of Nonlinear Science*, vol. 25, no. 9, p. 097620, 2015.

[175] K. Singh, P. Sethi, and N. Saini, “Effect of polarization force on head-on collision between multi-solitons in dusty plasma,” *Physics of Plasmas*, vol. 25, no. 3, p. 033705, 2018.

[176] D. E. Pelinovsky and R. H. Grimshaw, “Structural transformation of eigenvalues for a perturbed algebraic soliton potential,” *Physics Letters A*, vol. 229, no. 3, pp. 165–172, 1997.

[177] F. Baronio, A. Degasperis, M. Conforti, and S. Wabnitz, “Solutions of the vector nonlinear Schrödinger equations: evidence for deterministic rogue waves,” *Physical Review Letters*, vol. 109, no. 4, p. 044102, 2012.

[178] N. V. Priya, M. Senthilvelan, and M. Lakshmanan, “Akhmediev breathers, Ma solitons, and general breathers from rogue waves: A case study in the manakov system,” *Physical Review E*, vol. 88, no. 2, p. 022918, 2013.

[179] F. Baronio, M. Conforti, A. Degasperis, and S. Lombardo, “Rogue waves emerging from the resonant interaction of three waves,” *Physical Review Letters*, vol. 111, no. 11, p. 114101, 2013.

[180] Y. Ohta and J. Yang, “Rogue waves in the Davey-Stewartson I equation,” *Physical Review E*, vol. 86, no. 3, p. 036604, 2012.

[181] A. Tikan, C. Billet, G. El, A. Tovbis, M. Bertola, T. Sylvestre, F. Gustave, S. Randoux, G. Genty, P. Suret, *et al.*, "Universality of the Peregrine soliton in the focusing dynamics of the cubic nonlinear Schrödinger equation," *Physical Review Letters*, vol. 119, no. 3, p. 033901, 2017.

[182] P. Suret, R. El Koussaifi, A. Tikan, C. Evain, S. Randoux, C. Szwaj, and S. Bielawski, "Single-shot observation of optical rogue waves in integrable turbulence using time microscopy," *Nature Communications*, vol. 7, no. 1, pp. 1–8, 2016.

[183] K. Dysthe, H. E. Krogstad, and P. Müller, "Oceanic rogue waves," *Annu. Rev. Fluid Mech.*, vol. 40, pp. 287–310, 2008.

[184] I. Nikolkina and I. Didenkulova, "Catalogue of rogue waves reported in media in 2006-2010," *Natural Hazards*, vol. 61, no. 3, pp. 989–1006, 2012.

[185] A. Sergeeva, A. Slunyaev, E. Pelinovsky, T. Talipova, and D.-J. Doong, "Numerical modeling of rogue waves in coastal waters," *Natural Hazards and Earth System Sciences*, vol. 14, no. 4, p. 861, 2014.

[186] A. Laidler, "Bondi Beach wave death: Russian DJ named as victim." www.7news.com.au, 2020.

[187] K. B. Dysthe, "Modelling a Rogue Wave-speculations or a realistic possibility," pp. 255–264, Brest France, 2001.

[188] A. R. Osborne, "Nonlinear ocean wave and the inverse scattering transform," in *Scattering*, pp. 637–666, Elsevier, 2002.

[189] C. Kharif, E. Pelinovsky, and A. Slunyaev, *Rogue waves in the ocean. Springer Science and Business Media, 2008*.

[190] T. Soomere, "Rogue waves in shallow water," *The European Physical Journal Special Topics*, vol. 185, no. 1, pp. 81–96, 2010.

[191] V. E. Zakharov, "Stability of periodic waves of finite amplitude on the surface of a deep fluid," *Journal of Applied Mechanics and Technical Physics*, vol. 9, no. 2, pp. 190–194, 1968.

[192] V. I. Shrira and V. V. Geogjaev, "What makes the Peregrine soliton so special as a prototype of freak waves?," *Journal of Engineering Mathematics*, vol. 67, no. 1-2, pp. 11–22, 2010.

[193] Y. Kodama, "KP solitons in shallow water," *Journal of Physics A: Mathematical and Theoretical*, vol. 43, no. 43, p. 434004, 2010.

[194] D. J. Korteweg and G. De Vries, "XLI. on the change of form of long waves advancing in a rectangular canal, and on a new type of long stationary waves," *The London, Edinburgh, and Dublin Philosophical Magazine and Journal of Science*, vol. 39, no. 240, pp. 422–443, 1895.

[195] N. J. Zabusky and M. D. Kruskal, "Interaction of solitons in a collisionless plasma and the recurrence of initial states," *Physical Review Letters*, vol. 15, no. 6, p. 240, 1965.

[196] N. Zabusky and C. Galvin, "Shallow-water waves, the Korteweg-de Vries equation and solitons," *Journal of Fluid Mechanics*, vol. 47, no. 4, pp. 811–824, 1971.

[197] M. Kerszberg, "A simple model for unidirectional crystal growth," *Physics Letters A*, vol. 105, no. 4-5, pp. 241–244, 1984.

[198] N. Rao, P. Shukla, and M. Y. Yu, "Dust-acoustic waves in dusty plasmas," *Planetary and Space Science*, vol. 38, no. 4, pp. 543–546, 1990.

[199] Y. S. Kivshar, "Perturbation-induced dynamics of small-amplitude dark optical solitons," *Optics Letters*, vol. 15, no. 22, pp. 1273–1275, 1990.

[200] W. Hereman, "Shallow water waves and solitary waves," in *Mathematics of Complexity and Dynamical Systems* (R. A. Meyers, ed.), pp. 1520–1532, Springer, New York, 2012.

[201] A. Karczewska, P. Rozmej, and E. Infeld, "Shallow-water soliton dynamics beyond the Korteweg-de Vries equation," *Physical Review E*, vol. 90, no. 1, p. 012907, 2014.

[202] K. Brauer, "The Korteweg-de Vries equation: history, exact solutions, and graphical representation," *University of Osnabrück / Germany*, 2000.

[203] D. Levi, "Levi-Civita theory for irrotational water waves in a one-dimensional channel and the complex Korteweg-de Vries equation," *Theoretical and Mathematical Physics*, vol. 99, no. 3, pp. 705–709, 1994.

[204] Y. Zhang, Y.-n. Lv, L.-y. Ye, and H.-q. Zhao, "The exact solutions to the complex KdV equation," *Physics Letters A*, vol. 367, no. 6, pp. 465–472, 2007.

[205] J. Wu and J.-M. Yuan, "The effect of dissipation on solutions of the complex KdV equation," *Mathematics and Computers in Simulation*, vol. 69, no. 5-6, pp. 589–599, 2005.

[206] Y. C. Li, "Simple explicit formulae for finite time blow up solutions to the complex KdV equation," *Chaos, Solitons and Fractals*, vol. 39, no. 1, pp. 369–372, 2009.

[207] H. Abdel-Gawad, M. Tantawy, and R. Abo Elkhair, "On the extension of solutions of the real to complex KdV equation and a mechanism for the construction of rogue waves," *Waves in Random and Complex Media*, vol. 26, no. 3, pp. 397–406, 2016.

[208] A. Osborne and G. Boffetta, "The shallow-water nonlinear Schrödinger equation in Lagrangian coordinates," *Physics of Fluids A: Fluid Dynamics*, vol. 1, no. 7, pp. 1200–1210, 1989.

[209] A. Slunyaev, "A high-order nonlinear envelope equation for gravity waves in finite-depth water," *Journal of Experimental and Theoretical Physics*, vol. 101, no. 5, pp. 926–941, 2005.

[210] T. P. Horikis and D. J. Frantzeskakis, "On the NLS to KdV connection," *Rom. J. Phys*, vol. 59, pp. 195–203, 2014.

[211] G. Schneider, "Approximation of the Korteweg-de Vries equation by the nonlinear Schrödinger equation," *Journal of Differential Equations*, vol. 147, no. 2, pp. 333–354, 1998.

[212] G. Schneider, "Justification of the NLS approximation for the KdV equation using the Miura transformation," *Advances in Mathematical Physics*, vol. 2011, 2011.

[213] R. M. Miura, "Korteweg-de Vries equation and generalizations. I. A remarkable explicit nonlinear transformation," *Journal of Mathematical Physics*, vol. 9, no. 8, pp. 1202–1204, 1968.

[214] R. M. Miura, C. S. Gardner, and M. D. Kruskal, "Korteweg-de Vries equation and generalizations. II. Existence of conservation laws and constants of motion," *Journal of Mathematical physics*, vol. 9, no. 8, pp. 1204–1209, 1968.

[215] B. Buti, N. Rao, and S. Khadkikar, "Complex and singular solutions of KdV and mKdV equations," *Physica Scripta*, vol. 34, no. 6B, p. 729, 1986.

[216] J.-M. Yuan and J. Wu, "The complex KdV equation with or without dissipation," *Discrete & Continuous Dynamical Systems-B*, vol. 5, no. 2, p. 489, 2005.

[217] S. Ying-Ying, Y. Juan-Ming, and Z. Da-Jun, "Solutions to the complex Korteweg-de Vries equation: Blow-up solutions and non-singular solutions," *Communications in Theoretical Physics*, vol. 61, no. 4, p. 415, 2014.

[218] S. Wabnitz, C. Finot, J. Fatome, and G. Millot, "Shallow water rogue wavetrains in nonlinear optical fibers," *Physics Letters A*, vol. 377, no. 12, pp. 932–939, 2013.

[219] J. Cen and A. Fring, "Complex solitons with real energies," *Journal of Physics A: Mathematical and Theoretical*, vol. 49, no. 36, p. 365202, 2016.

[220] J. Cen, F. Correa, and A. Fring, "Time-delay and reality conditions for complex solitons," *Journal of Mathematical Physics*, vol. 58, no. 3, p. 032901, 2017.

[221] J. Boussinesq, *Essay on the theory of running water, Impr. National, 1877*.

[222] J. S. Russell, *Report on Waves, (Made to the Meetings of the British Association in 1842-43)*. Richard and John Taylor, London, 1845.

[223] A. Jeffrey, "Role of the Korteweg-de Vries equation in plasma physics," *Quarterly Journal of the Royal Astronomical Society*, vol. 14, p. 183, 1973.

[224] E. Belenov and A. Nazarkin, "Solutions of nonlinear-optics equations found outside the approximation of slowly varying amplitudes and phases," *JETP Lett*, vol. 51, no. 5, pp. 288–292, 1990.

[225] H. Leblond, "Half-cycle optical soliton in quadratic nonlinear media," *Physical Review A*, vol. 78, no. 1, p. 013807, 2008.

[226] D. Levi and M. Sanielevici, "Irrotational water waves and the complex Korteweg-de Vries equation," *Physica D: Nonlinear Phenomena*, vol. 98, no. 2-4, pp. 510–514, 1996.

[227] A. Shabat and V. Zakharov, "Exact theory of two-dimensional self-focusing and one-dimensional self-modulation of waves in nonlinear media," *Soviet Physics JETP*, vol. 34, no. 1, p. 62, 1972.

[228] G. P. Agrawal, "Nonlinear fiber optics," in *'Nonlinear Science at the Dawn of the 21st Century'* (P. L. Christiansen, M. P. Sorensen, and A. Scott, eds.), ch. 9, pp. 195–211, Springer, 2000.

[229] A. Biswas, Y. Yildirim, E. Yasar, Q. Zhou, S. P. Moshokoa, and M. Belic, "Optical solitons for Lakshmanan-Porsezian-Daniel model by modified simple equation method," *Optik*, vol. 160, pp. 24–32, 2018.

[230] A. Ankiewicz, D. Kedziora, A. Chowdury, U. Bandelow, and N. Akhmediev, "Infinite hierarchy of nonlinear Schrödinger equations and their solutions," *Physical Review E*, vol. 93, no. 1, p. 012206, 2016.

[231] Y. V. Sedletsky, "The fourth-order nonlinear Schrödinger equation for the envelope of stokes waves on the surface of a finite-depth fluid," *Journal of Experimental and Theoretical Physics*, vol. 97, no. 1, pp. 180–193, 2003.

[232] E. Tobisch and E. Pelinovsky, "Constructive study of modulational instability in higher order Korteweg-de Vries equations," *Fluids*, vol. 4, no. 1, p. 54, 2019.

[233] T. Marchant and N. Smyth, "The extended Korteweg-de Vries equation and the resonant flow of a fluid over topography," *Journal of Fluid Mechanics*, vol. 221, pp. 263–287, 1990.

[234] M. Hirata, S. Okino, and H. Hanazaki, “Numerical simulation of capillary gravity waves excited by an obstacle in shallow water,” *Proceedings of the Estonian Academy of Sciences*, vol. 64, no. 3, p. 278, 2015.

[235] J. K. Hunter and J. Scheurle, “Existence of perturbed solitary wave solutions to a model equation for water waves,” *Physica D: Nonlinear Phenomena*, vol. 32, no. 2, pp. 253–268, 1988.

[236] A. Misra, “Complex Korteweg-de Vries equation and nonlinear dust-acoustic waves in a magnetoplasma with a pair of trapped ions,” *Applied Mathematics and Computation*, vol. 256, pp. 368–374, 2015.

[237] T. Soomere, “Nonlinear ship wake waves as a model of rogue waves and a source of danger to the coastal environment: a review,” *Oceanologia*, vol. 48, no. S, 2006.

[238] T. Lennon, “Black sunday 1938: Hundreds washed out to sea on bondi beach as freak waves kill five, injure dozens.” www.dailytelegraph.com, 2015.

[239] V. Marinakis, “Higher-order equations of the KdV type are integrable,” *Advances in Mathematical Physics*, vol. 2010, 2010.

[240] A. Grünrock, “On the hierarchies of higher order mKdV and KdV equations,” *Open Mathematics*, vol. 8, no. 3, pp. 500–536, 2010.

[241] A.-M. Wazwaz, “A variety of negative-order integrable KdV equations of higher orders,” *Waves in Random and Complex Media*, vol. 29, no. 2, pp. 195–203, 2019.

[242] L. Zi-Liang, “Application of higher-order KdV-mKdV model with higher-degree nonlinear terms to gravity waves in atmosphere,” *Chinese Physics B*, vol. 18, no. 10, p. 4074, 2009.

[243] T. J. Bridges, G. Derks, and G. Gottwald, “Stability and instability of solitary waves of the fifth-order KdV equation: a numerical framework,” *Physica D: Nonlinear Phenomena*, vol. 172, no. 1-4, pp. 190–216, 2002.

[244] P. A. Clarkson, N. Joshi, and M. Mazzocco, “The Lax pair for the mKdV hierarchy,” *Théories asymptotiques et équations de Painlevé*, vol. 14, pp. 53–64, 2006.

[245] H. Leblond and F. Sanchez, “Models for optical solitons in the two-cycle regime,” *Physical Review A*, vol. 67, no. 1, p. 013804, 2003.

[246] A.-M. Wazwaz, “The simplified Hirota’s method for studying three extended higher-order KdV-type equations,” *Journal of Ocean Engineering and Science*, vol. 1, no. 3, pp. 181–185, 2016.

[247] A. Karczewska and P. Rozmej, "Shallow water waves-extended Korteweg-de Vries equations," *Oficyna Wydawnicza Uniwersyteu Zielonogórskiego, Zielona Góra*, 2018.

[248] N. A. Krall and A. W. Trivelpiece, "Principles of plasma physics," *American Journal of Physics*, vol. 41, no. 12, pp. 1380–1381, 1973.

[249] P. M. Bellan, *Fundamentals of plasma physics, Cambridge University Press, 2008*.

[250] R. C. Davidson, *Physics of nonneutral plasmas, Imperial College Press London, 2001*.

[251] P. K. Shukla and A. Mamun, *Introduction to dusty plasma physics, CRC press, 2015*.

[252] O. Havnes, T. Aslaksen, and A. Brattli, "Charged dust in the Earth's middle atmosphere," *Physica Scripta*, vol. 2001, no. T89, p. 133, 2001.

[253] J. Winter, "Dust: A new challenge in nuclear fusion research?," *Physics of Plasmas*, vol. 7, no. 10, pp. 3862–3866, 2000.

[254] C. Szopa, G. Cernogora, L. Boufendi, J. J. Correia, and P. Coll, "PAMPRE: A dusty plasma experiment for Titan's tholins production and study," *Planetary and Space Science*, vol. 54, no. 4, pp. 394–404, 2006.

[255] R. L. Merlino, "25 years of dust acoustic waves," *Journal of Plasma Physics*, vol. 80, no. 6, pp. 773–786, 2014.

[256] M. Bokaeeyan, "Dispersion characteristics of dust lattice waves in two-dimensional bi-crystal and mono-crystal," *Physica Scripta*, vol. 89, no. 9, p. 095601, 2014.

[257] I. Motie and M. Bokaeeyan, "Effect of the radio frequency discharge on the dust charging process in a weakly collisional and fully ionized plasma," *Physics of Plasmas*, vol. 22, no. 2, p. 023707, 2015.

[258] O. Bouzit and M. Tribeche, "Dust-acoustic waves modulational instability and rogue waves in a polarized dusty plasma," *Physics of Plasmas*, vol. 22, no. 10, p. 103703, 2015.

[259] M. Rahman, A. Mannan, N. Chowdhury, and A. Mamun, "Generation of rogue waves in space dusty plasmas," *Physics of Plasmas*, vol. 25, no. 10, p. 102118, 2018.

[260] H. Bailung, S. Sharma, and Y. Nakamura, "Observation of Peregrine solitons in a multicomponent plasma with negative ions," *Physical Review Letters*, vol. 107, no. 25, p. 255005, 2011.

[261] N. Akhtar, S. El-Tantawy, S. Mahmood, and A.-M. Wazwaz, "On the dynamics of dust-acoustic and dust-cyclotron freak waves in a magnetized dusty plasma," *Romanian Reports in Physics*, vol. 71, p. 403, 2019.

[262] W.-R. Sun, B. Tian, R.-X. Liu, and D.-Y. Liu, “Dust ion-acoustic rogue waves in a three-species ultracold quantum dusty plasmas,” *Annals of Physics*, vol. 349, pp. 366–373, 2014.

[263] S. Guo and L. Mei, “Three-dimensional dust-ion-acoustic rogue waves in a magnetized dusty pair-ion plasma with nonthermal nonextensive electrons and opposite polarity dust grains,” *Physics of Plasmas*, vol. 21, no. 8, p. 082303, 2014.

[264] W. Moslem, P. Shukla, and B. Eliasson, “Surface plasma rogue waves,” *EPL (Europhysics Letters)*, vol. 96, no. 2, p. 25002, 2011.

[265] S. Guo, L. Mei, and W. Shi, “Rogue wave triplets in an ion-beam dusty plasma with superthermal electrons and negative ions,” *Physics Letters A*, vol. 377, no. 34-36, pp. 2118–2125, 2013.

[266] N. Chowdhury, A. Mannan, M. Hasan, and A. Mamun, “Heavy ion-acoustic rogue waves in electron-positron multi-ion plasmas,” *Chaos: An Interdisciplinary Journal of Nonlinear Science*, vol. 27, no. 9, p. 093105, 2017.

[267] S. Khondaker, A. Mannan, N. Chowdhury, and A. Mamun, “Rogue waves in multi-pair plasma medium,” *Contributions to Plasma Physics*, vol. 59: e201800125, 2019.

[268] S. Sultana, S. Islam, A. Mamun, and R. Schlickeiser, “Modulated heavy nucleus-acoustic waves and associated rogue waves in a degenerate relativistic quantum plasma system,” *Physics of Plasmas*, vol. 25, no. 1, p. 012113, 2018.

[269] J. Sikta, N. Chowdhury, A. Mannan, S. Sultana, and A. Mamun, “Electrostatic dust-acoustic rogue waves in an electron depleted dusty plasma,” *arXiv:1909.12327*, 2019.

[270] H. Abdelwahed, E. El-Shewy, M. Zahran, and S. Elwakil, “On the rogue wave propagation in ion pair superthermal plasma,” *Physics of Plasmas*, vol. 23, no. 2, p. 022102, 2016.

[271] M. S. Ruderman, “Freak waves in laboratory and space plasmas,” *The European Physical Journal Special Topics*, vol. 185, no. 1, pp. 57–66, 2010.

[272] S. El-Labany, W. Moslem, N. El-Bedwehy, R. Sabry, and H. A. El-Razek, “Rogue wave in Titan’s atmosphere,” *Astrophysics and Space Science*, vol. 338, no. 1, pp. 3–8, 2012.

[273] M. Afify, W. Moslem, and M. Hassouba, “Non-linear dynamics of electron-hole plasma induced by an electron beam,” *Plasma Research Express*, vol. 1, no. 3, p. 035010, 2019.

[274] M. Tribeche and A. Merriche, “Nonextensive dust-acoustic solitary waves,” *Physics of Plasmas*, vol. 18, no. 3, p. 034502, 2011.

[275] A. Mamun and P. Shukla, “Spherical and cylindrical dust acoustic solitary waves,” *Physics Letters A*, vol. 290, no. 3-4, pp. 173–175, 2001.

[276] F. Deeba, S. Tasnim, and A. Mamun, “Gardner solitons in a dusty plasma,” *IEEE Transactions on Plasma Science*, vol. 40, no. 9, pp. 2247–2253, 2012.

[277] N. Jannat, M. Ferdousi, and A. Mamun, “Ion-acoustic Gardner solitons in a four-component nonextensive multi-ion plasma,” *Plasma Physics Reports*, vol. 42, no. 7, pp. 678–686, 2016.

[278] M. Hossain, A. Mamun, and K. Ashrafi, “Cylindrical and spherical dust ion-acoustic Gardner solitons in a quantum plasma,” *Physics of Plasmas*, vol. 18, no. 10, p. 103704, 2011.

[279] S. Guo, L. Mei, and Z. Zhang, “Time-fractional Gardner equation for ion-acoustic waves in negative-ion-beam plasma with negative ions and nonthermal nonextensive electrons,” *Physics of Plasmas*, vol. 22, no. 5, p. 052306, 2015.

[280] P. K. Shukla and A. Mamun, “Dust-acoustic shocks in a strongly coupled dusty plasma,” *IEEE transactions on plasma science*, vol. 29, no. 2, pp. 221–225, 2001.

[281] R. Grimshaw, D. Pelinovsky, E. Pelinovsky, and T. Talipova, “Wave group dynamics in weakly nonlinear long-wave models,” *Physica D: Nonlinear Phenomena*, vol. 159, no. 1-2, pp. 35–57, 2001.

[282] S. El-Tantawy, N. El-Bedwehy, and S. El-Labany, “Ion-acoustic super rogue waves in ultracold neutral plasmas with nonthermal electrons,” *Physics of Plasmas*, vol. 20, no. 7, p. 072102, 2013.

[283] A. Panwar, H. Rizvi, and C. Ryu, “Compressional alfvénic rogue and solitary waves in magnetohydrodynamic plasmas,” *Physics of Plasmas*, vol. 20, no. 8, p. 082101, 2013.

[284] K. C. Kao and G. A. Hockham, “Dielectric-fibre surface waveguides for optical frequencies,” *Proceedings of the Institution of Electrical Engineers*, vol. 113, no. 7, pp. 1151–1158, 1966.

[285] M.-J. Li and T. Hayashi, “Advances in low-loss, large-area, and multicore fibers,” in *Optical Fiber Telecommunications VII*, pp. 3–50, Elsevier, 2020.

[286] G. Brambilla, V. Finazzi, and D. J. Richardson, “Ultra-low-loss optical fiber nanotapers,” *Optics Express*, vol. 12, no. 10, pp. 2258–2263, 2004.

[287] A. Hasegawa, “Optical solitons in fibers,” in *Optical Solitons in Fibers*, pp. 1–74, Springer, 1989.

[288] M. Rosenbluh and R. Shelby, "Squeezed optical solitons," *Physical Review Letters*, vol. 66, no. 2, p. 153, 1991.

[289] P. Černỳ, P. G. Zverev, H. Jelinková, and T. T. Basiev, "Efficient Raman shifting of picosecond pulses using BaWO4 crystal," *Optics Communications*, vol. 177, no. 1-6, pp. 397–404, 2000.

[290] A. F. Runge, C. Aguergaray, N. G. Broderick, and M. Erkintalo, "Raman rogue waves in a partially mode-locked fiber laser," *Optics Letters*, vol. 39, no. 2, pp. 319–322, 2014.

[291] R. Driben and I. Babushkin, "Accelerated rogue waves generated by soliton fusion at the advanced stage of supercontinuum formation in photonic-crystal fibers," *Optics Letters*, vol. 37, no. 24, pp. 5157–5159, 2012.

[292] Z. Yuan, N. J. Taylor, R. Ramachandran, and T. B. Marder, "Third-order nonlinear optical properties of organoboron compounds: Molecular structures and second hyperpolarizabilities," *Applied organometallic chemistry*, vol. 10, no. 3-4, pp. 305–316, 1996.

[293] J. N. Kutz, W. L. Kath, R.-D. Li, and P. Kumar, "Long-distance pulse propagation in nonlinear optical fibers by using periodically spaced parametric amplifiers," *Optics Letters*, vol. 18, no. 10, pp. 802–804, 1993.

[294] V. V. Voronovich, V. I. Shrira, and G. Thomas, "Can bottom friction suppress freak wave formation?," *Journal of Fluid Mechanics*, vol. 604, pp. 263–296, 2008.

[295] A. Toffoli, D. Proment, H. Salman, J. Monbaliu, F. Frascoli, M. Dafilis, E. Stramignoni, R. Forza, M. Manfrin, and M. Onorato, "Wind generated rogue waves in an annular wave flume," *Physical Review Letters*, vol. 118, no. 14, p. 144503, 2017.

[296] B. Peng, N. Ma, and X. Gu, "Study on influence of wave-current interaction on prediction of rogue wave taking viscous effect into account," vol. 2A: Structures, Safety and Reliability of *The 32nd International Conference on Offshore Mechanics and Arctic Engineering*, American Society of Mechanical Engineers Digital Collection, 2013.

[297] Y. S. Kivshar and W. Królikowski, "Lagrangian approach for dark solitons," *Optics communications*, vol. 114, no. 3-4, pp. 353–362, 1995.

[298] A. Bondeson, M. Lisak, and D. Anderson, "Soliton perturbations: a variational principle for the soliton parameters," *Physica Scripta*, vol. 20, no. 3-4, p. 479, 1979.

[299] W. Chang, A. Ankiewicz, J. Soto-Crespo, and N. Akhmediev, "Dissipative soliton resonances," *Physical Review A*, vol. 78, no. 2, p. 023830, 2008.

[300] D. Anderson, "Variational approach to nonlinear pulse propagation in optical fibers," *Physical Review A*, vol. 27, no. 6, p. 3135, 1983.

[301] S. C. Cerda, S. B. Cavalcanti, and J. Hickmann, "A variational approach of nonlinear dissipative pulse propagation," *The European Physical Journal D-Atomic, Molecular, Optical and Plasma Physics*, vol. 1, no. 3, pp. 313–316, 1998.

[302] B. Jönsson, C. Peterson, and B. Söderberg, "Variational approach to correlations in charged polymers," *Physical Review Letters*, vol. 71, no. 3, p. 376, 1993.

[303] V. Skarka and N. Aleksić, "Stability criterion for dissipative soliton solutions of the one-, two-, and three-dimensional complex cubic-quintic Ginzburg-Landau equations," *Physical Review Letters*, vol. 96, no. 1, p. 013903, 2006.

[304] A. D. Boardman and L. Velasco, "Gyroelectric cubic-quintic dissipative solitons," *IEEE Journal of selected topics in quantum electronics*, vol. 12, no. 3, pp. 388–397, 2006.

[305] A. Sahoo, S. Roy, and G. P. Agrawal, "Perturbed dissipative solitons: A variational approach," *Physical Review A*, vol. 96, no. 1, p. 013838, 2017.

[306] P. Matthews and H. Susanto, "Variational approximations to homoclinic snaking in continuous and discrete systems," *Physical Review E*, vol. 84, no. 6, p. 066207, 2011.

[307] A. Ankiewicz, N. Akhmediev, and N. Devine, "Dissipative solitons with a Lagrangian approach," *Optical fiber technology*, vol. 13, no. 2, pp. 91–97, 2007.

[308] M. Manousakis, S. Droulias, P. Papagiannis, and K. Hizanidis, "Propagation of chirped solitary pulses in optical transmission lines: perturbed variational approach," *Optics communications*, vol. 213, no. 4-6, pp. 293–299, 2002.

[309] A. Maimistov and D. Parsons, "Evolution of solitary waves which are approximately solitons of a nonlinear Schrödinger equation," *Journal of experimental and theoretical physics*, vol. 77, no. 5, pp. 727–731, 1993.

[310] A. Ankiewicz and N. Akhmediev, "Comparison of Lagrangian approach and method of moments for reducing dimensionality of soliton dynamical systems," *Chaos: An Interdisciplinary Journal of Nonlinear Science*, vol. 18, no. 3, p. 033129, 2008.

[311] H. Feshbach, P. M. Morse, and M. Michio, *Methods of theoretical physics, Dover Publications, 2019*.

[312] N. Akhmediev and A. Ankiewicz, "Dissipative solitons in the complex Ginzburg-Landau and Swift-Hohenberg equations," in *Dissipative solitons*, pp. 1–17, Springer, 2005.

[313] Y. Kodama and A. Hasegawa, "Nonlinear pulse propagation in a monomode dielectric guide," *IEEE Journal of Quantum Electronics*, vol. 23, no. 5, pp. 510–524, 1987.

[314] A. Bhrawy, A. Alshaery, E. Hilal, W. N. Manrakhan, M. Savescu, and A. Biswas, "Dispersive optical solitons with Schrödinger–Hirota equation," *Journal of Nonlinear Optical Physics & Materials*, vol. 23, no. 01, p. 1450014, 2014.

[315] A. Ankiewicz, Y. Wang, S. Wabnitz, and N. Akhmediev, "Extended nonlinear Schrödinger equation with higher-order odd and even terms and its rogue wave solutions," *Physical Review E*, vol. 89, no. 1, p. 012907, 2014.

[316] A. Kundu, "Landau-Lifshitz and higher-order nonlinear systems gauge generated from nonlinear Schrödinger-type equations," *Journal of mathematical physics*, vol. 25, no. 12, pp. 3433–3438, 1984.

[317] X.-Y. Xie, B. Tian, W.-R. Sun, and Y. Sun, "Rogue-wave solutions for the Kundu-Eckhaus equation with variable coefficients in an optical fiber," *Nonlinear Dynamics*, vol. 81, no. 3, pp. 1349–1354, 2015.

[318] X. Wang, B. Yang, Y. Chen, and Y. Yang, "Higher-order rogue wave solutions of the Kundu-Eckhaus equation," *Physica Scripta*, vol. 89, no. 9, p. 095210, 2014.

[319] N. Taghizadeh, M. Mirzazadeh, and F. Tascan, "The first-integral method applied to the Eckhaus equation," *Applied Mathematics Letters*, vol. 25, no. 5, pp. 798–802, 2012.

[320] A. Osborne, A. Kirwan Jr, A. Provenzale, and L. Bergamasco, "The Korteweg-de Vries equation in Lagrangian coordinates," *The Physics of Fluids*, vol. 29, no. 3, pp. 656–660, 1986.

[321] Y. Nutku, "Lagrangian approach to integrable systems yields new symplectic structures for KdV," in *Integrable hierarchies and modern physical theories*, pp. 203–213, Springer, 2001.

[322] Y. Nutku and M. Pavlov, "Multi-Lagrangians for integrable systems," *Journal of Mathematical Physics*, vol. 43, no. 3, pp. 1441–1459, 2002.

[323] S. Chen, F. Baronio, J. M. Soto-Crespo, P. Grelu, and D. Mihalache, "Versatile rogue waves in scalar, vector, and multidimensional nonlinear systems," *Journal of Physics A: Mathematical and Theoretical*, vol. 50, no. 46, p. 463001, 2017.

[324] A. Choudhuri, B. Talukdar, and U. Das, "The modified Korteweg-de Vries hierarchy: Lax pair representation and Bi-Hamiltonian structure," *Zeitschrift für Naturforschung A*, vol. 64, no. 3-4, pp. 171–179, 2009.

[325] A. Maimistov and E. Manykin, "Propagation of ultrashort optical pulses in resonant non-linear light guides," *Zh. Eksp. Teor. Fiz*, vol. 85, pp. 1177–1181, 1983.

[326] P. Beaud, W. Hodel, B. Zysset, and H. Weber, “Ultrashort pulse propagation, pulse breakup, and fundamental soliton formation in a single-mode optical fiber,” *IEEE Journal of Quantum Electronics*, vol. 23, no. 11, pp. 1938–1946, 1987.

[327] A. Hasegawa and Y. Kodama, “Signal transmission by optical solitons in monomode fiber,” *Proceedings of the IEEE*, vol. 69, no. 9, pp. 1145–1150, 1981.

[328] A. Höök and M. Karlsson, “Ultrashort solitons at the minimum-dispersion wavelength: effects of fourth-order dispersion,” *Optics Letters*, vol. 18, no. 17, pp. 1388–1390, 1993.

[329] D. Christodoulides and R. Joseph, “Femtosecond solitary waves in optical fibers-beyond the slowly varying envelope approximation,” *Applied Physics Letters*, vol. 47, no. 2, pp. 76–78, 1985.

[330] D. Marcuse, “Pulse distortion in single-mode fibers,” *Applied Optics*, vol. 19, no. 10, pp. 1653–1660, 1980.

[331] D. Marcuse, A. R. Chraplyvy, and R. Tkach, “Effect of fiber nonlinearity on long-distance transmission,” *Journal of Lightwave Technology*, vol. 9, no. 1, pp. 121–128, 1991.

[332] S. Singh, V. Mishra, and S. Varshney, “Continuous-wave pumped, tunable mid-infrared fiber-optic parametric sources,” *JOSA B*, vol. 31, no. 11, pp. 2786–2791, 2014.

[333] J. Mores, G. Malheiros-Silveira, H. Fragnito, and H. Hernández-Figueroa, “Efficient calculation of higher-order optical waveguide dispersion,” *Optics Express*, vol. 18, no. 19, pp. 19522–19531, 2010.

[334] M. Tlidi and L. Gelens, “High-order dispersion stabilizes dark dissipative solitons in all-fiber cavities,” *Optics Letters*, vol. 35, no. 3, pp. 306–308, 2010.

[335] M. Piché, J. Cormier, and X. Zhu, “Bright optical soliton in the presence of fourth-order dispersion,” *Optics Letters*, vol. 21, no. 12, pp. 845–847, 1996.

[336] B. G. Bale, S. Boscolo, K. Hammani, and C. Finot, “Effects of fourth-order fiber dispersion on ultrashort parabolic optical pulses in the normal dispersion regime,” *JOSA B*, vol. 28, no. 9, pp. 2059–2065, 2011.

[337] S. Pitois and G. Millot, “Experimental observation of a new modulational instability spectral window induced by fourth-order dispersion in a normally dispersive single-mode optical fiber,” *Optics communications*, vol. 226, no. 1-6, pp. 415–422, 2003.

[338] P. T. Dinda and K. Porsezian, “Impact of fourth-order dispersion in the modulational instability spectra of wave propagation in glass fibers with saturable nonlinearity,” *JOSA B*, vol. 27, no. 6, pp. 1143–1152, 2010.

[339] M. Droques, A. Kudlinski, G. Bouwmans, G. Martinelli, A. Mussot, A. Armaroli, and F. Biancalana, “Fourth-order dispersion mediated modulation instability in dispersion oscillating fibers,” *Optics Letters*, vol. 38, no. 17, pp. 3464–3467, 2013.

[340] D. Christodoulides and R. Joseph, “Femtosecond solitary waves in optical fibres,” *Electronics Letters*, vol. 20, no. 16, pp. 659–660, 1984.

[341] E. Dianov, A. Y. Karasik, P. Mamyshev, A. Prokhorov, V. Serkin, M. Stelmakh, and A. Fomichev, “Stimulated-Raman conversion of multisoliton pulses in quartz optical fibers,” *JETP Lett.*, vol. 41, no. 6, p. 242, 1985.

[342] F. M. Mitschke and L. F. Mollenauer, “Discovery of the soliton self-frequency shift,” *Optics Letters*, vol. 11, no. 10, pp. 659–661, 1986.

[343] J. Lucek and K. Blow, “Soliton self-frequency shift in telecommunications fiber,” *Physical Review A*, vol. 45, no. 9, p. 6666, 1992.

[344] J. H. Lee, J. V. Howe, C. Xu, and X. Liu, “Soliton self-frequency shift: experimental demonstrations and applications,” *IEEE Journal of Selected Topics in Quantum Electronics*, vol. 14, no. 3, pp. 713–723, 2008.

[345] M. Romagnoli, F. Locati, F. Matera, M. Settembre, M. Tamburrini, and S. Wabnitz, “Role of pump-induced dispersion on femtosecond soliton amplification in erbium-doped fibers,” *Optics Letters*, vol. 17, no. 13, pp. 923–925, 1992.

[346] Q. Lin and G. P. Agrawal, “Raman response function for silica fibers,” *Optics Letters*, vol. 31, no. 21, pp. 3086–3088, 2006.

[347] N. Akhmediev, W. Królikowski, and A. Lowery, “Influence of the Raman-effect on solitons in optical fibers,” *Optics Communications*, vol. 131, no. 4-6, pp. 260–266, 1996.

[348] G. P. Agrawal and C. Headley III, “Kink solitons and optical shocks in dispersive nonlinear media,” *Physical Review A*, vol. 46, no. 3, p. 1573, 1992.

[349] P. D. Green, D. Milovic, D. A. Lott, and A. Biswas, “Optical solitons with higher order dispersion by semi-inverse variational principle,” *Progress in Electromagnetics Research*, vol. 102, pp. 337–350, 2010.

[350] A. Ankiewicz, “Simplified description of soliton perturbation and interaction using averaged complex potentials,” *Journal of Nonlinear Optical Physics and Materials*, vol. 4, no. 04, pp. 857–870, 1995.

[351] L. Gagnon and P. Bélanger, “Soliton self-frequency shift versus Galilean-like symmetry,” *Optics Letters*, vol. 15, no. 9, pp. 466–468, 1990.

[352] M. Facão, M. Carvalho, and D. Parker, "Soliton self-frequency shift: Self-similar solutions and their stability," *Physical Review E*, vol. 81, no. 4, p. 046604, 2010.

[353] R. Hirota, "Reduction of soliton equations in bilinear form," *Physica D: Nonlinear Phenomena*, vol. 18, no. 1-3, pp. 161–170, 1986.

[354] C. Babalic and A. S. Carstea, "Bilinear approach to the supersymmetric Gardner equation," *Theoretical and Mathematical Physics*, vol. 188, no. 2, pp. 1172–1180, 2016.